Aus dem Institut für Experimentelle Neurologie

der Medizinischen Fakultät Charité – Universitätsmedizin Berlin

DISSERTATION

Role of stroke-induced immunodepression in preventing central nervous system antigen specific immune responses

zur Erlangung des akademischen Grades

Doctor of Philosophy (PhD)

vorgelegt der Medizinischen Fakultät

Charité – Universitätsmedizin Berlin

von

Christine Römer

aus Tartu/Estland

Datum der Promotion: 27.02.2015

Table of contents

1. Abstract

1.1 Zusammenfassung

Nach Schlaganfall ist aufgrund einer systemischen Immundepression (CNS-injury induced immunodepression syndrome, CIDS) die Anfälligkeit gegenüber Infektionen, welche zu einer schlechteren neurologischen Prognose führen, erhöht. Ich habe untersucht, ob diese Immundepression ein adaptiver Mechanismus gegen eine Immunantwort auf spezifische Antigene des zentralen Nervensystems (ZNS) ist, und welche Auswirkungen die Unterdrückung dieses Mechanismus hat.

Im experimentellen Schlaganfallmodell (Okklusion der Arteria cerebri media, MCAo) wurden die Wirkungen des sympathischen Nervensystems (SNS) und der hypothalamisch-hypophyseal-adrenalen (HPA) Achse im Hinblick auf die Beeinflussung der CIDS pharmakologisch geblockt. Dazu wurden Propranolol und Mifepriston Wildtyp-C57Bl/6J-Mäusen gegeben, desweiteren 2D2-transgenen Mäusen mit $CD4^+$-T-Zellen, für die eine schädigende Wirkung durch Immunantwort auf das ZNS-Antigen MOG (Myelin-Oligodendrozyten-Glykoprotein) beschrieben ist. Die Rolle des β2-Adrenorezeptors bei der SNS-gesteuerten Immundepression nach Schlaganfall wurde in β2-Adrenorezeptor-Knockout-Mäusen untersucht. Zum besseren Verständnis der Schlaganfall-getriggerten $CD4^+$-T-Zell-Aggressivität wurden diese einer Gruppe 2D2-Mäusen nach MCAo und Behandlung mit Propranolol und Mifepriston entnommen und auf Lymphozyten-defiziente Rag-1KO-Mäuse nach MCAo übertragen.

Die Blockade der SNS-gesteuerten Immundepression nach Schlaganfall verringerte die Häufigkeit von pulmonalen Infektionen und erhöhte die MOG-spezifische Immunantwort von Typ1-T-Helferzellen (Th1) in ischämischen Gehirnen von 2D2-Mäusen, ohne dass sich der neurologische Zustand in der Langzeitbetrachtung verschlechterte.

Die gleichzeitige Blockade des SNS mit Propranolol und der HPA-Achse mit Mifepriston führte zu einem dauerhaft um zwei Drittel geringeren Infarktvolumen, einer geringeren Infektionsrate, einem verbesserten Gesundheitsstatus und einer verbesserten Langzeitüberlebensdauer von 2D2- und C57Bl/6J-Mäusen. Sie erhöhte die MOG-spezifische Th1-Typ-Immunantwort in ischämischen Gehirnen von 2D2-Mäusen. Dies ging jedoch nicht mit einem verschlechterten neurologischen Status dieser Mäuse einher, welcher mittels modifiziertem EAE-Score und CatWalk-Ganganalyse charakterisiert wurde. Nach

Schlaganfall entwickelten 2D2-Mäuse Symptome eines Polyradikulitis-ähnlichen Phänotyps. Durch die Blockade des SNS und der HPA-Achse wurde diese vermindert, wie mit Normalisierung der Latenzzeiten von F-Wellen nach Stimulation des Nervus ischiaticus gegenüber verlängerten Latenzzeiten nach Schlaganfall und verminderter T-Zell- und Makrophageninfiltration in Spinalnervenwurzeln nach MCAo gezeigt werden konnte. $CD4^+$-T-Zellen von behandelten 2D2-Mäusen verschlechterten nicht den langfristigen neurologischen Zustand von RAG-1KO-Mäusen, nachdem sie auf diesen Stamm übertragen wurden.

Zusammengefasst fällt unter pharmakologischer Blockade des SNS und der HPA-Achse mit Propranolol und Mifepriston das Infarktvolumen bei 2D2- und C57Bl/6J-Mäusen um zwei Drittel geringer aus, die MOG-spezifische Th1-Typ-Immunantwort war in ischämischen Gehirnen von 2D2-Mäusen erhöht, ohne dass sich der neurologische Zustand in der Langzeitbetrachtung verschlechterte.

1.2 Summary

Systemic immunodepression after stroke (central nervous system [CNS] injury induced immunodepression syndrome, CIDS) increases the susceptibility towards infections that have detrimental effects on neurological outcome. Here, I have investigated whether immunodepression after stroke represents an adaptive mechanism for reducing the likelihood of developing CNS antigen specific immune responses and consequences of suppressing this mechanism.

A murine model of middle cerebral artery occlusion (MCAo) and pharmacological blocking of the effects regarding CIDS mediated by sympathetic nervous system (SNS) and hypothalamic-pituitary-adrenal (HPA) axis were applied. Propranolol and mifepristone, respectively, were applied to wild-type C57Bl/6J and 2D2 transgenic mice, whose $CD4^+$ T cells have been described to exert detrimental effects against CNS-antigen myelin oligodendrocyte glycoprotein (MOG). The role of β2-adrenoreceptor in SNS mediated CIDS was investigated in β2-adrenoreceptor knockout mice. To elucidate the $CD4^+$ T-cell aggressiveness induced by stroke these cells were harvested from a group of 2D2 mice that received MCAo and treatment with propranolol and mifepristone, and were adoptively transferred to lymphocyte deficient Rag-1KO mice after MCAo.

Blocking SNS mediated CIDS decreased the rate of bronchopulmonary infections, increased MOG-specific type 1 T helper (Th1) cell responses in the ischemic brains of 2D2 mice but did not worsen the long-term neurological outcome in these mice.

Blocking simultaneously SNS with propranolol and HPA axis with mifepristone resulted in a stably two thirds smaller infarct volume, decreased infection rate, improved health status and long-term survival of 2D2 and C57Bl/6J mice. It increased MOG-specific Th1 cell responses in the ischemic brains of 2D2 mice. This was not accompanied by worse functional neurological outcome in these mice based on EAE like disease development and locomotor deficits. After stroke, 2D2 mice developed polyradiculitis-like phenotype, the symptoms of which were diminished by blocking SNS and HPA axis illustrated by normalization of stroke-induced elongated F-wave latencies upon sciatic nerve stimulation and diminished T cell and macrophage infiltration into spinal nerve roots after MCAo. $CD4^+$ T cells from treated 2D2 mice did not worsen long-term neurological outcome in RAG-1KO mice following adoptive transfer.

In conclusion, pharmacological blocking of SNS and HPA axis with propranolol and mifepristone resulted in infarct volumes sustainably smaller by two thirds in 2D2 as well as in C57Bl/6J mice, increased MOG-specific Th1-type immune responses in the ischemic brains of 2D2 mice but did not worsen long-term neurological outcome.

2. Introduction

2.1 Stroke

Stroke is after ischemic heart disease globally the second most common reason for death and the third most common medical condition causing disability. Over the last 20 years, the incidence of stroke has increased worldwide while the age at onset has decreased (Krishnamurthi, 2013). One out of five or six people, depending on region and gender, experiences stroke in a lifetime (Krishnamurthi, 2013). Stroke is a cerebrovascular accident caused by obstructed cerebral blood flow. This involves typically large cranial arteries, often the middle cerebral artery (MCA) or its branches. Globally, from all strokes that occurred in 2010, 68.5% were ischemic (Krishnamurthi, 2013) resulting from an obstruction, such as a clot, inside the artery.

Despite the urgency to find alleviation for stroke-induced deficits, the current treatment options are poor. In acute stage (within 3 h [or 4.5 h in Europe] after the onset), only recombinant tissue-type plasminogen activator for thrombolysis has been proven effective (NINDS, 1995). Due to the narrow time-window, it is applied on 1-8.5% of hospitalized stroke patients (Millan and Davalos, 2006). Other methods include mechanical retrieval of the clot and intervening complications. Further efforts in elucidating the pathophysiology of stroke might provide novel therapeutic targets in stroke treatment.

Models of focal cerebral ischemia, most prominently embolic stroke and transient MCA occlusion (MCAo) are invaluable sources for information regarding stroke pathophysiology (Durukan and Tatlisumak, 2007). Development of ischemic damage is a long process initiated immediately and lasting for days and weeks (Dirnagl et al., 1999). Occlusion in the artery reduces cerebral blood flow (CBF) and thereby the transport of oxygen and glucose to brain tissue, leading within minutes to neuronal and glial depolarization in the ischemic core. Excitotoxic environment triggers necrosis and apoptosis. Developing edema restricts the CBF around the ischemic core. Events like free radical production, lipid peroxidation, activation of proteolytic enzymes and phospholipases aggravate tissue damage. Mitochondria becomes dysfunctional, cells accumulate lactic acid leading to tissue acidosis. Initial ischemic core enlarges as cells in penumbra depolarize gradually (Dirnagl et al., 1999).

An important contributor to stroke pathophysiology is inflammation. In stroke patients, this occurs within hours after stroke and leukocytes infiltrate ischemic lesion even five weeks later

(Wang et al., 1993). It has been shown in a murine MCAo model that early leukocyte infiltration to ischemic lesion follows certain dynamics. Microglia, macrophages and natural killer cells accumulate within hours after stroke onset. Neutrophils and dendritic cells, mainly of myeloid origin, reach peak numbers on day three after stroke. B and T cells are within the first seven days after MCAo recruited to lesion site in low numbers (Gelderblom et al., 2009). However, a second and larger wave of T cell infiltration is initiated seven days after stroke, reaching maximal levels by day 14. This high infiltration is maintained at least until 30 days after stroke. This second wave of T cell recruitment coincides with increased infiltration of antigen presenting cells such as microglia, dendritic cells and macrophages that often contact T cells directly (Stubbe et al., 2013). Within ischemic lesion, T cells accumulate initially at the border to penumbra and enter ischemic core at their peak infiltration (Schroeter et al., 1994).

Therefore, the pathophysiology of stroke is comprised of diverse events contributing to augmentation of ischemic damage. Since this is a process lasting for weeks, it carries potential for therapeutic interventions by targeting the mechanisms involved to save the brain tissue surrounding ischemic core and thereby improve neurological outcome after stroke.

2.2 Infections after stroke

In 85% of the cases stroke is followed by a complication (Langhorne et al., 2000), which directly affects stroke outcome (Czlonkowska et al., 1979; Davenport et al., 1996). One of the most commonly observed complication in this patient population is infection (Brown and Glassenberg, 1973) which mostly involves urinary tract or bronchopulmonary infections (Czlonkowska et al., 1979). Urinary tract infections develop in about 24% and pneumonia in 22% of stroke patients (Langhorne et al., 2000; Weimar et al., 2002). Respiratory infections such as pneumonia are together with cardiovascular complications the leading cause of death in post-acute phase (Vernino et al., 2003) and, compared with urinary tract infections, have a stronger impact on neurological outcome (Emsley and Hopkins, 2008). Until relatively recently it was widely believed that prolonged hospitalization and aspiration increase pneumonia susceptibility in stroke patients. Even though the link between altered cellular immunity, infections caused by proteus, pseudomonas, staphylococci and Escherichia coli, and neurological outcome in stroke patients had been described (Czlonkowska et al., 1979), it was formulated only in 2005 that CNS injury itself is a risk factor for infections by inducing

secondary immunodepression [CNS injury induced immunodepression syndrome (CIDS)] (Meisel et al., 2005).

2.3 Crosstalk between the nervous and the immune system

The CNS and immune system interact with each other actively to maintain homeostasis in the body. This is achieved through a bidirectional communication via nerve pathways, hormonal cascades and cellular contacts. The key pathways mediating the crosstalk between the nervous and immune system are the sympathetic nervous system (SNS), the hypothalamic-pituitary-adrenal (HPA) axis and the cholinergic anti-inflammatory pathway. The SNS and the HPA axis are highly conserved and well-known as stress systems, eliciting effects on many parts and functions of the body. In addition to these pathways, other mediators participate in homeostasis maintenance including calcitonin gene-related peptide, substance P, neuropeptide Y, vasoactive intestinal peptide, α-melanocyte stimulating hormone and β-endorphin (Woiciechowsky et al., 1999a; Meisel et al., 2005).

When inflammation occus in the periphery, pro-inflammatory mediators such as tumor necrosis factor-α (TNF-α), interleukin-1β (IL-1β), IL-6 are produced to activate immune response. Locally released cytokines bind their cognate receptors on vagal afferents (Woiciechowsky et al., 1999a; Meisel et al., 2005). Circulating cytokines reach the CNS through active carrier-mediated transport (Banks et al., 1995) or, more commonly, by passive transport through the capillary endothelium of the chemosensitive circumventricular organs (Buller, 2001). Circumventricular organs are the pineal gland, the subfornical organ, the median eminence, the posterior lobe of the pituitary, the subcommissural organ, the vascular organ of the lamina terminalis, the area postrema. Many of those are either located in or form extensive connections with the hypothalamus (Squire, 2003) which plays a key role in mediating the crosstalk between the CNS and the immune system. Projections from circumventricular organs to the paraventricular nucleus of the hypothalamus modulate the activity of the SNS and the HPA axis. The hypothalamus is also connected to the vagus nerve via the nucleus tractus solitarius and the locus coeruleus. TNF-α, IL-1β and IL-6 trigger the activation of the SNS, the HPA axis, and the cholinergic anti-inflammatory pathway, stimulating the release of catecholamines, glucocorticoids, and acetylcholine, respectively, which all function to counter-balance peripheral inflammation (Woiciechowsky et al., 1999a; Pavlov et al., 2003; Meisel et al., 2005).

2.3.1 Sympathetic nervous system

Anatomically, the sympathetic nervous system (SNS) is composed of a chain of preganglionic neurons in the lateral horn of the thoraco-lumbar spinal cord, paravertebral sympathetic chain ganglia along the vertebral column and prevertebral collateral ganglia. Axons arising from the paravertebral sympathetic chain ganglia and the prevertebral collateral ganglia innervate an enormous range of target organs, joining segmental spinal nerves, and the viscera, respectively. Sympathetic nerve fibers form an extensive mash around the blood vessels, regulating blood pressure and lumen diameter. Brain centers involved in regulation of sympathetic activity include the rostral ventrolateral medulla and the locus coeruleus which projects to the paraventricular nucleus of the hypothalamus (Squire, 2003).

Among other functions, the SNS is involved in regulation of immune cell development and function. A fundament for this is formed by abundant sympathetic nerve fibers innervating both the primary (bone marrow, thymus) and secondary lymphoid organs (lymph nodes, spleen) (Felten et al., 1985). Compartments of T cells and macrophages are affected by SNS more than those of B cells. SNS appears to affect more the compartments of T cells and macrophages than those of B cells (Felten et al., 1987). The state of SNS activity influences T cell function, lymphocyte trafficking as well as antigen processing and presentation directly (Madden et al., 1995).

When stimulated, sympathetic nerve fibers release catecholamines, mainly noradrenaline but also adrenaline. Small amount of catecholamines are secreted from the adrenal medulla. Released noradrenaline is bound by an adrenoreceptor (AR) on a neighboring cell, as SNS nerve terminals form immediate contacts with lymphocytes and macrophages in spleen (Felten and Olschowka, 1987) or further in the parenchyma through diffusion (Madden et al., 1995). These routes enhance the effects of SNS activation and allow diverse local and systemic effects. ARs are abundant on the cells of immune system and the CNS. ARs are divided into α-ARs (mainly excitatory) and β-ARs (mainly inhibitory) (Ahlquist, 1948). Based on localization, pharmacological and molecular characteristics α-ARs are subdivided into α1A-, α1B-, α1D-AR and α2A-, α2B-, α2C-AR (Bylund et al., 1994; Hieble et al., 1995) and β-ARs into β1-AR, β2-AR (Lands et al., 1967) and β3-AR (Emorine et al., 1989). All ARs are G protein coupled receptors composed of seven transmembrane helical segments forming a pore. Ligand binding stabilizes receptor's active conformation and G protein(s) are recruited to the intracellular domain that determine the direction of the signal through activation of various second messengers. G proteins are divided based on their subunit to

stimulatory (G_s), adenylate cyclase inhibitory (G_i) and phospholipase C coupled (G_q) G proteins (Squire, 2003). The most common AR on immune cells is the β-AR which is found on neutrophils, basophils, eosinophils (Plaut, 1987; Yukawa et al., 1990), macrophages (Abrass et al., 1985) and lymphocytes (Loveland et al., 1981; Fuchs et al., 1988). All β-ARs couple to G_s protein (Squire, 2003) and β2-AR additionally to G_i protein (Azzi et al., 2003). The key AR for immune function is the β2-AR.

SNS activation can induce a multitude of responses with opposing polarity, affecting initiative, proliferative and effector phases of immune response (Madden et al., 1995). Sudden raise in noradrenaline concentration initially increases the numbers of circulating lymphocytes and granulocytes (Benschop et al., 1996), followed by a more pronounced reduction, cytotoxic T cells and natural killer cells being the most sensitive (Elenkov et al., 2000). SNS activation suppresses endotoxin-induced production of pro-inflammatory TNF-α, IL-1, IL-12, IFN-γ, and nitric oxide but increases the release of anti-inflammatory IL-10. At the same time promoting neutrophil recruitment by increasing IL-6 and IL-8 levels (Elenkov et al., 2000). Chronic SNS stimulation desensitizes and down-regulates β2-AR on lymphocytes (Aarons et al., 1983; Motulsky et al., 1986).

SNS activation affects most prominently cell-mediated immune responses. Both, T and B cells, express high affinity β2-ARs (Loveland et al., 1981; Khan et al., 1986; Fuchs et al., 1988). Nevertheless, subpopulations of T cells differ in their responsiveness to noradrenaline (Elenkov et al., 2000). SNS activation elicits strong effects on type 1 helper T (Th1) cells but not on Th2 cells that lack β2-AR (Sanders et al., 1997), introducing Th2 bias (Webster et al., 2002). Noradrenaline binding to the β2-AR impairs Th1 cell differentiation through inhibition of IL-12 secretion from monocytes and dendritic cells (Panina-Bordignon et al., 1997), suppresses Th1 cell ability to produce IFN-γ and IL-2 (Sanders et al., 1997; Borger et al., 1998) and priming (Panina-Bordignon et al., 1997). Enhanced secretion of anti-inflammatory IL-10 from monocytes and macrophages upon binding the β2-AR (Elenkov et al., 1996; Woiciechowsky et al., 1998) down-regulates major histocompatibility (MHC) class II expression, inhibits TNF-α, IL-1β and IL-12 secretion from monocytes (Howard and O'Garra, 1992) and leads to defective antigen presentation. Decreased IL-12 and TNF-α production from antigen presenting cells combined with decreased IFN-γ secretion from Th1 and natural killer cells impairs cellular immunity mediated by cytotoxic T cells, natural killer cells and macrophages (Elenkov et al., 2000).

2.3.2 Hypothalamic-pituitary-adrenal axis

The hypothalamic-pituitary-adrenal (HPA) axis is a neurohormonal pathway involving three main anatomical centers. Upon appropriate stimulus, neurons of the hypothalamic paraventricular nucleus produce corticotropin releasing hormone and vasopressin which stimulate the release of pro-opiomelanocortin-derived peptides like adrenocorticotropin hormone (ACTH) from the anterior pituitary. ACTH, in turn, induces the adrenal cortex to produce glucocorticoids (corticosterone in rodents and cortisol in humans), the end-products of the HPA axis. Besides ACTH and corticotropin releasing hormone, glucocorticoid synthesis is regulated by catecholamines and acetylcholine (Joels and de Kloet, 1994).

Glucocorticoids are bound by intracellular mineralocorticoid and glucocorticoid receptors. Both are abundant on neuronal and glial cells of the brain. While mineralocorticoid receptors are crucial for maintenance and permissive actions of corticosterone, glucocorticoid receptors are more sensitive to increased corticosterone concentration and stress. Continuous stress leads to a lasting down-regulation of the receptors (Joels and de Kloet, 1994; Sapolsky et al., 2000).

Glucocorticoids elicit their effects through a variety of molecular mechanisms which primarily end with modifying gene expression. Most commonly, ligand binding changes receptor conformation and heat shock protein 90 dissociates. Receptor complex translocates into the nucleus, binds hormone responsive element on deoxyribonucleic acid (DNA) and modulates gene expression (Joels and de Kloet, 1994). Glucocorticoids can also bind other transcription factors, such as nuclear factor-κB. Alternatively, non-genomic effects can occur when binding membrane-bound receptors or interfering with glucocorticoid receptor signal transduction components like inositol-1,4,5-triphosphate (Tischner and Reichardt, 2007). The exact mechanism of action is determined by the amino-terminal isoform of the glucocorticoid receptor, phosphorylation, promoter choice, corticosterone concentration, interactions with signaling cascades and diurnal rhythm (Joels and de Kloet, 1994; Sapolsky et al., 2000).

Activation of the HPA axis leads to a plethora of effects in the periphery and the CNS affecting metabolic homeostasis, transmitter systems, ionic conductance, cognition and immune system. Glucocorticoids inhibit the synthesis of pro-inflammatory mediators IL-1β, IL-2, IL-6, IL-12, TNF-α, IL-8, granulocyte-macrophage colony stimulating factor, prostaglandins and nitric oxide (Kwon et al., 1994; Szabo et al., 1994; Wilckens and De Rijk, 1997; Webster et al., 2002) while promoting anti-inflammatory IL-4, IL-10 and TGF-β

release (AyanlarBatuman et al., 1991; Hodge et al., 1999; Barrat et al., 2002; Webster et al., 2002). In addition, glucocorticoids up-regulate cytokine receptor gene expression which can either augment (IL-6 receptor) or antagonize (IL-1 and TNF-α receptors) cytokine function (Munck and Naray-Fejes-Toth, 1994). The HPA axis induced immunomodulation is coarsely immunodepressive, particularly under lasting stress. The effects of this immunodepression affect maturation, differentiation, proliferation and recruitment of immune cells to inflammatory site (Webster et al., 2002).

Similar to the SNS, activation of the HPA axis has profound effects on cell-mediated immune responses affecting most prominently T cells and antigen presenting cells. In T cells, glucocorticoids initiate caspase activation, cathepsin B release, increase hydrogen peroxide concentration and introduce sodium/potassium imbalance (Herold et al., 2006). The most sensitive T cells to glucocorticoid-induced apoptosis are the immature T cells (Compton et al., 1987; Tuosto et al., 1994) and $CD4^+$ helper T cells (Migita et al., 1997) while memory T cells and $CD8^+$ cytotoxic T cells are more resistant (Migita et al., 1997; Sapolsky et al., 2000). Glucocorticoids inhibit T cell proliferation and homing (Tischner and Reichardt, 2007). Furthermore, they inhibit Th1 cell differentiation and IFN-γ production which is further enhanced by suppression of IL-12 synthesis from antigen presenting cells (Blotta et al., 1997; Franchimont et al., 2000). Th1 cells (Franchimont et al., 2000) and antigen presenting cells become less responsive to IFN-γ, resulting in defective antigen presentation (Pan et al., 2001) and impaired T cell priming (Tischner and Reichardt, 2007). HPA axis activation does not impair and might even promote the differentiation and function of Th2 cells (Ramirez et al., 1996). This together with enhanced synthesis of anti-inflammatory IL-4 and IL-10 promote B cell proliferation (McGillis et al., 1989) and immunoglobulin synthesis (Sapolsky et al., 2000; Webster et al., 2002).

2.3.3 Crosstalk between the sympathetic nervous system and the hypothalamic-pituitary-adrenal axis

A high degree of interaction (mainly synergistic) in immune response regulation exists between the SNS and the HPA axis. They both affect predominantly cell-mediated immune responses, suppress Th1 cell function and induce Th2 cell bias. SNS stimulates release of IL-10 which, in turn, augments the anti-inflammatory properties of the HPA axis activation (Woiciechowsky et al., 1999a; Meisel et al., 2005). The two pathways are also anatomically connected. Glucocorticoid receptors are expressed in the brain stem monoaminergic cells and

in areas where monoaminergic neurons project. Hypothalamic noradrenaline activity increases corticosterone synthesis (Smythe et al., 1983) and glucocorticoids regulate the synthesis of noradrenaline (McEwen et al., 1987). Catecholamines enhance glucocorticoid receptor transactivation through a mechanism involving β2-AR (McEwen et al., 1987). Glucocorticoids, on the other hand, enhance β2-AR gene transcription and prevent its desensitization (Collins et al., 1988; Hadcock and Malbon, 1988). Thus, the interplay between these two pathways is essential for modulating immune response.

2.3.4 Cholinergic anti-inflammatory pathway

Cholinergic anti-inflammatory pathway is conveyed by the vagus nerve. It mediates rapid and local effects on immune response. Upon immunogenic stimuli, dendritic cells, macrophages or chemoreceptive cells in vagal paraganglia stimulate vagal afferents that terminate mainly in the nucleus tractus solitarius, the dorsal motor nucleus of the vagus and the area postrema, the latter being a circumventricular organ. The area postrema is positioned centrally to connect the cholinergic anti-inflammatory pathway with the SNS and the HPA axis (Pavlov et al., 2003). From the CNS, vagal efferent fibers project to the organs of reticuloendothelial system (spleen, heart, liver and gastrointestinal tract) (Tracey, 2002). Stimulation of vagal efferents triggers a release of acetylcholine that binds to muscarinic (metabotropic) and nicotinic (ionotropic) receptors on local macrophages (Pavlov et al., 2003). Immunodepression by the cholinergic anti-inflammatory pathway is mediated by acetylcholine binding to α-bungarotoxin sensitive nicotinic acetylcholine receptors containing α7 subunit. The net effect of this interaction is post-translational suppression of pro-inflammatory cytokine, such as TNF-α, IL-1β, IL-6 and IL-18, release whereas the levels of anti-inflammatory cytokine IL-10 remain unchanged (Borovikova et al., 2000; Wang et al., 2003). Stimulation of the vagus nerve enables therefore rapid and targeted depression of immediate immune responses and through tight anatomical connections provides additional input to the primary communication pathways between the CNS and the immune system: the SNS and the HPA axis.

2.4 Central nervous system (CNS) injury induced immunodepression

An injury to the CNS can physically disrupt the neuroinflammatory pathways or alter systemic immune responses through local inflammation in the CNS, causing CNS injury induced immunodepression syndrome (CIDS) (Meisel et al., 2005) which lasts for weeks after stroke (Czlonkowska et al., 1979). In CIDS, neuroinflammatory pathways are activated in the absence of peripheral infections. That lesions physically interfering with the key centers

mediating crosstalk between the CNS and the immune system, such as hypothalamus, modify cell-mediated immune responses, was recognized about 40 years ago (Stein et al., 1976). CIDS is also triggered by local inflammatory milieu in the brain and affects primarily cellular immunity and lymphocytic function (Czlonkowska et al., 1979). Intracerebroventricular injection of pro-inflammatory cytokine IL-1β activates the SNS and the HPA axis to stimulate rapid ACTH, glucocorticoid and catecholamine release in rats (Katsuura et al., 1988; Rivier et al., 1989) and primates (Sullivan et al., 1997). This leads to impaired cellular immune responses by decreasing the numbers of circulating lymphocytes, suppressing the functions of monocytes, macrophages, natural killer cells and T cells, inhibiting lymphocyte migration and T cell proliferation (Czlonkowska et al., 1979; Sundar et al., 1989; Brown et al., 1991; Cruse et al., 1992; Meert et al., 1995; Sullivan et al., 1997; Woiciechowsky et al., 1999b). Indicative of communication with immune system is also the mixture of increased concentration of pro- (IL-6, IL-8, TNF-α) and anti-inflammatory mediators (IL-10, IL-1 receptor antagonist) of the immune response in the plasma and/or cerebrospinal fluid of those that have undergone neurosurgery (Asadullah et al., 1995) or suffered either subarachnoid haemorrhage (Mathiesen et al., 1993; Mathiesen et al., 1997), severe traumatic brain injury (Bell et al., 1997) or stroke (Fassbender et al., 1994b; Beamer et al., 1995). Increased synthesis of glucocorticoids causes down-regulation of adhesion molecules on blood-brain-barrier, preventing its disruption, and promoting axonal remyelination (Tischner and Reichardt, 2007).

The severity of CNS injury and involvement of brain parenchyma determine the extent of CIDS (Czlonkowska et al., 1979). In stroke, the size of the ischemic lesion correlates with the magnitude of the HPA axis activation that aggravates hypoxic damage to neurons further (Fassbender et al., 1994a). The severity of CIDS, in turn, predicts poorer the neurological outcome and higher likelihood of infections (Czlonkowska et al., 1979; Asadullah et al., 1995; Woiciechowsky et al., 1998). One of the hallmarks of CIDS severity is reduced lymphocytic IFN-γ production which rapidly impairs the microbiocidal activity of macrophages and neutrophils after stroke (Prass et al., 2003). Importantly and in addition to worse neurological status, inflammatory insult, such as systemic lipopolysaccharide administration, predisposes for the development of autoreactivity towards CNS antigens (Becker et al., 2005). Therefore, CIDS is directly linked with neurological outcome after CNS injury such as stroke.

2.5 Pathophysiological basis for autoreactive immune responses after stroke

Stroke is accompanied by damage to blood-brain-barrier and brain parenchyma leading to myelin deliberation and exposure of brain antigens to immune system. Interstitial fluid and solutes carry the brain antigens along basement membranes in capillary and artery walls to cervical lymph nodes (Weller et al., 2009) where T cells accumulate in areas of high neuroantigen presentation (Planas et al., 2012). CNS-antigen specific T cells infiltrate the injured brain and, when recognizing their antigen in correct MHC context, remain in the parenchyma or re-enter in cycles to aggravate inflammation (Hickey et al., 1991).

The antibodies and T cells specific for various CNS-antigens are elevated after stroke. The concentration of circulating neurofilament-specific antibodies increases gradually over six months after stroke and potentially increases the risk for dementia and cognitive deficits (Bornstein et al., 2001). Autoreactive T cells recognizing myelin components like myelin basic protein and proteolipid protein are found in the blood and cerebrospinal fluid of stroke patients at levels resembling those in multiple sclerosis patients (Wang et al., 1992). The CNS-antigen specific T cells can be both, detrimental and beneficial. Immunoreactivity towards myelin basic protein predicts larger infarct volume and poorer neurological outcome whereas immunoreactivities towards microtubule-associated protein 2 and N-methyl D-aspartate receptor subunit NR-2A are related with smaller infarct volumes and improved functional outcome (Planas et al., 2012).

The autoreactive CNS-antigen specific T cells carry mainly regulatory potential (Becker et al., 1997; Becker et al., 2005). Also, regulatory T cells are more resistant to apoptosis induced by elevated glucocorticoid levels like those occurring in CIDS (Tischner and Reichardt, 2007). Mucosal tolerization to myelin basic protein (Becker et al., 1997) or MOG_{35-55} (Frenkel et al., 2003) decreases infarct volume and improves functional outcome one month after stroke through a mechanism involving regulatory T cells. At three months post-stroke, however, these beneficial effects disappear and, instead, the Th1 type autoreactive immune responses are promoted (Gee et al., 2008; Gee et al., 2009). This emphasizes the need for long-term studies following immunomodulation in stroke which, to date, are only a few.

Typically, the autoreactive Th1 and Th17 cells that secrete IFN-γ and IL-17, respectively, are related to worse outcome (Ando et al., 1989; Cua et al., 2003). The effects of CNS-antigen specific T cell subpopulations on stroke outcome, however, appear to be more complex. CNS-

antigen specific Th1 and Th2 cells have been shown to accelerate healing in a model of severe aseptic cryoinjury to brain (Hofstetter et al., 2003) and myelin basic protein specific pro-inflammatory Th1 cells improve neuronal survival after the CNS injury (Kipnis et al., 2002). The polarity of autoreactive T cell responses is therefore likely determined by several factors contributing to the CNS injury.

One of these factors in stroke patients is infection. Inflammatory stimulus promotes detrimental Th1 (Becker et al., 2005; Becker et al., 2011) and Th2 cell responses (Hofstetter et al., 2003) supported by enhanced priming of antigen presenting cells when microbial agents are present in the brain (Hofstetter et al., 2003). This appears not to be antigen specific as lipopolysaccharide administration at the time of stroke directs the development of Th1 type autoreactive responses towards several CNS-antigens, such as myelin basic protein, neuron specific enolase and proteolipid protein. All these are associated with poorer neurological outcome (Zierath et al., 2010). In fact, lipopolysaccharide administration alone is sufficient for triggering EAE disease in mice overexpressing TCR for myelin basic protein (Nogai et al., 2005). In patients, occurrence of pneumonia within 15 days after stroke increases myelin basic protein specific Th1 responses and is linked to poorer neurological outcome at three months (Becker et al., 2011). Post-stroke infections determine thus the polarity of CNS-directed autoreactive responses and long-term neurological outcome.

2.6 Myelin oligodendrocyte glycoprotein and experimental autoimmune encephalomyelitis

MOG is a myelin component, building up 0.01-0.05% of all myelin proteins (Amiguet et al., 1992). It is expressed on the outer surface of myelin sheaths and on mature oligodendrocytes of the CNS. Small amounts of MOG can be found in the lamellae of compacted myelin and the myelin/axon border zone (Brunner et al., 1989; Scolding et al., 1989). In ten-fold lower amounts than in the CNS, MOG is expressed in rodent and primate peripheral nervous system, including in Schwann cells from the sciatic nerve (Pagany et al., 2003).

MOG is highly conserved across the species and comprised of 218 amino acids anchored into the membrane. MOG belongs to the Ig superfamily with extracellular amino-terminus (aa 1-118) forming an immunoglobulin variable region like domain (Pham-Dinh et al., 1993; Kroepfl et al., 1996). It functions likely as an adhesion molecule between individual myelin sheaths. It also participates in the CNS inflammation by activating complement through binding the C1q component, resulting in damage to mature oligodendrocytes (Scolding et al.,

1989; Johns and Bernard, 1999). Its localization on the outmost layer of myelin makes it easily accessible for immune cells.

MOG is an important target antigen in multiple sclerosis and its animal model experimental autoimmune encephalomyelitis (EAE) (Mendel et al., 1995; Hjelmstrom et al., 1998). Multiple sclerosis is the most prevalent neuroinflammatory disease and chronic CNS-directed autoreactivity with the key involvement of ($CD4^+$) Th1 cells (Tischner and Reichardt, 2007). EAE can be induced either by administration of myelin components in adjuvant or by adoptive transfer of encephalitogenic T cells. MOG-induced EAE mimics best the axonal damage and demyelination occurring in multiple sclerosis patients (Tischner and Reichardt, 2007). The whole amino-terminal Ig variable region like domain of MOG is capable of inducing significant MOG-specific T cell responses (Mendel et al., 1995). In addition, a transmembrane/intracellular fragment of the MOG peptide (aa 146-154) induces $CD4^+$ T cell activation and IFN-γ secretion (Weissert et al., 2002). The strongest encephalitogenic potential and highest capability to induce neurological deficits is characteristic to the peptide fragment with aa 35-55 situated within the loop of the Ig Variable region like domain (Mendel et al., 1995). EAE pathology and demyelination induced by $pMOG_{35-55}$ is predominantly mediated by T cells while B cells appear not essential for this (Linington et al., 1993; Genain et al., 1996; Hjelmstrom et al., 1998). T cell response to MOG is MHC class II restricted (Sun et al., 1991) and different T cell subpopulations, such as Th1 and Th17 cells, contribute to characteristic histopathological damage (Jager et al., 2009). In EAE, MOG-specific Th1 cells invade brain (Jager et al., 2009) and spinal cord (Stromnes et al., 2008) but poorly, accumulating preferentially at perivascular cuffs (Linington et al., 1993; Genain et al., 1996; Bettini et al., 2009). Inflammatory infiltrates characteristic to $pMOG_{35-55}$ induced EAE contain primarily activated and memory T cells as well as macrophages (Linington et al., 1993; Genain et al., 1996; Hjelmstrom et al., 1998). It is not clear if the number of IFN-γ secreting MOG-specific T cells is elevated in multiple sclerosis patients (Sun et al., 1991; Van der Aa et al., 2003) but stimulation of these T cells with MOG results in a predominant IFN-γ secreting Th1 phenotype, higher TNF-α production and induction of cytolysis of autologous MOG-pulsed peripheral blood mononuclear cells (Van der Aa et al., 2003).

Identification of the highly encephalitogenic fragment of MOG and the relevance of $CD4^+$ T cells in MOG-induced EAE pathology led to the creation of MOG TCR transgenic mouse (2D2 mouse) in which over 80% of the peripheral $CD4^+$ cells express a functional receptor for $pMOG_{35-55}$ (Bettelli et al., 2003). Under normal conditions, the MOG-specific $CD4^+$ T cells

have restricted access to MOG in the CNS and thus only 4% of 2D2 mice develop EAE spontaneously (Bettelli et al., 2003). To transfer EAE, MOG TCR $CD4^+$ (Th1) cells need to differentiate into effector/memory T cells that express adhesion molecule CD44 (Jager et al., 2009; Williams et al., 2011). Therefore, 2D2 mice provide an interesting, though artificial, model for investigating autoreactive changes after stroke when dysfunctional blood-brain-barrier enables the MOG TCR $CD4^+$ T cells the access to the CNS.

2.7 The role of hyperactivation of sympathetic nervous system and hypothalamic-pituitary-adrenal axis in autoimmune responses

The neuroimmunomodulatory pathways SNS and HPA axis are well known stress systems and stress suppresses the development of clinical and histological signs of EAE (Levine et al., 1962). The importance of adrenal gland and elevated corticosterone levels in relieving the course of EAE disease have been shown (MacPhee et al., 1989) and high doses of methylprednisolone are routinely used for treating acute relapses in multiple sclerosis (Milligan et al., 1987). Majority of the autoimmune diseases, including multiple sclerosis, is associated with Th1/Th2 cell imbalance towards Th1 cells and consequent production of excess IL-12 and TNF-α. HPA axis activation provides resistance via promoting Th2 bias (Webster et al., 2002). Glucocorticoids target preferentially potentially autoreactive lymphocytes like those that are less active and those producing antibodies with lower affinities for the antigen (Sapolsky et al., 2000). Additionally, they interfere directly with the effector functions of encephalitogenic T cells (Tischner and Reichardt, 2007).

SNS stress system elicits comparable effects on autoimmune diseases in that the activation of SNS is protective against EAE and promotes Th2 cell bias. Chemical sympathectomy, on the other hand, potentiates EAE in a rat (Chelmicka-Schorr et al., 1988) even when corticosterone levels remain elevated, suggesting that both stress systems are relevant for EAE suppression. Decreased noradrenaline levels and accompanying up-regulation of cell surface β-AR characterize the pre-clinical phase of EAE (Mackenzie et al., 1989). The key noradrenaline receptor involved in suppressing the chronic/relapsing EAE in Lewis rat is the β(2)-AR (Wiegmann et al., 1995). Activation of the stress and neuroimmunomodulatory pathways SNS and the HPA axis in stroke patients might thus comprise a mechanism to protect the vulnerable brain against CNS-directed autoreactive immune responses.

3. Aims of the study

Within the scope of my doctoral thesis I have focussed on investigating if and how CIDS affects the development of CNS antigen specific autoreactive immune responses. To elucidate that, the following central questions were addressed:

1. Does blocking the SNS axis of CIDS with propranolol aggravate symptoms of CNS-inflammation and functional neurological outcome in a murine model of MCAo? If and how does blocking the SNS axis of CIDS alter the cellular composition and autoreactive potential of ischemic brain infiltrating MNCs and would this effect be limited to the CNS?

2. Does blocking simultaneously the SNS and HPA axes of CIDS with propranolol and mifepristone aggravate symptoms of CNS-inflammation and functional neurological outcome in long-term follow-up after MCAo? If and how does blocking the SNS and HPA axes of CIDS alter the autoreactive potential of ischemic brain infiltrating MNCs and would this effect be limited to the CNS?

3. Would the adoptive transfer of $CD4^+$ T cells from stroked 2D2 mice, that have undergone simultaneous blocking of the SNS and HPA axes of CIDS, to functional B and T cell deficient stroked Rag-1KO mice boost neurological deficits indicative of CNS antigen specific autoreactive immune responses in these mice?

4. Materials and Methods

4.1 Materials

4.1.1 Animals

Strain	Provider
2D2 TCR strain name: C57BL/6-Tg(Tcra2D2, Tcrb2D2)1Kuch/J stock number: 006912	The Jackson Laboratory, Bar Harbor, ME, USA
β2-adrenoreceptor knockout (β2-AR ko)	gift from Dr. Michel Barrot, Institute of Cellular and Integrative Neurosciences, Strasbourg, France
C57Bl/6J	Charles River Laboratories, Sulzfeld, Germany
Rag-1KO strain name: B6.129S7-Rag1tm1Mom/J stock number: 002216	The Jackson Laboratory, Bar Harbor, ME, USA

4.1.2 Cage enrichment

Item	Provider
igloo	Plexx B.V, Elst, The Netherlands
running wheel	Plexx B.V, Elst, The Netherlands
tunnel	Plexx B.V, Elst, The Netherlands

4.1.3 Pharmaceuticals

Item	Provider
2% Xylocain gel	AstraZeneca GmbH, Wedel, Germany
2.5% enrofloxacin	Baytril, Leverkusen, Germany
atipamezolhydrochloride	Orion Pharma, Espoo, Finland
flumazenil	Inresa Arztneimittel GmbH, Freiburg, Germany
isoflurane	Forene, Abbott, Wiesbaden, Germany
ketamine	Deltaselect, Dreieich, Germany
medetomidinhydrochloride	Orion Pharma, Espoo, Finland
midazolam	Roche Pharma AG, Grenzach-Wyhlen, Germany
mifepristone	Sigma-Aldrich, St Louis, MO, USA
S-(-) propranolol	Sigma-Aldrich, St Louis, MO, USA
saline	Fresenius Kabi Deutschland GmbH, Bad Homburg, Germany
xylazine	Bayer Vital, Leverkusen, Germany

4.1.4 Chemicals

Item	Provider
2-methylbutan	Carl Roth GmbH-Co. KG, Karlsruhe, Germany
2-propanol	Carl Roth GmbH & Co. KG, Karlsruhe, Germany
3,3′-diaminobenzidine-tetra-hydrochloride	Sigma-Aldrich, St Louis, MO, USA
3-amino-9-ethylcarbazole	Sigma-Aldrich, St Louis, MO, USA
4',6-diamidino-2-phenylindole (DAPI)	Invitrogen, Life Technologies GmbH, Darmstadt, Germany
10x Citrate buffer pH 6.0	Sigma-Aldrich, St Louis, MO, USA
acetic acid glacial	Merck KGaA, Darmstadt, Germany
agar	Sigma-Aldrich, St Louis, MO, USA
agarose	Carl Roth GmbH & Co. KG, Karlsruhe, Germany
bacto-tryptone	Carl Roth GmbH & Co. KG, Karlsruhe, Germany
bacto-yeast extract	Carl Roth GmbH & Co. KG, Karlsruhe, Germany
boric acid	Merck KGaA, Darmstadt, Germany
bovine serum albumin (BSA) fraction V	Sigma-Aldrich, St Louis, MO, USA
chloroform	Carl Roth GmbH-Co. KG, Karlsruhe, Germany
D(+)-sucrose	Carl Roth GmbH-Co. KG, Karlsruhe, Germany
disodium phosphate	Sigma-Aldrich, St Louis, MO, USA
EDTA	Sigma-Aldrich, St Louis, MO, USA
EDTA buffer pH 8.5	Sigma-Aldrich, St Louis, MO, USA
ethanol (70%, 80%, 96%, absolute)	Rotipuran, Carl Roth GmbH & Co. KG, Karlsruhe, Germany
Green GoTaq Flexi Buffer	Promega Corporation, Madison, WI, USA
hydrogen peroxide	Merck KGaA, Darmstadt, Germany
magnesium chloride	Promega Corporation, Madison, WI, USA
mounting medium DABCO	Sigma-Aldrich, St Louis, MO, USA
nuclease-free distilled water	B. Braun Melsungen AG, Melsungen, Germany
Osteosoft	Merck KGaA, Darmstadt, Germany
paraformaldehyde (PFA)	Sigma-Aldrich, St Louis, MO, USA
Paraplast Plus Tissue Embedding Media	Leica Biosystems, St Louis, USA
Roti-Histol	Carl Roth GmbH & Co. KG, Karlsruhe, Germany
sesame oil	Fluca Analytical, Sigma-Aldrich, St Louis, MO, USA
sodium acetate	Sigma-Aldrich, St Louis, MO, USA
sodium azide	Carl Roth GmbH-Co. KG, Karlsruhe, Germany
sodium chloride	Sigma-Aldrich, St Louis, MO, USA

sodium dihydrogen phosphate monohydrate	Sigma-Aldrich, St Louis, MO, USA
sodium dodecyl sulfate (SDS)	Carl Roth GmbH&Co. KG, Karlsruhe, Germany
tris(hydroxymethyl)aminomethane (Tris)	Carl Roth GmbH-Co. KG, Karlsruhe, Germany
Triton X	LABORAT GmbH, Germany
Vitro-Clud mounting medium	R.Langenbrinck, Emmendingen, Germany
Tween 20	Sigma-Aldrich, St Louis, MO, USA

4.1.5 Cell culture media and supplements

Item	Provider
Ampuwa distilled water	Fresenius Kabi Deutschland GmbH, Bad Homburg, Germany
Easycoll gradient	Biochrom AG, Berlin, Germany
fetal calf serum (FCS Gold)	PAA Laboratories, Pasching, Austria
HL-1 medium	Lonza, Verviers, Belgium
L-alanyl-L-glutamine	Biochrom AG, Berlin, Germany
normal goat serum	BIOZOL Diagnostica Vertrieb GmbH, Germany
penicillin-streptomycin	Biochrom AG, Berlin, Germany
Pharm Lyse lysis buffer	BD Pharmingen, San Diego, CA, USA
phosphate buffered saline (PBS)	PAA Laboratories, Pasching, Austria
Roswell Park Memorial Institute (RPMI) 1640 medium	Biochrom AG, Berlin, Germany
Trypan Blue dye	Biochrom AG, Berlin, Germany

4.1.6 Commercial kits

Item	Provider
$CD4^+$ T cell isolation kit	Miltenyi Biotec, Bergisch Gladbach, Germany
Vectastain Avidin/Biotin Complex (ABC) Elite reagent kit	Vector Laboratories, Burlingame, CA, USA

4.1.7 Enzymes

Item	Provider
GoTaq DNA polymerase	Promega Corporation, Madison, WI, USA
proteinase K	Bioline GmbH, Luckenwalde, Germany
streptavidin-horseradish peroxidase	BD Biosciences, Franklin Lakes, NJ, USA

4.1.8 Polymerase chain reaction primers, nucleotide mix and deoxyribonucleic acid visualization reagents

Item	Provider
2-Log DNA Ladder	New England BioLabs, Ipswich, MA, USA
6x Gel Loading Dye Orange	New England BioLabs, Ipswich, MA, USA
B1 primer (5' TGT GCG TCA CAG CCA GCA TCG AG 3')	Eurofins MWG Operon, Ebersberg, Germany
B2 primer (5' AGC TGC CTT TTG GCC ACC TGG AAG 3')	Eurofins MWG Operon, Ebersberg, Germany
P7 primer (5' ACC GCT TCC TCG TGC TTT ACG GTA 3')	Eurofins MWG Operon, Ebersberg, Germany
polymerase chain reaction (PCR) nucleotide mix	Roche Diagnostics GmbH, Mannheim, Germany
Serva DNA Stain G	SERVA Electrophoresis GmbH, Heidelberg, Germany

4.1.9 Fluorescence-activated cell sorting (FACS) staining panel for phenotyping 2D2 mice

Raised against	Conjugation	Clone	µg per 10^6 cells	Provider
CD4	APC	RM4-5	0.2 µg	BD Pharmingen, Franklin Lakes, NJ, USA
IgG2α κ chain	APC		0.2 µg	BD Pharmingen, Franklin Lakes, NJ, USA
IgG2β κ chain	PE		0.2 µg	BD Pharmingen, Franklin Lakes, NJ, USA
Vβ11 TCR	PE	RR3-15	0.2 µg	BD Pharmingen, Franklin Lakes, NJ, USA

4.1.10 FACS staining panel for spleen

Raised against	Conjugation	Clone	µg per 10^6 cells	Provider
B220/CD45RO	PO	RA3-6B2	0.2 µg	Caltag Medsystems Limited, Buckingham, UK
CD11b	PE-Texas Red	M1/70.15	0.1 µg	Life Technologies, Invitrogen GmbH, Darmstadt, Germany
CD3ε	APC	145-2C11	0.4 µg	eBioscience, San Diego, CA, USA
CD4	Alexa Fluor 700	RM4-5	0.2 µg	BD Pharmingen, Franklin Lakes, NJ, USA
CD45	PE-Cy7	30-F11	0.2 µg	BD Pharmingen, Franklin Lakes, NJ, USA
CD8α	PB	53-6.7	0.2 µg	BD Pharmingen, Franklin Lakes, NJ, USA
Vα3.2	FITC	RR3-16	0.2 µg	BD Pharmingen, Franklin Lakes, NJ, USA
	Biotin	RR3-16	0.2 µg	BD Pharmingen, Franklin Lakes, NJ, USA

4.1.11 FACS staining panel for thymus

Raised against	Conjugation	Clone	µg per 10^6 cells	Provider
CD3ε	PerCP	145-2C11	0.4 µg	BD Pharmingen, Franklin Lakes, NJ, USA
	PE-Cy7	145-2C11	0.4 µg	eBioscience, San Diego, CA, USA
CD4	Alexa Fluor 700	RM4-5	0.2 µg	BD Pharmingen, Franklin Lakes, NJ, USA
CD8α	PB	53-6.7	0.2 µg	BD Pharmingen, Franklin Lakes, NJ, USA
Vα3.2	FITC	RR3-16	0.2 µg	BD Pharmingen, Franklin Lakes, NJ, USA

4.1.12 FACS staining panel for brain

Raised against	Conjugation	Clone	µg per 10^6 cells	Provider
B220/CD45RO	PO	RA3-6B2	0.2 µg	Caltag Medsystems Limited, Buckingham, UK
CD11b	PE-Texas Red	M1/70.15	0.1 µg	Life Technologies, Invitrogen GmbH, Darmstadt, Germany
CD16/CD32		2.4G2	2.5 µg	BD Pharmingen, Franklin Lakes, NJ, USA
CD25	APC-Cy7	PC61	0.4 µg	BD Pharmingen, Franklin Lakes, NJ, USA
CD3ε	APC	145-2C11	0.4 µg	eBioscience, San Diego, CA, USA
CD4	Alexa Fluor 700	RM4-5	0.2 µg	BD Pharmingen, Franklin Lakes, NJ, USA
CD44	PE	IM7	0.2 µg	BD Pharmingen, Franklin Lakes, NJ, USA
CD45	PE-Cy7	30-F11	0.034 µg	BD Pharmingen, Franklin Lakes, NJ, USA
CD8α	FITC	53-6.7	0.2 µg	BD Pharmingen, Franklin Lakes, NJ, USA
Gr1	PB	RB6-8C5	0.2 µg	Caltag Medsystems Limited, Buckingham, UK
Streptavidin	PerCP		0.2 µg	BD Pharmingen, Franklin Lakes, NJ, USA
Vα3.2	Biotin	RR3-16	0.2 µg	BD Pharmingen, Franklin Lakes, NJ, USA

4.1.13 Enzyme-linked immunospot (ELISpot) antibodies and stimulation peptide

Item	Provider
Coating antibodies	
interferon-gamma (IFN-γ)	eBioscience, San Diego, CA, USA
interleukin-4 (IL-4)	BD Biosciences, Franklin Lakes, NJ, USA
interleukin-17 (IL-17)	eBioscience, San Diego, CA, USA
Stimulation antibodies	
CD3Ɛ (clone 145-2C11)	eBioscience, San Diego, CA, USA
CD28 (clone 37.51)	eBioscience, San Diego, CA, USA
Stimulation peptide	
mouse myelin oligodendrocyte glycoprotein (MOG) peptide amino acid (aa) sequence: MEVGWYRSPFSRVVHLYRNGK	Gift from Dr. Rudolf Volkmer, Institute of Medical Immunology, Berlin, Germany
Detection antibodies	
against IFN-γ	eBioscience, San Diego, CA, USA
against IL-4	BD Biosciences, Franklin Lakes, NJ, USA
against IL-17	eBioscience, San Diego, CA, USA

4.1.14 Immunohistochemistry antibodies

Antibody (conjugation)	Clone	Dilution	Provider
Primary antibodies			
mouse anti- β-APP		1/500	Chemicon International Inc; Hampshire, UK
rabbit anti-CD3	SP7	1/500	Thermo scientific, Fremont, CA, USA
rabbit anti-Iba1		1/200	Wako Chemicals GmbH, Germany
rat anti-CD4	RM4-5	1/200	BD Biosciences, Franklin Lakes, NJ, USA
rat anti-Mac3	M3/84	1/100	BD Biosciences, Franklin Lakes, NJ, USA
rat anti-Vα3.2 T cell receptor (biotin)	RR3-16	1/100	BD Pharmingen, Franklin Lakes, NJ, USA
Secondary antibodies			
goat anti-rabbit (Alexa Fluor 568)		1/400	Invitrogen, Life Technologies GmbH, Darmstadt, Germany
goat anti-rat (Alexa Fluor 488)		1/400	Invitrogen, Life Technologies GmbH, Darmstadt, Germany

4.1.15 Laboratory supplies

Item	Provider
0.19±0.01 mm diameter silicon-rubber coated monofilament	Doccol Corporation, MA, USA
10 cm diameter Petri dishes	Greiner Bio-One GmbH, Frickenhausen, Germany
100-µm cell strainer	BD Falcon, Franklin Lakes, NJ, USA
2-ml syringe	BD Discardit, Franklin Lakes, NJ, USA
35 mm diameter Petri dish	Greiner Bio-One GmbH, Frickenhausen, Germany
40-µm cell strainer	BD Falcon, Franklin Lakes, NJ, USA
70-µm cell strainer	BD Falcon, Franklin Lakes, NJ, USA
96-well ELISpot plates	EMD Millipore Corporation, Billerica, MA, USA
digitalthermometer GMH 3210	Greisinger, Regenstauf, Germany
ethylenediaminetetraacetic acid (EDTA) coated tubes	MiniCollect, Greiner Bio-One International AG, Kremsmünster, Austria
Fuchs-Rosenthal chamber	Paul Marienfeld GmbH & Co. KG; Lauda-Königshofen, Germany
homeothermic blanket system	Harvard Apparatus, Holliston, MA, USA
MACS column (LS)	Miltenyi Biotec, Bergisch Gladbach, Germany
magnetic-activated cell sorting (MACS) Separator	Miltenyi Biotec, Bergisch Gladbach, Germany
Microscope slides (SuperFrost Plus)	R. Langenbrinck, Emmendingen, Germany
Pur-Zellin cotton pads	Paul Hartmann AG, Heidenheim, Germany
recovery box	MediHEAT PecoServives Ltd. Brough, Cumbria, UK
RET-3 rectal probe for mice	Physitemp Instruments Inc, Clifton, NJ, USA
sterile scalpel #21	B.Braun AESCULAP, Tuttlingen, Germany
Tissue embedding molds	Polysciences, Eppelheim, Germany

4.1.16 Machines and technical equipment

Item	Provider
^{1}H (300 MHz) mouse head surface radiofrequency (RF) coil	RAPID Biomedical GmbH, Rimpar, Germany
20 mm quadrature volumeresonator radiofrequency (RF) coil	RAPID Biomedical GmbH, Rimpar, Germany
72-mm linear volumeresonator	RAPID Biomedical GmbH, Rimpar, Germany
7T Bruker PharmaScan 70/16 magnet	Bruker, Karlsruhe, Germany
bronchoscope	PolyDiagnost, Pfaffenhofen, Germany
CasyTon cell counter	Casy-Technology, Innovatis AG, Reutlingen, Germany

CatWalk	Noldus Information Technology, Wageningen, the Netherlands
cell incubator	NuAire, Plymouth, MN, USA
centrifuge	Eppendorf Vertrieb Deutschland GmbH, Hamburg, Germany
Dräger Vapor 2000 vaporizer	Drägerwerk AG & Co. KGaA, Lübeck, Germany
FACSCalibur flow cytometer	BD Pharmingen, Franklin Lakes, NJ, USA
fluorescence microscope	Leica DMRE, Nussloch, Germany
GeliX Geldoku iNTAS imager	INTAS Science Imaging Instruments GmbH, Göttingen, Germany
horizontal gel system	PEQLAB Biotechnologie GmbH, Erlangen, Germany
incubator for bacteria	Thermo Scientific GmbH, Vantaa, Finland
laminar flow	NuAire, Plymouth, MN, USA
Leica confocoal microscope	Leica TCS SPE, Nussloch, Germany
LSR II flow cytometer	BD Pharmingen, Franklin Lakes, NJ, USA
Mastercycle personal thermocycler	Eppendorf Vertrieb Deutschland GmbH, Hamburg, Germany
microtome MICROM HM 330	Thermo Scientific, Waldorf, Germany
microwave	Braun, Kronberg, Deutschland
MouseOxTM Small Animal Oximeter	STARR Life Sciences Corporation, March-Hugstetten, Germany
NanoDrop ND2000 spectrophotometer	Thermo Scientific GmbH, Asheville, NC, USA
optical microscope	Leica Microsystems, Wetzlar, Germany
peqpower 300 powersupply	PEQLAB Biotechnologie GmbH, Erlangen, Germany
pH522 pH meter	Wissenschaftlich-Technische Werkstätten GmbH, Weilheim, Germany
sliding microtome	Leica SM2000R, Nussloch, Germany
Small Animal Monitoring and Gaiting System	SA Instruments Inc., NY, USA
Thermomixer 5436 heating block	Eppendorf Vertrieb Deutschland GmbH, Hamburg, Germany

4.1.17 Software

Item	Provider
Bruker Paravision 4.0	Bruker, Karlsruhe, Germany
CasyTon cell counter and analyser system	Casy-Technology, Innovatis AG, Reutlingen, Germany
CatWalk XT	Noldus Information Technology, Wageningen, the Netherlands
FACSDiva 6.1.3	BD Pharmingen, Franklin Lakes, NJ, USA
FlowJo 7.6.5	Tree Star, Ashland, OR, USA
GraphPad Prism	GraphPad, San Diego, CA, USA
ImageJ	ImageJ 1.42q Wayne Rasband, NIH, Bethesda, USA
ImmunoSpot 4.013	Cellular Technology Limited, Bonn, Germany
Intas GDS	INTAS Science Imaging Instruments GmbH, Göttingen, Germany
MATLAB	The Mathworks, Natick, MA, USA
Mayo Clinic Analyze 5.0	Biomedical Imaging Resource, Analyze Direct, Overland Park, KS, USA
Medtronic KeyPoint Portable V5.11	Medtronic Inc., Minneapolis, MN, USA
MouseOx	STARR Life Sciences Corporation, March-Hugstetten, Germany
Small Animal Monitoring and Gaiting System	SA Instruments Inc., NY, USA
SPSS Statistics 21.0 for Windows	IBM Somers, NY, USA
Stereo Investigator software	MBF Bioscience, VT, USA

4.2 Methods

4.2.1 Experiments with live animals

4.2.1.1 Animals and housing

Experiments on mice were conducted in a blinded manner. Animals were randomly assigned between the treatment groups and mice from different groups were housed in a cage together.

Four different mouse strains were used in the present thesis:

- C57Bl/6J, 12 weeks old, male and female.
- 2D2 (transgenic) mice, created on a C57Bl/6J background, [strain name: C57BL/6-Tg(Tcra2D2,Tcrb2D2)1Kuch/J], 9-16 weeks old, male and female. 2D2 mice overexpress

$CD4^+$ T cells with a functional T cell receptor for MOG peptide fragment, amino acid (aa) sequence MEVGWYRSPFSRVVHLYRNGK ($pMOG_{35-55}$) (see 3.1.1).

- Rag-1KO mice, created on a C57Bl/6J background, (strain name: B6.129S7-*Rag1*$^{tm1Mom/J}$), 11-14 weeks old, male and female. Rag-1KO mice lack mature B and T cells (see 3.1.1).
- β2-adrenoreceptor knockout (β2-AR ko) mice, created on a mixed background of C57Bl/6J and Sv129 strain (Prof. Dr. Lutz Hein, University of Freiburg, Freiburg, Germany, personal communication), 19 weeks old and male. The β2-AR ko mice were originally created by the groups of Dr. Brain Kobilka by targeted disruption of β2-AR gene resulting in a production of non-functional receptor segments.

Housing conditions were standardized and involved a 12-hour light/dark cycle (lights on from 7:00 until 19:00), *ad libitum* access to food (standard chow) and water (where indicated, water was replaced with an antibiotic). During the first three post-operative days, mice received daily soft pellet food (standard chow moistened with water/antibiotic). Cages were lined with chip bedding and enrichment was provided through mouse tunnel, igloo and running wheel. The latter was allowed until the middle cerebral artery occlusion (MCAo) surgery.

Animal experiments were approved by local authority (Landesamt für Gesundheit und Soziales, Berlin, Germany) and performed according to the European Community Council Directives 86/609/EEC and German national laws.

4.2.1.2 Pharmacological manipulation of mice

Core pharmacological manipulation of mice in the present thesis involved blocking SNS axis of CIDS with S-(-) propranolol [30 mg/kg or 15 mg/kg, injected intraperitoneally (i.p.) at the time of MCAo and 4 h and 8 h after MCAo; Figure 1A], blocking HPA axis of CIDS with mifepristone [30 mg/kg or 20 mg/kg injected i.p. 24 h and 5 h before MCAo and at reperfusion, i.e. 60 minutes after MCAo; Figure 1A], or combined treatment with propranolol and mifepristone to simultaneously block SNS and HPA axes of CIDS. Mice from vehicle groups received diluents without active substance.

Original injection schemes for blocking SNS and HPA mediated CIDS with 30 mg/kg propranolol and 30 mg/kg mifepristone, respectively, have been described (Prass et al., 2003). Here, I optimized the dosage and preparation of pharmaceutical agents to increase absorption and animal well-being. Injection solution of propranolol was prepared as follows: propranolol was dissolved in saline at 3 mg/ml using regular vortexing. Preparation of mifepristone

injection solution was optimized: mifepristone was carefully dissolved in absolute ethanol at 30 mg/ml on a heated water bath, regularly vortexed, diluted with sesame oil until the end concentration of 3 mg/ml mifepristone was reached, and vortexed until homogenous. Injection solutions were prepared freshly for each injection time point.

Where indicated by experiment design, mice received preventive antibiotic to reduce interdependencies between infection and outcome parameters (Engel and Meisel, 2010; Hetze et al., 2013). A fluoroquinolone enrofloxacin was dissolved in drinking water and provided from 24 h before MCAo until seven days after the surgery (Figure 1C, D, and E). Due to post-operative dehydration, mice received additional 10 mg/kg enrofloxacin i.p. once a day for the first three days after MCAo.

4.2.1.3 Middle cerebral artery occlusion

MCAo was performed according to the standard operating procedures of the laboratory (Dirnagl, 2012). Anaesthesia was induced in mice with 2.5% isoflurane and maintained at 1.0-1.5% isoflurane in oxygen/nitrous oxide mixture (1/2) through a face mask. Body temperature was kept stable at 36.5±0.5 °C with a heating pad. Silicon-rubber coated monofilament with a diameter of 0.19±0.01 mm was inserted into the common carotid artery, advanced along the internal carotid artery to the origin of the middle cerebral artery (MCA), and left there for 60 min until reperfusion. Where indicated, sham surgery was performed for a control. Filament in sham mice was withdrawn immediately after reaching MCA. A drop of 2% xylocain gel was applied onto the wound for pain relief. Neurological deficits were assessed using modified Bederson score (Bederson et al., 1986) where 0 stood for no observable deficit, 1 for forelimb flexion, 2 for circling and forelimb flexion, 3 for complex motoric abnormalities. After surgery, animals were allowed to regain consciousness in a recovery box at 30 °C before being returned to a home cage.

4.2.1.4 Magnetic resonance imaging

4.2.1.4.1 Cerebral blood flow measurements

Flow sensitive alternating inversion recovery magnetic resonance imaging (FAIR-MRI) and diffusion-weighted imaging (DWI) were used to analyze alterations in CBF after MCAo and simultaneous blocking of SNS and HPA axes of CIDS in female 2D2 and C57Bl/6J mice. Measurements were performed immediately after filament insertion and 3 h after MCAo (Figure 1B).

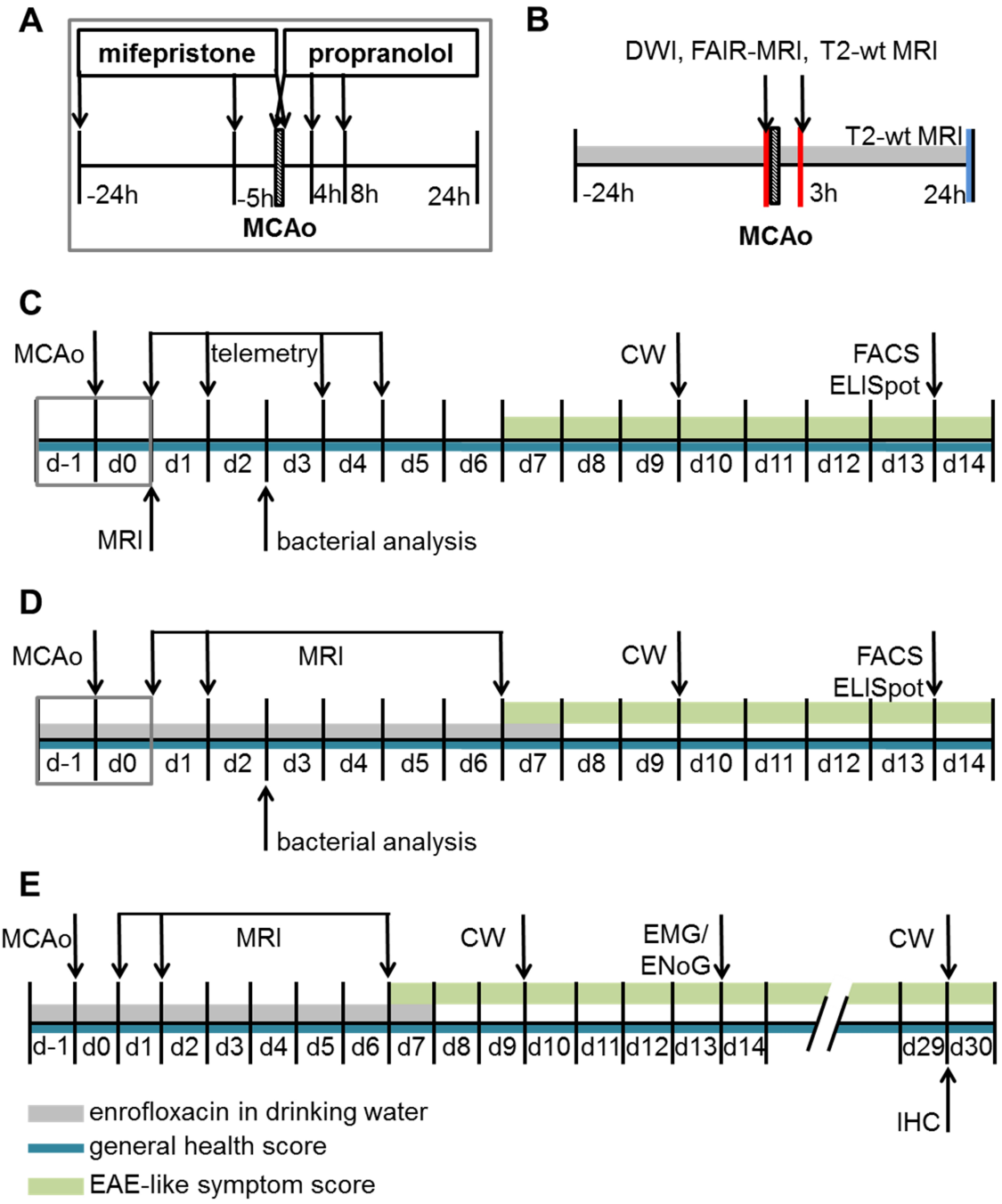

Figure 1. Treatment scheme. Experimental design. ***A***, Injection times of propranolol and mifepristone for blocking SNS and HPA mediated CIDS relative to MCAo time. ***B***, Alterations in CBF were assessed with FAIR-MRI and DWI at the time of MCAo and 3 h after MCAo in experiments where SNS and HPA mediated CIDS was simultaneously blocked. Infarct volume was measured by T2-weighted MRI. ***C***, Time flow of an experiment where only the SNS axis of CIDS was blocked. ***D***, Time flow of a dual CIDS block experiment (SNS&HPA) with focus on cellular immunological outcome. ***E***, Time flow of a dual CIDS block experiment with a focus on long-term functional neurological outcome. Pre-MCAo baseline measurements (CW and EMG/ENoG) are not shown. CW, CatWalk; DWI, diffusion-weighted imaging; EAE, experimental autoimmune encephalomyelitis; ELISpot, enzyme-linked immunospot; EMG/ENoG, electromyography/electroneurography; FACS, fluorescence-activated cell sorting; FAIR-MRI, flow sensitive alternating inversion recovery magnetic resonance imaging; IHC, immunohistochemistry; MCAo, middle cerebral artery occlusion; MRI, magnetic resonance imaging; T2-wt MRI, T2-weighted magnetic resonance imaging.

For the measurement immediately after filament insertion, post-operative anaesthesia was maintained at 0.6-1.0% isoflurane in oxygen/nitrous oxide mixture (1/2) regulated through a vaporizer and delivered through a face mask. For the measurement 3 h after MCAo, anaesthesia was induced with 2.0% isoflurane and maintained as described. Body temperature was kept stable at 36.5±0.5 °C with a heating pad. Vital signs, such as rectal temperature, electrocardiogram and respiration rate were monitored with Small Animal Monitoring and Gating System. Head of the mouse was fixed in the magnet bore using ^{1}H (300 MHz) mouse head surface radiofrequency (RF) coil. Since the latter was a receive-only coil, a 72 mm linear volume resonator was used for transmission. FAIR-MRI and DWI were performed on a 7 Tesla Bruker PharmaScan 70/16 magnet using Bruker Paravision 4.0 software as described in detail elsewhere (Leithner et al., 2008). Pilot images were collected with a Fast Low Angle Shot (FLASH) sequence [time to echo (TE) 5 ms, time of repetition (TR) 307.7 ms, field of view (FOV) 25 mm, total of 27 slices with a thickness of 600 µm in three views, 128x128 in plane resolution] to select the area between the olfactory bulb and cerebellum. FAIR-MRI images were collected with a spin echo echo planar imaging (EPI; TE 42.55 ms, TR 9122.7 ms, FOV 20 mm, imaging slice thickness 2 mm, 64x64 in plane resolution, inversion slab thickness 6 mm, inversion recovery time 15.55 ms, increment of inversion recovery time 800 ms). Three slices with 2-mm interval were selected. For each slice two series of 11 images (alternating slice selective inversion and slice non-selective inversion) were collected (Leithner et al., 2010). FAIR-MRI was immediately followed by DWI using spin echo EPI sequence (TE 40.93 ms, TR 3000 ms, FOV 20 mm, imaging slice thickness and inter-slice distance 1 mm, 128x128 in plane resolution, total of 10 slices and 6 averages).

Hemispheric CBF was calculated from FAIR-MRI data as described elsewhere (Leithner et al., 2008; Royl et al., 2009) using custom script routines based on MATLAB. DWI images were used for calculating apparent diffusion coefficient (ADC) maps to outline the lesions and calculate lesion volumes through multiplication with voxel size.

4.2.1.4.2 Infarct volume determination

All the mice that were subjected to MCAo, underwent T2-weighted MRI for ischemic lesion quantification. MRI was performed on one or several of the following time points: 24 h, 48 h and seven days after MCAo (Figure 1C, D and E).

Anaesthesia was induced with 2.0% isoflurane and maintained at 1.0-1.5% isoflurane in oxygen/nitrous oxide mixture (1/2) regulated through a vaporizer and delivered through a face mask. Animal vital signs were monitored as described above. Head of a mouse was fixed in

the magnet bore. Measurements were performed on a 7 T Bruker PharmaScan 70/16 magnet with a 20 mm quadrature volume resonator RF coil and using Bruker Paravision 4.0 software. Pilot scan was run with a multi-slice multi-echo (MSME) sequence (TE 11 ms, TR 200 ms, FOV 500 mm, three slices with a thickness of 2000 µm, 128x128 in plane resolution). T2-weighted images were collected with Rapid Acquisition with Relaxation Enhancement (RARE) sequence (TE 36 ms, TR 4200 ms, FOV 28 mm, 20 slices with a thickness of 500 µm and inter-slice distance 500 µm, 256x256 in plane resolution). Axial slices covered the distance between the olfactory bulb and the cerebellum.

The format of acquired images was converted using ImageJ software. Lesions were outlined and infarct volumes were calculated using Mayo Clinic Analyze software version 5.0. Infarct volumes were corrected for edema by dividing the difference between hemispheric volumes (excluding the lesion) with the volume of ipsilateral hemisphere and converting into percent.

4.2.1.5 Heart rate measurements

Heart rate was measured in naïve 2D2 mice and in 2D2 mice where simultaneously the SNS and HPA axes of CIDS or solely SNS axis of CIDS was blocked around the time of MCAo. Measurements were performed between days one and five after MCAo at the same day-time in non-anaesthesized mice using MouseOx Small Animal Oximeter and attached software according to manufacturer's instructions.

4.2.1.6 Bronchoalveolar lavage

Bronchoalveolar lavage (BAL) fluid was collected for microbiological analysis from mice three days after MCAo. This is the optimal time point for identifying mice with pulmonary infections based on bacterial load in the BAL fluid and minimizing mortality bias (Prass et al., 2003). Before BAL, mice were anaesthetized with an i.p. injection of 5.0 mg/kg midazolam and 0.5 mg/kg medetomidin dissolved in saline. Mouse was fixed on a vertical board under 75°. Bronchi were reached using a camera-guided bronchoscope and illumination with fiber optic (Bettini et al., 2009). BAL fluid was collected by flushing with 300 µl saline using a 2-ml syringe. Anesthesia was antagonized with a subcutaneous (s.c.) injection of 0.5 mg/kg flumazenil and 2.5 mg/kg atipamezolhydrochloride dissolved in saline.

4.2.1.7 General health score

Animal well-being was assessed daily in a detailed manner for the duration of the experiment (Figure 1C, D and E). For the exact scoring criteria see (Hetze et al., 2013). Briefly, assessed

were behavior, posture, skin/fur, eyes, breathing, gastrointestinal tract, rectal temperature and body weight. Each of these parameters was evaluated with a score from 0 (no deficits) to 2 (major deficits).

4.2.1.8 Modified experimental autoimmune encephalomyelitis score

Mice were observed to develop symptoms of a disease reminiscent to EAE. Development of autoreactive deficits in mice was assessed daily with modified EAE score starting with day seven after MCAo (Figure 1C, D and E). Neurological scoring criteria (modified from (Adelmann et al., 1995) were following: 0, no disease; 0.5, partial tail paralysis; 1.0, complete tail paralysis; 1.5, limb weakness without tail paralysis; 2.0, limb weakness with tail paralysis; 2.5, partial limb and tail paralysis; 3.0, complete limb paralysis; 3.5, paraplegia; 4.0, quadriplegia.

The procedure of EAE scoring included monitoring of gait and walking behavior on a smooth surface. Mice were then transferred onto a metal grid to detect foot faults while walking. Tail tone was examined by grabbing the mouse by the scruff of the neck and observing spontaneous tail raise reflex.

4.2.1.9 CatWalk gait analysis

To detect subtle stroke-induced deficits in mice over a longer period after MCAo, gait of the mice was assessed using CatWalk gait analysis method as described in detail elsewhere (Hetze et al., 2012). Measurements were performed before MCAo (baseline values), 10 days and, where indicated, 30 days after MCAo.

Briefly, analysis was carried out in a silent and dim (<20 lux of illumination) room to maximize signal-to-noise ratio. Walkway consisted of a dark tunnel on a 1.3 m long glass plate illuminated by a fluorescent light. Mouse was placed into one end of the walkway and its home cage served as a bait in the opposite end. During the run, paw contact with the glass plate induced a change in the refractive index of light: it scattered at the paw and illuminated the area. Illuminated paw prints were captured by a camera below. Captured images were processed, runs automatically classified and manually quality-controlled by CatWalk XT software.

Prior to the acquisition of pre-MCAo baseline values, mice were trained on CatWalk system in three sessions (three runs each) on three consecutive days for familiarization. Duration of compliant runs was 0.5-5.0 s, speed variation less than 60% and interruptions were not

accepted. Stroke-sensitive individual paw and gait parameters were determined (Hetze et al., 2012) and used for gait assessment in the present thesis. These parameters included individual paw characteristics, positioning of footprints, and gait coordination (spatial, kinetic and comparative statistics of gait). Swing speed was normalized to run speed.

4.2.1.10 Electrophysiology

Electrophysiology [electromyography/electroneurography (EMG/ENoG)] was performed in 2D2 and Rag-1KO mice in experiments investigating the role for simultaneously blocking SNS and HPA axes of CIDS in post-stroke autoreactivity. Sciatic nerve was stimulated and latencies to F-wave and F-wave chronodispersion [difference between the shortest and longest F-wave latency within one animal (Fisher, 2007)] measured before MCAo (baseline) and 14 days after MCAo.

Anaesthesia was induced with 2.5% isoflurane and maintained at 0.8-1.2% isoflurane in oxygen/nitrous oxide mixture (1/2) regulated through a vaporizer and delivered through a face mask. Body temperature was kept stable at 36.5±0.5 °C with a heating pad. Two pairs of needle electrodes were used: a) reference and stimulation; and b) reference and recording electrodes. Electrical stimulus was applied at the sciatic notch. Reference electrode was inserted s.c. into peritoneal cavity, recording electrode into the muscle innervated by sciatic nerve and reference electrode into lower extremity with minimal activity. Surface electrode served as ground to connect the fields of stimulation and recording and to increase signal-to-noise ratio. It was kept moist with saline throughout the procedure to minimize artefacts. Acquisition and stimulation parameters were controlled with Medtronic KeyPoint Portable software V5.11. Single stimulus lasted 0.2 s at 1.2 mA.

4.2.1.11 Intravenous transfer of $CD4^+$ T cells

Anaesthesia was induced in recipient Rag-1KO mice 6 h after MCAo with 2.0% isoflurane and maintained at 0.8-1.0% of isoflurane in oxygen/nitrous oxide mixture (1/2) regulated through a vaporizer and delivered through a face mask. Tail vein was visualized through dilation via warming with infrared lamp. Two million untouched $CD4^+$ T cells [$1x10^6$ cells per 100 µl phosphate buffered saline (PBS)] were injected intravenously (i.v.) per recipient. Bleeding from the tail vein was stopped using cotton pads and pressure. Mice were returned to home cage only after the bleeding from vein had completely stopped.

4.2.1.12 Perfusion and tissue harvesting

At the end of the study (Figure 1C, D and E) mice were deeply anaesthesized with an i.p. injection of 150 mg/kg ketamine and 15 mg/kg xylazine. Mice were fastened on a board under 45° and the fur was cleaned with 70% ethanol before incision. Spleen, lymph nodes (cervical, mesenteric, inguinal and lumbar) and, where indicated, lungs and blood (under sterile conditions from *vena cava*) were collected and animal was transcardially perfused with 20 ml ice cold saline at 80 cm water height. Brains were removed from the skull and placed into Roswell Park Memorial Institute (RPMI) 1640 medium, supplemented with 10% fetal calf serum (FCS), 50 U/ml penicillin, 50 µg/ml streptomycin and 2 mM L-alanyl-L-glutamine (referred to as complete RPMI1640 medium). Tissue processing followed immediately.

In experiments designed for the assessment of long-term functional neurological outcome (Figure 1E), perfusion with saline was followed by perfusion with 20 ml ice cold 4% paraformaldehyde (PFA) in 0.1 M Sörensen buffer (consisting of 80 mM disodium phosphate, 20 mM sodium dihydrogen phosphate monohydrate in distilled water; pH 7.4) per mouse. Brains were removed, post-fixed for 24 h in 4% PFA, incubated for five days in 30% D+(-) sucrose in PBS for cryoprotection and snap-frozen with 2-methylbutan. Vertebral columns were removed, post-fixed for 24 h in 4% PFA and transferred into 0.1 M PBS. Decalcification of bone structures was achieved by 24 h incubation with Osteosoft. Tissue was preserved in 0.1 M PBS until further processing.

4.2.1.13 Microbiological analysis of lungs, bronchoalveolar lavage and blood

The lungs, BAL and blood of 2D2 and C57Bl/6J mice were collected under sterile conditions three days after MCAo for microbiological analysis. Lungs were homogenized mechanically and 100 µl of tissue homogenate, BAL or blood were serially diluted in liquid Lysogeny Broth (LB) medium (1% bacto-tryptone, 0.5% bacto-yeast extract and 1% sodium chloride in distilled water; pH was set to 7.0 using a pH meter) and plated under sterile laminar flow onto 10-cm diameter Petri dishes pre-filled with polymerized LB agar (liquid LB medium supplemented with 15% agar) and incubated at 37 °C, 5% carbon dioxide, 20% oxygen in nitrogen gas in an incubator for 24 h. Bacterial colonies were quantified and used for calculating colony forming units (CFUs). Data are presented as LOG10 (CFU/ml). Criteria for infection were met when LOG10 of CFU/ml exceeded 5.

4.2.2 Cell culture, molecular and immunological methods

All procedures with living cells except from fluorescence-activated cell sorting (FACS) were performed under sterile conditions using sterile laminar flow.

4.2.2.1 Cell isolation from brain, thymus, spleen and lymph nodes

The brains were transferred from complete RPMI1640 medium onto a 35 mm diameter Petri dish where the cerebellum was removed and hemispheres separated using a sterile scalpel. Singe cell suspension was achieved by forcing the brain tissue through a 70 µm pore size cell strainer into complete RPMI1640 medium using a 2-ml syringe stamp. Procedure was repeated until the strainer appeared clear. Cells were washed with complete RPMI1640 medium by centrifugation at 250 g at room temperature (RT) for 10 minutes. Easycoll gradient dilutions (35% and 70%) were prepared in complete RPMI1640 medium. Cell pellet was resuspended in 6 ml of 35% Easycoll gradient and pipetted, using gravity alone, on a top of the 4 ml of 70% Easycoll gradient. Gradients were centrifuged at 900 g at RT for 30 minutes, without acceleration and brake. Mononuclear cells (MNCs) were isolated from the interface of 35% and 70% Easycoll gradient. After washing with complete RPMI1640 medium, a fraction of MNCs was stained with Trypan Blue dye, pipetted into Fuchs-Rosenthal chamber (depth 0.200 mm; area 0.0625 mm^2) and quantified under optical microscope.

Single cell suspension from thymus was achieved by forcing the tissue through a 70-µm pore size cell strainer with a 2-ml syringe stamp until the strainer appeared clear. Cells were washed with complete RPMI1640 medium and a fraction of thymocytes was used for quantification on a Trypan Blue method (see above).

Spleen and lymph node tissue was in a first step forced through a 100-µm pore size cell strainer with a 2-ml syringe stamp and washed with complete RPMI1640 medium [or a magnetic-activated cell sorting (MACS) buffer containing 2% FCS in sterile PBS]. For MACS assay, erythrocytes in spleen were lysed with a 30-second incubation with distilled water. In a second step, splenocytes/lymphocytes were pipetted through a 40-µm cell strainer and washed with complete RPMI1640 medium (or MACS buffer). For quantification of splenocytes a program was installed on CasyTon cell counter and analyzer system. Lymphocytes were quantified on a Trypan Blue method (see above).

4.2.2.2 Untouched $CD4^+$ T cell magnetic-activated cell sorting (MACS)

$CD4^+$ T cells were sorted from the spleens and lymph nodes of naïve and treated (simultaneous blocking of SNS and HPA axes of CIDS or vehicle) 2D2 donor mice seven days after MCAo before transfer to Rag-1KO recipient mice (receiving no treatment but preventive enrofloxacin) 6 h after MCAo.

Single cell suspensions from spleens and lymph nodes (cervical, mesenteric, inguinal and lumbar) were prepared and cells were quantified as described above. Untouched $CD4^+$ T cell sorting was performed with $CD4^+$ T cell isolation kit for mice and MACS separator together with LS columns according to manufacturer's instructions. Non-$CD4^+$ T cells (cytotoxic T cells, B cells, natural killer cells, dendritic cells, macrophages, granulocytes, remaining erythrocytes) were labelled with biotin-conjugated antibody cocktail consisting of CD8α (Ly-2), CD45R (B220), DX5, CD11b (Mac-1) and Ter-119 antibodies. Biotin was detected with anti-biotin microbeads carrying a magnetic tag. LS columns were rinsed with 3 ml MACS buffer on a MACS separator before cell suspension was allowed to run through the column. After MACS was completed, the columns were washed four times with 3 ml MACS buffer to increase the number of untouched $CD4^+$ T cells in MACS product. Magnetically labelled non-$CD4^+$ T cells were retained in the column and eluted outside of the magnetic field into another container. The percentage of untouched $CD4^+$ cells was verified with FACS.

4.2.2.3 Fluorescence-activated cell sorting (FACS)

4.2.2.3.1 Phenotyping 2D2 mice

2D2 mice from the breeding were phenotyped using FACS for use in the present thesis. The blood from 2D2 mice was collected into ethylenediaminetetraacetic acid (EDTA) coated tubes and analyzed within 24 h. Erythrocytes were lysed with Pharm Lyse lysis buffer according to manufacturer's instructions. Leukocytes were separated with centrifugation at 252 g at RT for 6 min. Cells were washed with FACS buffer (2% FCS and 15.4 mM sodium azide in PBS) and their surfaces were stained with a cocktail of monoclonal antibodies: allophycocyanin (APC) conjugated anti-CD4 to detect helper T cells and phycoerythrin (PE) conjugated anti-Vβ11 TCR for 2D2 TCR (see 4.1.9.). Staining was performed by incubating the samples light-protected on ice for 30 minutes. Isotype controls were stained with APC-rat immunoglobulin (Ig) G2α κ chain for CD4-specific staining and PE-rat IgG2β κ chain for Vβ11 TCR-specific staining. Samples were washed with FACS buffer to remove unbound antibodies, acquired on FACSCalibur flow cytometer and analyzed with FlowJo software

version 7.6.5. Lymphocyte population was gated by comparing cell size against granularity using forward light scatter (FSC) channel and side light scatter (SSC) channel and Vβ11 expressing $CD4^+$ helper T cells were identified. Animal was considered transgenic if the number of $CD4^+$ T cells carrying MOG TCR (based on transgenity of the TCR variable region Vβ11) was above 80%.

4.2.2.3.2 FACS for immunological comparison of treatment groups

Brain MNCs, splenocytes and thymocytes were resuspended in FACS buffer and centrifuged at 252 g at 4 °C for 6 min. Unspecific binding of immunoglobulin G to FcγII/III receptors [present on phagocytes, B cells, natural killer and follicular dendritic cells (Murphy, 2008)] was blocked by incubation with anti-CD16/32 antibody at 4 °C for 15 minutes. Cellular surfaces were stained with a cocktail of monoclonal antibodies (for staining panels see 4.1.10 for spleen, 4.1.11 for thymus and 4.1.12 for brain). Samples were incubated with antibody-cocktails light-protected on ice for 30 min. Unbound antibodies were removed by washing with FACS buffer and, where indicated, cell surfaces were stained in a second step for the detection of Vα3.2 receptor with biotin-binding PerCP-conjugated streptavidin antibody. Samples were measured immediately on a LSR II flow cytometer using FACSDiva software version 6.1.3. Data were analyzed with FlowJo software 7.6.5.

Gating strategy for brain is shown (Figure 2). In the analysis of splenocytes and thymocytes cell aggregates (doublets and triplets) were excluded by comparing FSC-area against FSC-height, cell fragments and dead cells by comparing FSC against SSC. This was followed by analysis of specific cell populations based on fluorescence signal from cell surface marker conjugates.

4.2.2.3.3 FACS analysis of $CD4^+$ cell purity in MACS product

The purity of untouched $CD4^+$ T cells in MACS product was analyzed with FACS following the same basic procedure. Cells were stained with APC-conjugated anti-CD4 monoclonal antibody at concentration 0.2 µg per 10^6 cells. Samples were measured on FACSCalibur flow cytometer and analyzed with FlowJo software version 7.6.5.

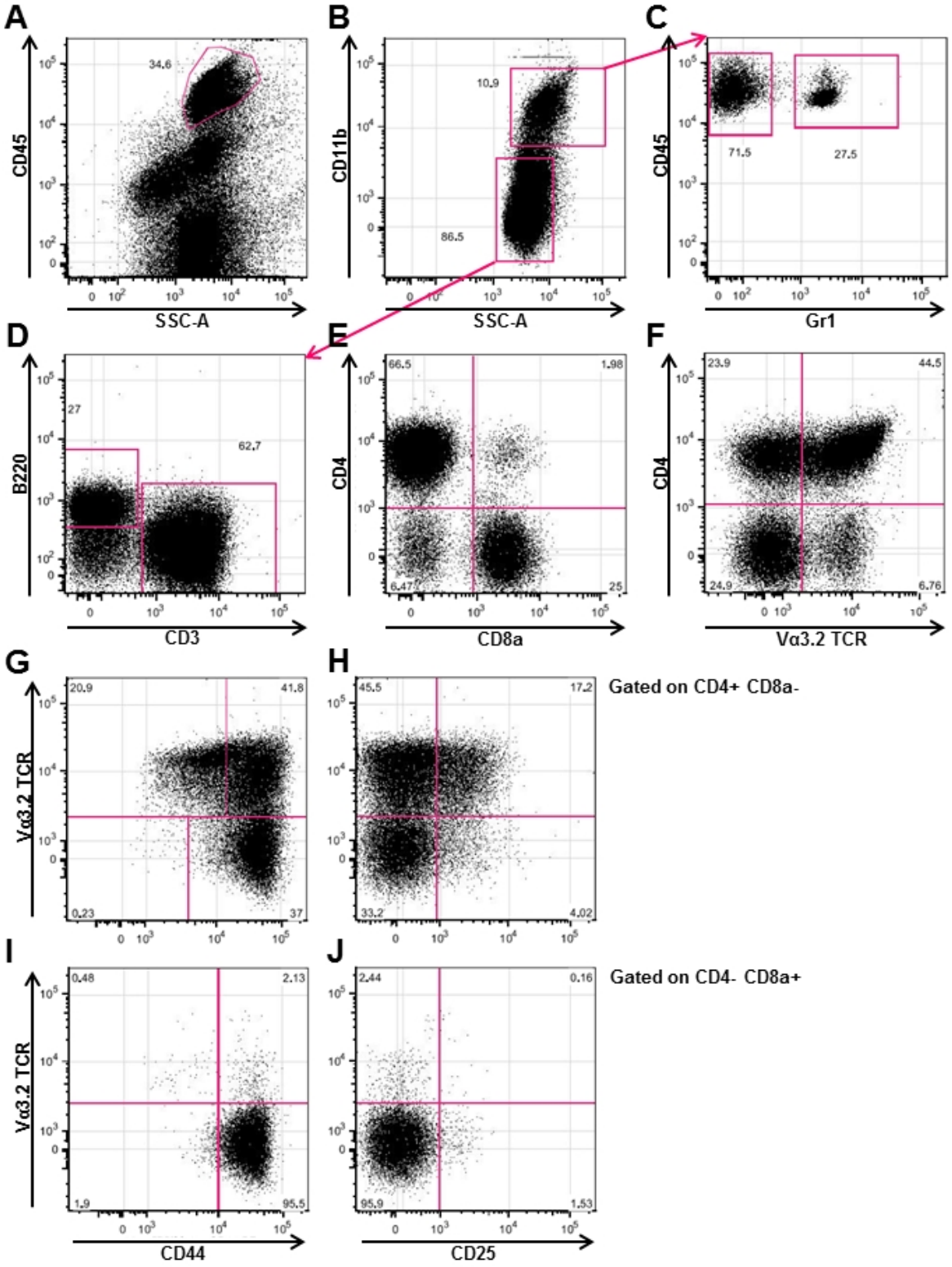

Figure 2. FACS gating strategy for the analysis of brain samples. CD45$^+$ bright leukocytes were selected (***A***) and divided into CD11b$^+$ bright monocytes/macrophages and CD11b$^-$ lymphocytes (***B***). CD11b$^+$ cell population was further analyzed for Gr1 expression to differentiate between Gr1$^-$ monocytes/macrophages and Gr1$^+$ granulocytes (***C***). CD11b$^-$ lymphocytes were splitted into B220$^+$ B cells and CD3$^+$ T cells (***D***). Since T cells were of particular interest in the present thesis, CD3$^+$ T cells were further divided between CD4$^+$ helper T cells and CD8α$^+$ effector T cells (***E***). MOG TCR expressing Vα3.2$^+$ CD4$^+$ T cells were identified (***F***) and the numbers of antigen-experienced (CD44$^+$) and regulatory (CD25$^+$) CD4$^+$ (***G*** and ***H***) and CD8$^+$ (***I*** and ***J***) transgenic Vα3.2$^+$ T cells quantified.

4.2.2.4 Enzyme-linked immunospot assay (ELISpot)

ELISpot was performed from brain MNCs and splenocytes of 2D2 mice 14 days after MCAo to assess the cytokine-profile of CNS-antigen specific self-reactive cells. Resulting from a need for high numbers of brain MNCs for this assay, brain MNCs from mice belonging to one group were pooled.

ELISpot plates (96-welled plates with hydrophobic polyvinyl difluoride membrane, 0.45 µm pore size) were coated with 7.5 µg/ml of a) interferon-γ (IFN-γ); b) interleukin-4 (IL-4); or c) interleukin-17 (IL-17) specific capture antibody in sterile PBS and incubated for 24 h at +4 °C light-protected. Plates were washed four times with sterile PBS (200 µl per well) and blocked with 1% bovine serum albumin (BSA) fraction V in PBS (100 µl per well) for 2 h at RT. Blocking solution was removed and wells were filled with 100 µl of stimulation medium consisting of a) HL-1 medium (specific for differentiated lymphoid cells) enriched with 2 mM L-alanyl-L-glutamine, 50 U/ml penicillin and 50 µg/ml streptomycin (referred to as complete HL-1 medium), with 2 µg/ml CD3Ɛ and 0.2 µg/ml CD28; duplicates per sample (positive control); b) complete HL-1 medium with 0.2 µg/ml CD28 and 40 µg/ml $pMOG_{35-55}$; triplicates per sample (peptide stimulation); and c) complete HL-1 medium with 0.2 µg/ml CD28; triplicates per sample (negative control). (Due to low overall numbers of brain MNCs, in ELISpot from brain MNCs only one positive and negative control per cytokine was used per experiment.) MNCs were added at $1.75x10^5$ together with $1x10^6$ naïve C57Bl/6J splenocytes in 100 µl of complete HL-1 medium. In spleen ELISpot, splenocytes were added at $3.75x10^5$ (IFN-γ) or $1x10^6$ (IL-4 and IL-17) in 100 µl of complete HL-1 medium per well. Cells were incubated at 37 °C, 5% CO_2 for 24 h (IFN-γ plates) or 48 h (IL-4 and IL-17 plates). Plates were washed four times with sterile PBS and four times with 0.05% Tween 20 in sterile PBS (each wash with 200 µl/well) before incubation with a biotinylated secondary antibody raised against IFN-γ (1.5 µg/ml), IL-4 (3 µg/ml) or IL-17 (3 µg/ml) in a solution of 0.05% Tween 20 and 1% BSA V in PBS at 4 °C overnight. Plates were washed four times with 0.05% Tween 20 in PBS (200 µl/well). To visualize secondary antibody binding, enzyme streptavidin-horseradish peroxidase was diluted at 2 µg/ml in 0.05% Tween 20 and 1% BSA V in PBS and added to wells (100 µl/well). Plates were incubated at RT for 2 h followed by washing four times with PBS (200 µl/well). Thereafter wells were filled with 200 µl of a solution containing 50 mM 3-amino-9-ethylcarbazole (enzyme substrate) in 30 mM acetic acid glacial, 117 mM sodium acetate and 5 µM hydrogen peroxide. Reaction was stopped

with tap water. Plates were air-dried. Formed spots were quantified automatically and quality-controlled manually using ImmunoSpot software 4.013.

4.2.2.5 Histology and immunohistochemistry

4.2.2.5.1 Immunohistochemistry from free-floating brain sections

Frozen brains from Rag-1KO mice 30 days after MCAo were cut into 30 µm-thick sections on a sliding microtome. Free-floating sections were washed with Tris-buffered saline (TBS), consisting of 50 mM Tris and 150 mM sodium chloride in distilled water (pH 7.5). This was followed by incubation with 10% normal goat serum and 0.3% Triton X in TBS at RT for 1 h to block unspecific antibody binding. Sections were stained with rat anti-CD4 (for $CD4^+$ T cells) and rabbit anti-Iba-1 (for microglia/macrophages) primary antibodies at 4 °C overnight. Then, sections were washed and stained with Alexa Fluor 488 conjugated goat anti-rat and Alexa Fluor 568 conjugated goat anti-rabbit secondary antibodies at RT for 2 h. All antibodies were diluted in 1% normal goat serum and 0.3% Triton X in TBS. Nuclei were counterstained with 4',6-diamidino-2-phenylindole (DAPI). Sections were mounted on gelatinized glass slides and coverslipped using anti-fading mounting medium. Microphotographs were taken with Leica confocal microscope. Stereological analysis was performed using fluorescence microscope and Stereo Investigator software. Hemispheres were outlined and positively stained cells in ipsilateral hemisphere were counted using Meander scan. Resident microglia were distinguished from activated microglia/macrophages based on location and morphology. Data are presented as number of immunopositive cells per mm^2 ipsilateral hemisphere.

4.2.2.5.2 Immunohistochemistry from paraffin-embedded tissue

Vertebral columns containing spinal nerve roots of 2D2 and Rag-1KO mice from 30 days after MCAo were dehydrated through ascending series of ethanol baths. Tissue samples were incubated with 70% ethanol for 4 h, with 80% ethanol for an overnight, with 96% ethanol twice and with absolute ethanol three times, 1 h each. Subsequently, samples were incubated with a mixture of absolute ethanol and chloroform (with ratio 2:1, ratio 1:1 and ratio 1:2, 20 minutes each). This was followed by incubation with chloroform for 1 h, then 40 minutes and finally 20 minutes before transfer to tissue embedding molds and paraffin incubation at 60 °C. After 1 h, paraffin around tissue blocks was renewed and incubation was continued for an overnight. Tissue blocks were cooled at RT for another overnight.

Paraffin-embedded tissue blocks containing vertebral columns and nerve roots were cut into 2-3 µm-thick sections on a microtome and collected onto microscope glass slides. Sections

were deparaffinized and rehydrated. For this, slides were incubated three times in Roti-Histol for 5 minutes each, and in descending series of ethanol baths: 100%, 96%, 80% and 70% each lasting for 5 minutes. After the last ethanol incubation, slides were transferred into PBS. Immunohistochemistry was performed in adjacent serial sections. Slides were cooked for 1 h in citrate (pH 6.0) or, for Vα3.2 staining, with EDTA buffer (pH 8.5) for antigen retrieval, cooled and washed with PBS. Thereafter, slides were incubated overnight with rat anti-Mac3 (for macrophages), rabbit anti-CD3 (for T cells) or mouse anti-beta-amyloid precursor protein (β-APP, for axonal injury) primary antibodies. Biotin-conjugated rat anti-Vα3.2 TCR antibody was used for detecting MOG TCR immunoreactivity. All antibody dilutions were prepared in 10% FCS in PBS. Bound primary antibody was visualized with biotin–avidin technique using avidin/biotin complex kit according to manufacturer's instructions and 1.4 mM 3,3′-diaminobenzidine-tetra-hydrochloride (0.5 mg/ml) with 6.6 µM hydrogen peroxide as chromogen. Control sections were stained in the absence of primary antibody. Slides were dehydrated through ascending series of ethanol baths, immersed in Roti-Histol and coverslipped using Vitro-Clud mounting medium. All available nerve root cross sections were examined and their cumulative areas were quantified under light microscope using an optical grid. All $Mac3^+$, $CD3^+$ and $V\alpha3.2^+$ cells and APP^+ axons were counted. Data are presented as numbers of immunopositive structures per mm^2 nerve root.

4.2.2.6 Genotyping β2-Adrenoreceptor knockout mice

4.2.2.6.1 Deoxyribonucleic acid (DNA) isolation and DNA concentration measurement

To identify β2-AR knockout (ko) mice from the litter for the use in this thesis, DNA was analyzed from tail tip samples that were stored at -20 °C. Lysis buffer was prepared from 100 mM tris(hydroxymethyl)aminomethane (Tris), 5 mM EDTA, 200 mM sodium chloride, 0.2% sodium dodecyl sulfate (SDS) and 2% proteinase K (added immediately before use) diluted with distilled water and 510 µl of it was pipetted on a tail tip. Samples were incubated on a heating block at 55 °C overnight, vortexed briefly and centrifuged at 20000 g at RT for 10 minutes. Supernatants containing DNA were mixed through inversion with an equal volume of 2-propanol and centrifuged at 20000 g at RT for 10 minutes. Precipitated DNA was washed with 250 µl of 70% ethanol, centrifuged at 20000 g at RT for 2 minutes and dissolved in 200 µl of buffer containing 10 mM Tris and 1mM EDTA in distilled water. Samples were incubated on a heating block at 55 °C for 45 minutes and mixed by inversion at 15-minute intervals. DNA was precipitated with 20 µl 5 M sodium chloride and 600 µl absolute ethanol,

washed with 250 µl of 70% ethanol and dissolved in 100 µl of buffer containing 10 mM Tris and 0.1 mM EDTA in distilled water. Samples were incubated on a heating block at 55 °C for another 45 minutes and mixed by inversion at 15-minute intervals. DNA samples were vortexed and 1 µl of sample was used for DNA concentration and sample purity measurements on NanoDrop ND2000 spectrophotometer.

4.2.2.6.2 Polymerase chain reaction

The volume of Polymerase chain reaction (PCR) mixture for one reaction was 25 µl and it contained dissolved in nuclease-free distilled water: 25 ng of DNA (10 ng/µl), 2.1 mM magnesium chloride, 210 nM PCR nucleotide mix [desoxyadenosintriphosphat (dATP), desoxycytidintriphosphat (dCTP), desoxyguanosintriphosphat (dGTP), desoxythymidin-triphosphat (dTTP], 5xGreen GoTaq Flexi Buffer (5 µl) and 0.03 U GoTaq DNA polymerase. From the following primers 0.416 µM was added to the PCR mixture: B1 (5’ TGT GCG TCA CAG CCA GCA TCG AG 3’) and B2 (5’ AGC TGC CTT TTG GCC ACC TGG AAG 3’) and template P7 (5' ACC GCT TCC TCG TGC TTT ACG GTA 3').

PCR was performed on Mastercycle personal thermocycler using a following program: 1) 94 °C for 2 minutes; 2) 94 °C for 45 seconds; 3) 55 °C for 25 seconds; 4) 72 °C for 1 minute; 5) 29x repetition of steps 2 through 4; 6) 72 °C for 5 minutes; and 7) cooling and holding at 10 °C.

Agarose (final concentration 1%) was added into Tris-boric acid-EDTA (TBE) buffer (9 M Tris, 9 M boric acid and 0.2 M EDTA in double distilled water) and dissolved in microwave. Serva DNA Stain G was added to the fully homogenous solution (final concentration 0.001%). Solution was poured into a gel chamber supplied with a comb for sample insertion. Fully polymerized gel was lifted to a horizontal gel system filled with TBE buffer. For orientation in DNA fragment sizes, 0.1 µg 2-Log DNA Ladder was diluted in 10% gel loading buffer prepared from 6x Gel Loading Dye Orange and 80% of nuclease-free distilled water. Ten µl of this solution was loaded onto the agarose gel. PCR product (200 ng) was diluted in gel loading buffer (final volume 12 µl) and 10 µl of it was loaded onto a gel. The gel was run for 50 minutes at 100 mV, controlled by a power supply peqpower 300. Copied DNA strands were visualized with 312 nm ultraviolet (UV) light using GeliX Geldoku iNTAS imager with Intas GDS software.

Mice were considered β2-AR ko when a DNA fragment of 580 base pairs (bp) occurred, heterozygous when 346 and 580 bp DNA fragments occurred and wild-type when 346 bp DNA fragment was detected.

4.2.3 Statistical Analysis

Data were analyzed with SPSS Statistics 21.0 software for Windows. Normality of data distribution was analyzed with Kolmogorov-Smirnov test. Parametric data were analyzed with two-tailed Student's *t*-test (paired/unpaired) or, where applicable, one-way analysis of variance (ANOVA) for multiple comparisons with Bonferroni correction. Non-parametric data were analyzed with Kruskal-Wallis and Mann Whitney *U*-test. Paired parameters with non-parametric distribution were analyzed with Wilcoxon signed rank test. All non-parametric tests were performed with exact two-tailed *p*-values. Survival curves were analyzed with Chi-Square test. *P*-value < 0.05 was considered significant (*, $p<0.05$; **, $p<0.01$; ***, $p<0.001$). Spearman's *rho* correlation coefficient (non-parametric data) was used for correlations. Figures for statistical data presentation were prepared using GraphPad Prism software. Data in text are expressed in a form of mean±standard deviation. Health score and EAE data are presented as median(±range). Survival data are plotted on Kaplan-Meier curve.

5. Results

Results of my doctoral thesis are divided into three main parts:

First, data are summarized from experiments where only the SNS-mediated CIDS was blocked with propranolol, a non-specific β-AR antagonist. Here, also the results from β2-AR ko mice are presented due to the suggested critical involvement of β2-AR in SNS-mediated immunomodulation.

Second, data are summarized from experiments where both, the SNS and HPA axis mediated CIDS was simultaneously blocked with a combined treatment of propranolol and mifepristone (glucocorticoid receptor antagonist). The SNS and the HPA axis function in additive fashion to modulate cellular immune responses and CNS antigen specific autoreactive immune response.

Third, data are presented from an adoptive transfer experiment where the $CD4^+$ T cells from lymph nodes and spleens of stroked 2D2 mice were transferred i.v. to Rag-1KO recipients 6 h after MCAo. This aimed at elucidating the role of MOG TCR $CD4^+$ T cells primed by stroke for inflammatory processes in the ischemic brain in a setting of a second stroke and to overcome infarct-size bias from combined propranolol and mifepristone treatment.

5.1 The role of sympathetic nervous system (SNS) in CNS antigen specific immune responses

5.1.1 SNS block with propranolol did not increase mortality or worsen health status

2D2 mice where SNS axis of CIDS was blocked with propranolol around the time of MCAo did not differ from vehicle-treated mice in terms of survival, general health score, body weight loss and temperature in experiments with and without preventive enrofloxacin (Figure 3A-G).

The propranolol dose (3x30 mg/kg within 8 hours) necessary to block the SNS axis of CIDS is very high (LD_{50} for a mouse per i.p. route is 80 mg/kg propranolol). In order to verify, how the substance was tolerated by 2D2 mice after MCAo, heart rate of the treated mice was measured one (353±43 beats per minute), two (335±51 beats per minute), four (347±122 beats per minute) and five days after MCAo (438±153 beats per minute).

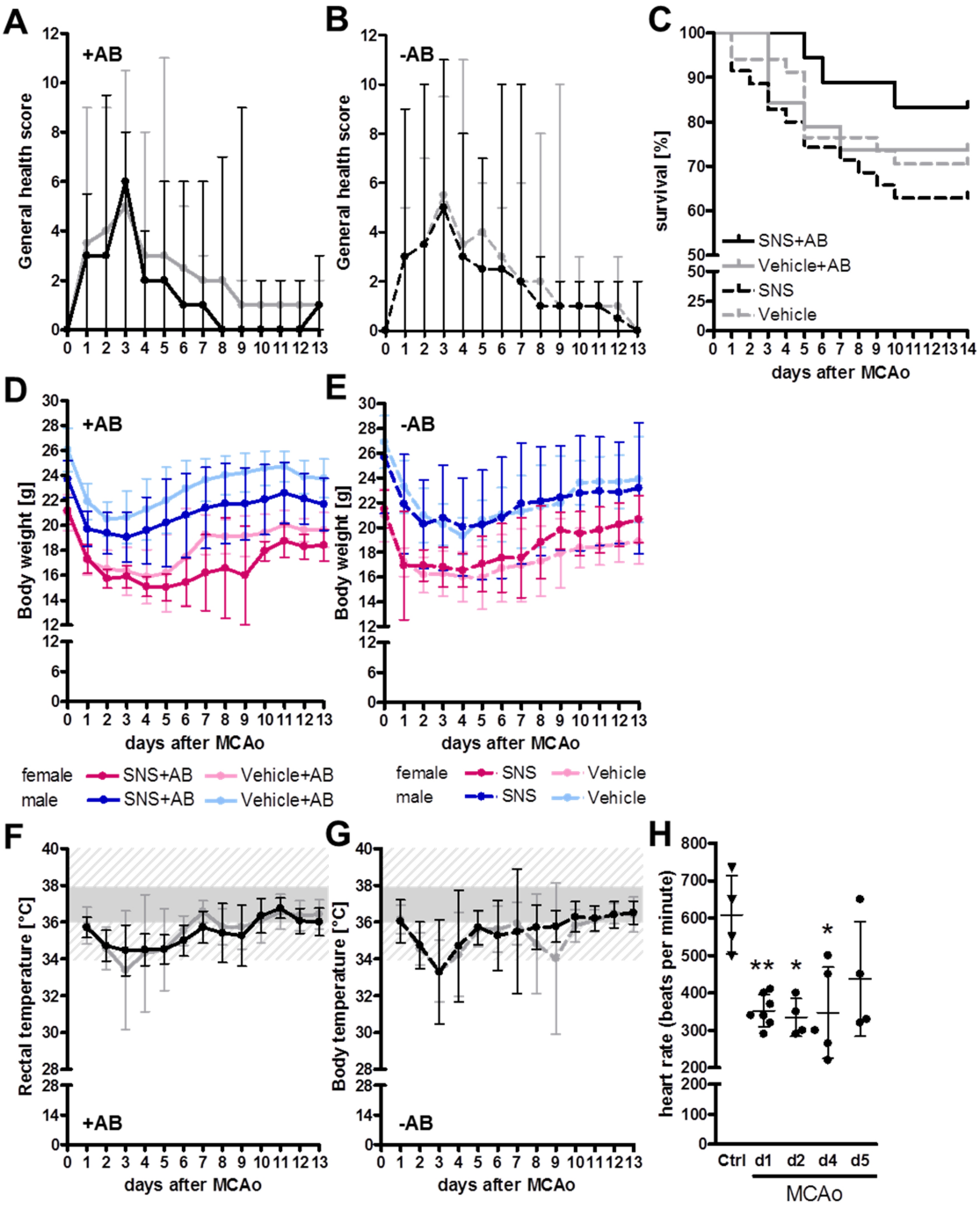

Figure 3. Health status follow-up over a period of 13 days after MCAo of 2D2 mice treated with vehicle or propranolol. Experiments with and without preventive enrofloxacin. 2D2 mice treated with propranolol for blocking the SNS axis of CIDS (SNS block, N=36; SNS block+AB, N=19) did not differ from vehicle-treated mice (vehicle, N=35; vehicle+AB, N=19) in terms of general health score (***A*** and ***B***), survival (***C***), body weight loss (***D*** and ***E***) and post-stroke alterations in rectal temperature (***F*** and ***G***). Optimal body temperature for a mouse is presented as a grey bar, and yet acceptable body temperature with grey streaked area on a background. Mice from vehicle and SNS block groups were similar regarding health status in experiments with (***B***, ***D***, and ***F***) and without preventive enrofloxacin (***C***, ***E***, and ***G***). ***H***, Heart rate was reduced in propranolol- and enrofloxacin-treated 2D2 mice (N=4-7) up to four days after MCAo compared with non-operated 2D2 mice which did nor receive propranolol but were treated preventively with enrofloxacin (N=4; Mann-Whitney *U*-test: day one: U=0.0, p=0.006; day two: U=0.0, p=0.029; day four: U=0.5, p=0.024). Abbreviations: AB, antibiotic (enrofloxacin); MCAo, middle cerebral artery occlusion; SNS, sympathetic nervous system block group.*, p<0.05; **, p<0.01.

Mice were given preventively enrofloxacin to exclude a possible bias due to post-stroke infections. Obtained heart rate values were compared with those from 2D2 mice that were neither operated nor treated with propranolol but received preventively enrofloxacin (609±105 beats per minute). Blocking SNS axis of CIDS with propranolol reduced the heart rate for up to four days after MCAo (Figure 3H). Five days after MCAo the heart rate no longer differed from control values.

5.1.2 Infarct volume was smaller in male 2D2 mice following SNS block with propranolol

Treatment with propranolol resulted in smaller infarct volume in male 2D2 mice 24 h after MCAo (from 29±12% in vehicle group to 18±12% in SNS block group; Figure 4). This effect was not observed in male C57Bl/6J mice (vehicle, 32±12% and SNS block, 27±10%). Infarct volumes in female 2D2 mice (vehicle, 22±6% and SNS block, 20±11%) were not affected by propranolol-treatment. This effect was likely not mediated by the β2-AR (wild-type mice: 19±8% and β2-AR ko mice: 18±7%). Also, preventive antibiotic treatment did not alter the size of ischemic lesion 24 h after MCAo (Figure 4).

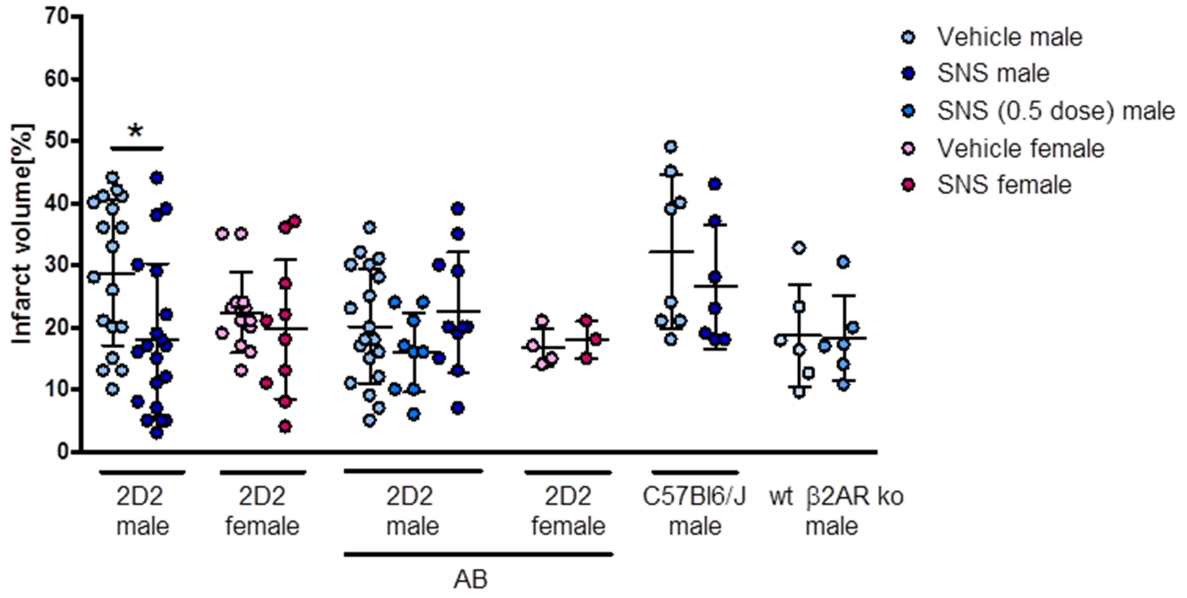

Figure 4. Blocking SNS axis of CIDS with propranolol resulted in smaller infarct volume in male 2D2 mice. Infarct volumes, measured 24 h after MCAo by T2-weighted MRI, were smaller in male 2D2 mice (N=18) after blocking SNS axis of CIDS with propranolol compared with vehicle-treated (N=20) mice (One-way ANOVA with Bonferroni post-hoc, F=2.1; p=0.039). Treatment with propranolol did not significantly affect the infarct volume in male C57Bl/6J mice (vehicle, N=8; SNS block, N=7) and in female 2D2 mice (vehicle, N=13; SNS block, N=10). Mice lacking β2-adrenoreceptor [β2-AR ko mice (N=6)] developed with their wild-type littermates (N=6) identical infarct volumes. Preventive antibiotics did not affect the size of ischemic lesion neither in vehicle (male, N=19; female, N=4) nor in SNS block groups of mice [SNS block (0.5 dose), male, N=9; SNS block, male, N=11; female, N=3). Abbreviations: AB, antibiotic (enrofloxacin); β2-AR ko, β2-adrenoreceptor knockout, SNS, sympathetic nervous system block group; wt, wild-type. *, p<0.05.

5.1.3 SNS block with propranolol decreased the incidence of pulmonary infections in male 2D2 mice

To investigate if and how blocking the SNS axis of CIDS affects post-stroke bacterial burden in the body, BAL fluid and blood were collected and lung homogenates were prepared from 2D2 mice three days after MCAo and analyzed microbiologically.

Largest bacterial loads were found in BAL fluid followed by lung and blood in both, vehicle and SNS block group (Figure 5A). Larger bacterial load in the BAL fluid was in both groups associated with larger bacterial load in the lung tissue (Figure 5B). In vehicle group, higher levels of bacteria in the blood predicted higher bacterial levels in BAL fluid and lung.

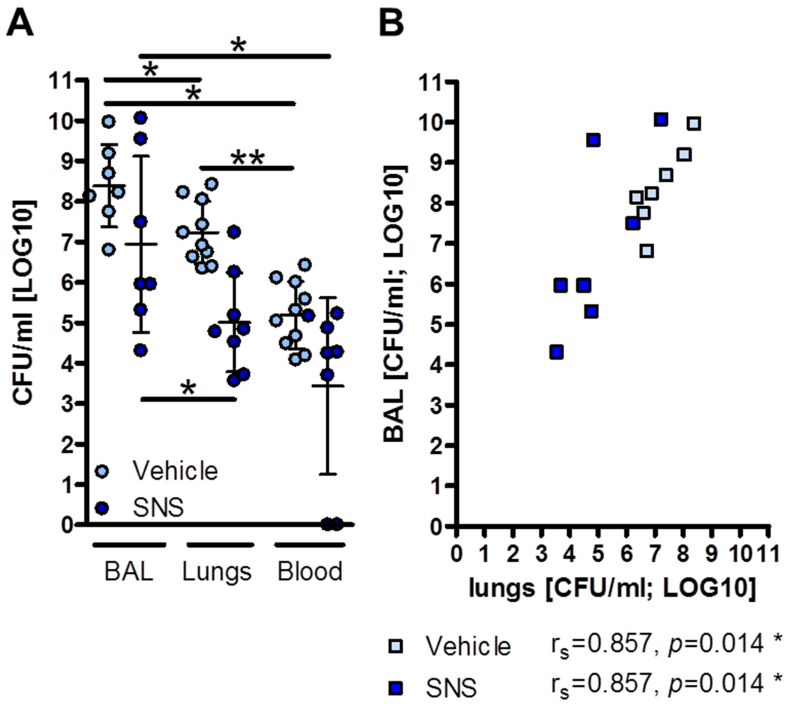

Figure 5. Interdependencies between bacterial burdens in BAL fluid, lungs and blood among vehicle- and propranolol-treated male 2D2 mice. ***A*** Compared with BAL fluid, less bacteria was found in the lungs (all paired parameters were analysed with Wilcoxon signed-rank test; vehicle: N=7, *Z*=-2.4, *p*=0.016; SNS block: N=7, *Z*=-2.4, *p*=0.016) and blood (vehicle: *Z*=-2.4, *p*=0.016; SNS block, *Z*=-2.4, *p*=0.016). In vehicle group, the amount of bacteria in lung exceeded that in blood (vehicle: *Z*=-2.8, *p*=0.002). ***B***, The bacterial loads in the BAL fluid of vehicle-treated and SNS block group mice were strongly and positively correlated (Spearman's rank-order correlation) with the bacterial load in lungs. Abbreviations: BAL, bronchoalveolar lavage; CFU, colony forming units; SNS, sympathetic nervous system block group. *, *p*<0.05; **, *p*<0.01; ***, *p*<0.001.

Blocking SNS axis of CIDS with propranolol effectively reduced the bacterial burden in the BAL fluid [vehicle, 8.0±1.0 CFU/ml (LOG10); SNS block, 6.9±1.4 CFU/ml (LOG10)] and lungs of male 2D2 mice [vehicle, 7.2±0.8 CFU/ml (LOG10); SNS block, 5.0±1.2 CFU/ml

(LOG10); Figure 6A]. Microbiological comparisons of BAL fluid from β2-AR ko mice and wild-type littermates did not reveal a significant role for the β2-AR in this effect [wild-type, 7.8±0.6 CFU/ml (LOG10); β2-AR ko, 6.9±1.0 CFU/ml (LOG10); Figure 6A]. Preventive enrofloxacin administration reduced bacterial load in the BAL fluid of 2D2 mice from both, vehicle and SNS block groups [vehicle, 5.7±1.1 CFU/ml (LOG10); SNS block, 5.9±0.6 CFU/ml (LOG10)]. However, the effect of propranolol was here no longer distinguishable (Figure 6B). Higher numbers of bacterial CFUs, and thus higher infection rate, were found in those vehicle-treated gender-mixed mice that suffered larger infarcts. Such correlation was not observed in propranolol-treated gender-mixed mice (Figure 6C).

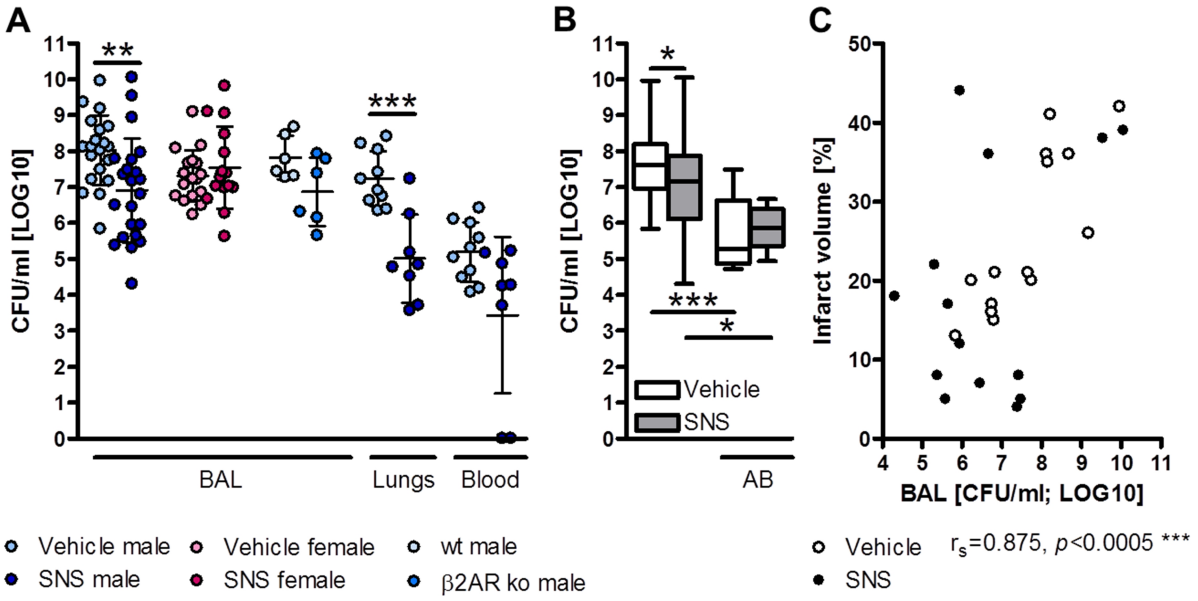

Figure 6. Blocking SNS axis of CIDS effectively reduced bacterial load in BAL fluid and lungs of male 2D2 mice three days after MCAo. ***A***, Bacterial burden [CFU/ml(LOG10)] in the BAL fluid of male 2D2 mice after blocking the SNS axis of CIDS (N=22) was lower than in vehicle-treated mice (N=20; Kruskal-Wallis, Chi-Square=13.4, df=5, p=0.020; Mann-Whitney *U*-test: BAL, U=107.0; p=0.004). This effect was not observed in female 2D2 mice (vehicle, N=17; SNS, N=15) and did not reach significance in male β2-AR ko mice (N=6) compared with male wild-type littermates (N=6). Bacterial burden was also reduced in the lungs of male 2D2 mice after propranolol treatment (N=8) compared with mice receiving vehicle (N=10; Mann-Whitney *U*-test: BAL, U=6.0; p=0.001). Bacterial burden in blood was not affected (vehicle, N=10; SNS, N=8). ***B***, Bacterial load in BAL fluid was smaller in gender-mixed 2D2 mice from SNS block group compared with vehicle (enrofloxacin was not provided; Mann-Whitney *U*-test, U=496.0; p=0.042). This difference disappeared when enrofloxacin was applied. Preventive antibiotics reduced bacterial burden in the BAL fluid (vehicle, N=37; SNS, N=37; vehicle+AB, N=8; SNS+AB, N=6; Kruskal-Wallis, Chi-Square=23.1, df=3, p<0.0005; Mann-Whitney *U*-test: between vehicle groups, U=27.0; p<0.0005; between SNS block groups, U=43.0; p=0.015). ***C***, Infarct volume (measured 24 h after stroke) in vehicle but not SNS block group of gender-mixed mice correlated strongly with bacterial load in the BAL fluid (Spearman's rank-order correlation). Abbreviations: AB, antibiotic (enrofloxacin); BAL, bronchoalveolar lavage; β2-AR ko, β2-adrenoreceptor knockout; CFU, colony forming units; SNS, sympathetic nervous system block group; wt, wild-type.*, p<0.05; **, p<0.01; ***, p<0.001.

Taken together, blocking SNS axis of CIDS with propranolol did not worsen post-MCAo health status in 2D2 mice. Furthermore, propranolol treatment resulted in smaller infarct volumes measured 24 h after MCAo through a mechanism not involving β2-AR, and bacterial burden in the BAL fluid and lungs of male 2D2 mice.

5.1.4 SNS block with propranolol did not worsen symptoms of experimental autoimmune encephalomyelitis reminiscent disease

2D2 mice differ from C57Bl/6J mice in that they overexpress MOG-specific TCR on $CD4^+$ T cells. Upon appropriate stimulus, these mice can develop autoreactive responses towards myelin structures. To assess the development of CNS-directed autoreactive immune responses after stroke, I investigated 2D2 mice treated with vehicle or propranolol for EAE score between days 7 and 13 after MCAo.

Majority of 2D2 mice developed EAE-like symptoms within 13 days after MCAo. In experiments where animals did not receive enrofloxacin, the fraction of mice with EAE-like symptoms was 83% in vehicle and 92% in SNS block group. Both male (Figure 7A) and female 2D2 mice (Figure 7B) developed EAE-like symptoms at similar rate and severity independent of blocking the SNS axis of CIDS.

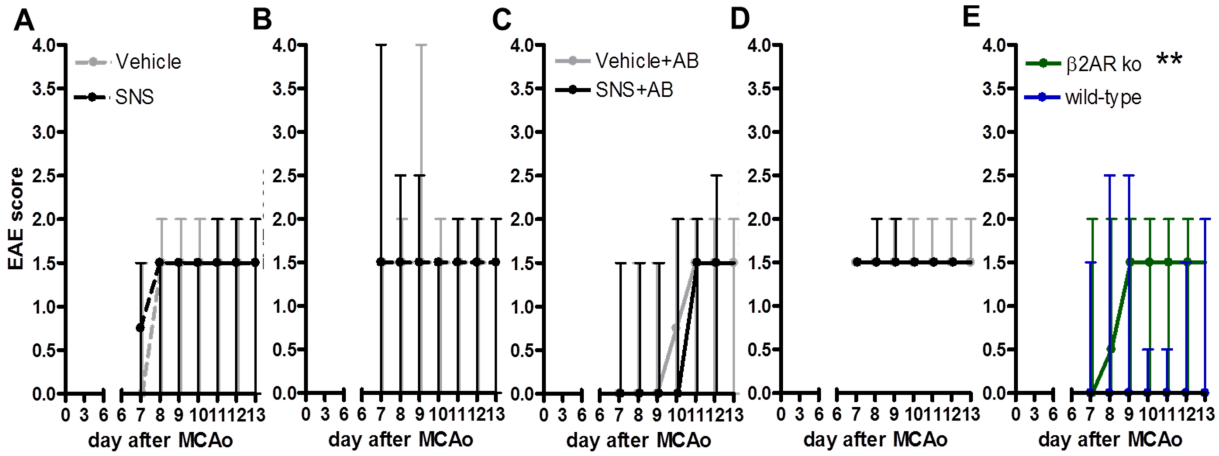

Figure 7. EAE disease development was similar in vehicle- and propranolol-treated 2D2 mice. ***A***, EAE score in male (vehicle, N=8; SNS block, N=14) and ***B***, in female 2D2 mice (vehicle, N=15; SNS block, N=12) in the absence of preventive antibiotics. ***C***, EAE score in male (vehicle, N=8; SNS block, N=9) and ***D***, female 2D2 mice (vehicle, N=5; SNS, N=3) which received preventive antibiotics. ***E***, β2-AR ko mice developed more severe EAE-like disease compared with their wild-type littermates (Mann-Whitney *U*-test, U=2.0; p=0.002). Abbreviations: AB, antibiotic (enrofloxacin); β2-AR ko, β2-adrenoreceptor knockout; EAE, experimental autoimmune encephalomyelitis; MCAo, middle cerebral artery occlusion; SNS, sympathetic nervous system block group. **, p<0.01.

Even in experiments where enrofloxacin was preventively used, 85% of vehicle and 75% of SNS block group mice showed symptoms of EAE-like disease by day 13 after MCAo, with equal severity in male and female 2D2 mice (Figure 7C and D). Comparatively, appearance of EAE and its progression were followed in β2-AR ko mice and their wild-type littermates (enrofloxacin was not provided). Post-stroke EAE-like symptom progression was more advanced in mice lacking the β2-AR compared with wild-type littermate controls (Figure 7E).

5.1.5 SNS block with propranolol did not aggravate locomotor deficits

CatWalk gait analysis as a method for detecting locomotor deficits in male C57Bl/6J mice 10 days after MCAo was perfected to represent individual paw characteristics, gait coordination and kinetics regularly affected by stroke.

Here, I investigated whether and how blocking SNS axis of CIDS with propranolol affected mid (10 days after MCAo) and long-term (30 days after MCAo) post-stroke locomotor behavior in comparison with vehicle treatment. 2D2 mice from both, vehicle and SNS block group displayed some of the typical spatial and kinetic alterations in gait induced by cerebral ischemia but did not differ from each other (Table. 1). Gait of β2-AR ko mice 10 days after MCAo was not generally different from wild-type littermates and pre-MCAo baseline values, except from the phase dispersion from left front to left hind paw, reflecting worse gait coordination in wild-type mice (Table 1).

To conclude, blocking SNS axis of CIDS with propranolol did not aggravate functional neurological outcome indicative of MOG-specific autoreactive immune responses in comparison with vehicle-treated mice over the period of 14 days after MCAo.

Table 1. CatWalk gait analysis of 2D2 and β2-AR knockout (ko) mice before and 10 days after middle cerebral artery occlusion (MCAo).

Parameter	Definition	Paw	2D2					β2-AR ko		
			Baseline	Vehicle	Vehicle+AB	SNS	SNS+AB	Baseline	wild-type	β2AR ko
Spatial characteristics										
Max contact area (mm^2)	Area of a paw print at maximal plate contact	RF	26,97±5,004	23,63±4,596	27,44±4,444	25,91±5,571	26,60±3,776	34,23±4,642	34,36±4,477	34,89±3,526
		RH	25,67±5,653	18,57±5,779 ***	22,49±5,287	19,45±7,842 **	19,90±3,152 *	26,46±8,090	28,87±9,579	26,51±6,650
		LF	26,89±4,785	25,15±3,957	28,19±3,360	25,70±5,961	26,77±3,779	33,54±5,085	35,81±5,159	33,69±3,205
		LH	25,52±6,040	19,65±8,868 *	25,34±7,834	21,78±9,105	24,51±7,899	25,46±7,714	35,26±7,437	30,85±7,246
Kinetic characteristics										
Run duration (s)	Time for passing the walkway		2,850±0,641	2,865±0,801	2,913±0,655	3,013±0,722	2,858±0,761	2,760±0,545	3,337±0,183	2,782±0,377
Normalized swing speed (s)	Swing speed*Run duration	RF	1449±291,2	1299±201,0	1405±182,0	1375±170,0	1358±169,8	1346±136,7	1385±88,16	1316±68,90
		RH	1360±259,6	1077±179,4 ***	1133±168,0 *	1124±204,2 ***	1105±111,8 *	1352±221,4	1403±200,6	1262±301,9
		LF	1403±231,4	1317±178,9	1384±174,8	1381±252,3	1392±187,5	1342±104,1	1434±200,4	1277±139,4
		LH	1401±295,8	1192±253,3 *	1316±260,5	1263±295,7	1308±301,4	1358±183,6	1552±187,7	1383±225,3
Stand (s)	Duration of a paw contact with plate	RF	0,156±0,032	0,165±0,038	0,181±0,042	0,182±0,036 *	0,175±0,032	0,182±0,034	0,210±0,123	0,179±0,020
		RH	0,149±0,034	0,135±0,033	0,140±0,030	0,143±0,027	0,139±0,038	0,171±0,042	0,199±0,029	0,163±0,035
		LF	0,156±0,035	0,167±0,037	0,177±0,042	0,179±0,041	0,173±0,038	0,176±0,027	0,201±0,030	0,173±0,027
		LH	0,153±0,035	0,141±0,045	0,162±0,050	0,157±0,034	0,163±0,056	0,172±0,027	0,224±0,029 *	0,189±0,040
Comparative statistics										
Regularity index (%)	Regularity of gait		90,52±5,800	89,91±8,119	88,57±4,570	89,38±8,624	89,06±6,354	91,07±7,312	91,81±5,610	93,08±1,609
Base of support (mm)	Distance between paws	RF-LF	14,96±5,700	14,27±5,759	18,08±2,146 ‡‡	11,39±7,036	18,16±1,796 ‡	12,72±6,358	6,917±1,592	9,875±6,985
		RH-LH	28,80±11,35	25,92±10,41	35,79±3,758 ‡‡	20,69±13,78 *	33,47±3,283 ‡	21,98±10,62	13,03±3,999	16,71±10,79
Stride length (mm)	Distance between successive steps with one paw	RF	56,96±8,725	56,23±7,967	61,42±5,541	59,90±9,508	61,98±10,13	60,36±5,974	56,50±1,445	59,27±6,449
		RH	51,51±9,561	51,52±8,381	51,03±7,031	50,17±9,391	53,48±10,81	52,95±6,815	50,00±4,741	51,01±5,405
		LF	56,63±8,834	56,63±7,748	60,79±5,205	56,86±9,520	62,58±9,963	59,38±5,679	52,41±4,025	57,83±7,537
		LH	52,17±8,947	51,34±7,233	52,94±5,206	50,89±9,935	55,70±6,240	53,74±7,983	53,21±2,702	56,61±4,811
Phase dispersions (%)	Contact of a target paw in relation to step cycle of the anchor paw	RF-LH	9,664±13,87	14,08±15,88	28,99±20,59 **	15,43±16,83	12,12±14,60	9,502±6,598	5,758±4,762	7,834±6,260
		LF-RH	12,96±16,22	9,252±9,260	10,53±5,951	13,65±15,32	16,24±18,48	10,62±6,624	13,17±3,644	12,15±8,050
		LH-RH	42,04±7,392	39,56±6,473	39,01±7,934	42,17±7,525	41,26±5,815	38,76±9,744	40,99±8,301	40,27±6,525
		LF-RF	49,09±3,542	48,37±4,671	49,57±3,176	50,27±2,918	51,79±1,603	50,30±2,533	52,26±2,641	49,30±3,385
		RF-RH	45,83±6,192	48,69±6,559	46,73±5,568	50,02±5,614	45,98±4,320	48,73±5,969	51,68±5,587	48,88±2,258
		LF-LH	45,98±5,836	47,08±6,372	48,27±4,980	49,34±6,745	49,79±6,995	49,42±4,315	57,20±4,519 **	51,12±2,819 #

* compared with baseline: One-way ANOVA for multiple comparisons with Bonferroni correction (*, $p<0.05$; **, $p<0.01$; ***, $p<0.001$)

‡ compared with SNS: One-way ANOVA for multiple comparisons with Bonferroni correction (‡, $p<0.05$; ‡‡, $p<0.01$)

compared with wild-type on day 10 after MCAo: One-way ANOVA for multiple comparisons with Bonferroni correction (#, $p<0.05$)

Abbreviations: RF, right front paw; RH, right hind paw; LF, left front paw; LH, left hind paw; 2D2, myelin oligodendrocyte glycoprotein T-cell-receptor transgenic mouse; SNS, sympathetic nervous system block group; AB, antibiotic (preventively administered enrofloxacin); β2-AR ko, β2-adrenoreceptor knock-out

2D2 mice: Gender mixed. Baseline N=65; SNS N=20; SNS+AB N=10; Vehicle N=22; Vehicle+AB N=13

β2-AR ko mice: Males. Baseline N=13; β2AR ko N=7; wild-type N=5

5.1.6 SNS block with propranolol or lack of β2-adrenoreceptor did not affect the cellular composition of leukocytes in the spleen

Spleen, innervated by the SNS (Felten et al., 1985), is a peripheral lymphoid organ where dendritic cells present circulating antigens to T cells. I investigated and characterized the cellular composition of the spleen after blocking SNS axis of CIDS with propranolol in 2D2, C57Bl/6J and β2-AR ko mouse strains.

Compared with naïve non-manipulated C57Bl/6J mice, the number of splenocytes was decreased in 2D2 mice 3 and 14 days after MCAo and in C57Bl/6J mice 3 days after MCAo. Preventive administration of enrofloxacin did not affect splenocyte numbers in 2D2 mice 14 days after MCAo. Splenocyte numbers in β2-AR ko mice and their wild-type littermates 14 days after MCAo did not differ significantly from naïve C57Bl/6J mice (Figure 8A).

A detailed analysis of the cellular composition of spleen was performed using FACS. Cell populations of interest were myeloid cells (expressing CD11b, and their subpopulations $CD11b^+$ $Gr1^-$ monocytes and $CD11b^+$ $Gr1^+$ granulocytes) and lymphoid cells ($B220^+$ B cells, $CD3^+$ T cells and T cell subpopulations $CD4^+$ helper T cells with the fraction of $CD4^+$ $V\alpha3.2^+$ MOG-specific helper T cells, $CD8^+$ cytotoxic T cells, and, where indicated, $CD8^+$ $V\alpha3.2^+$ MOG-specific cytotoxic T cells).

Blocking SNS axis of CIDS did not affect cellular composition of spleen three days after MCAo neither in C57Bl/6J (Figure 8B) nor in 2D2 mice (Figure 8C and D) compared with vehicle treatment. Mice did not receive enrofloxacin. However, certain strain-specific differences were detected. 2D2 mice where the SNS axis of CIDS was blocked (N=8) had more $B220^+$ B cells (Mann-Whitney *U*-test, $U=9.0$; $p=0.029$) and $CD4^+$ helper T cells (Mann-Whitney *U*-test, $U=7.0$; $p=0.014$) among splenocytes than C57Bl/6J mice from SNS block group (N=7). The quantity of cytotoxic $CD8^+$ T cells among splenocytes, on the other hand, was larger in C57Bl/6J mice than in 2D2 mice (Mann-Whitney *U*-test; between SNS block groups: $U=0.0$; $p<0.0005$; between vehicle groups: $U=2.0$; $p<0.0005$). Spleens of β2-AR ko mice and their wild-type littermates (enrofloxacin was not administered) were investigated for cellular composition 14 days after MCAo and no significant differences were found (Figure 8E).

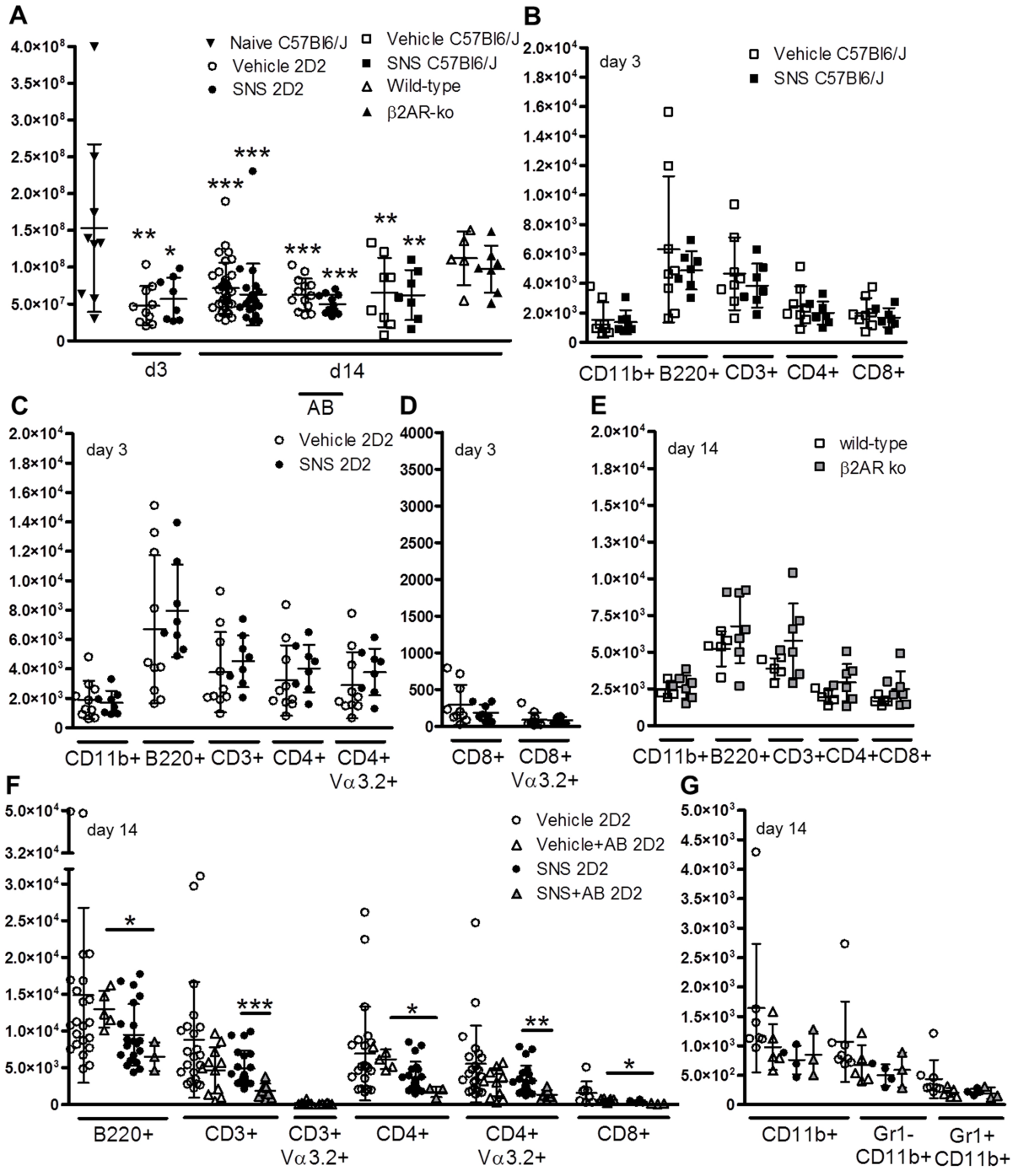

Figure 8. Semi-automatic analysis of absolute splenocyte numbers and cellular composition of spleen (presented per 1x10^5 splenocytes) using FACS in vehicle and propranolol-treated C57Bl/6J and 2D2 mice and β2-AR ko mice 3 and/or 14 days after MCAo. Where indicated, enrofloxacin was provided. ***A***, Absolute numbers of splenocytes (significances indicate differences from naïve non-manipulated C57Bl/6J mice). Absolute numbers of splenocytes were reduced in 2D2 mice (vehicle, N=10; SNS block, N=8) compared with naïve non-manipulated C57Bl/6J mice (N=9) three days after MCAo (One-way ANOVA with Bonferroni post-hoc, F=6.4, vehicle: p=0.009; SNS block: p=0.026). Splenocyte counts in C57Bl/6J mice (vehicle, N=8; SNS, N=7) three days after MCAo were, independent of group assignment, reduced compared with naïve mice (F=4.7, vehicle: p<0.004; SNS: p<0.004). The numbers of splenocytes in 2D2 mice (vehicle, N=34; SNS block, N=22) remained reduced 14 days after MCAo (F=4.7, vehicle: p<0.0005; SNS block: p<0.0005) and after preventive enrofloxacin treatment (vehicle, N=13; SNS block, N=11; F=4.7, vehicle: p<0.0005; SNS: p<0.0005). Splenocyte numbers 14 days after MCAo in β2-AR ko mice (N=7) and their wild-type littermates (N=5), however, did not differ

significantly from those in naïve C57Bl/6J mice. ***B***, Three days after MCAo, similar quantities of $CD11b^+$ myeloid cells, $B220^+$ B cells, $CD3^+$ T cells, $CD4^+$ helper T cells and $CD8^+$ cytotoxic T cells were observed in vehicle (N=8) and SNS block (N=7) groups of C57Bl/6J mice. ***C*** and ***D***, Cellular composition of spleen three days after MCAo was similar also in 2D2 mice from vehicle (N=10) and SNS block group (N=8; $CD4^+$ $V\alpha3.2^+$ and $CD8^+$ $V\alpha3.2^+$ cells are the MOG TCR transgenic T cells). ***E***, Fourteen days after MCAo, cellular composition of spleen was similar between β2-AR ko mice (N=7) and their wild-type littermates (N=5). ***F***, Cellular distribution of lymphocytes in the spleens of 2D2 mice. Data were analyzed with Kruskal-Wallis ($B220^+$: Chi-Square=9.1; df=3, p=0.029; $CD3^+$: Chi-Square=18.4; df=3, p<0.0005; $CD4^+$: Chi-Square=9.5; df=3, p=0.023; $CD4^+$ $V\alpha3.2^+$: Chi-Square=15.3; df=3, p=0.002; $CD8^+$: Chi-Square=11.2; df=3, p=0.011) and Mann-Whitney U-test. The fractions of lymphocytes, such as $B220^+$ B cells, $CD3^+$ T cells, $CD4^+$ helper T cells, $CD4^+$ $V\alpha3.2^+$ MOG-specific helper T cells (for all: vehicle, N=22; SNS block, N=20) and $CD8^+$ cytotoxic T cells (vehicle, N=8; SNS block, N=4) were similar in vehicle and SNS block groups of mice. In experiments where preventive enrofloxacin was used, propranolol-treated 2D2 mice had lower frequencies of splenic $B220^+$ B cells (vehicle+AB, N=11; SNS block+AB, N=9; U=6.0; p=0.036), $CD4^+$ helper T cells (vehicle+AB, N=5; SNS block+AB, N=3; U=6.0; p=0.036) and $CD8^+$ cytotoxic T cells (vehicle+AB, N=5; SNS block+AB, N=3; U=6.0; p=0.036) than vehicle-treated mice. While preventive enrofloxacin did not change the splenic cellular distribution in vehicle group, it strongly reduced the frequencies of $CD3^+$ T cells (SNS block, N=20; SNS block+AB, N=9; U=13.0; p<0.0005) and $CD4^+$ $V\alpha3.2^+$ MOG-specific helper T cells (U=26.0; p=0.002) in the spleens of propranolol-treated mice. ***G***, The numbers of myeloid cells among splenocytes did not differ between the groups and were not affected by preventive antibiotic treatment (vehicle, N=8; vehicle+AB, N=5; SNS block, N=4; SNS block+AB, N=3). Abbreviations: AB, antibiotic (enrofloxacin); β2-AR ko, β2-adrenoreceptor knockout; SNS, sympathetic nervous system block group. *, p<0.05; **, p<0.01; ***, p<0.001.

Compared with measurements from three days after MCAo, lymphocyte numbers in spleens of 2D2 mice belonging to vehicle group were increased on day 14 (Mann-Whitney U-test). This involved $B220^+$ B cells (day 3, N=10; day 14, N=22; U=46.0; p=0.008), $CD3^+$ T cells (day 3, N=10; day 14, N=22; U=43.0; p=0.005), $CD4^+$ helper T cells (day 3, N=10; day 14, N=22; U=55.0; p=0.025) and $CD8^+$ cytotoxic T cells (day 3, N=10; day 14, N=8; U=9.0; p=0.004). Within SNS block groups, lymphocyte numbers in spleen on day 14 after MCAo did not significantly differ from those on day 3. Also, vehicle and propranolol-treated mice did not differ regarding lymphocyte numbers in spleen 14 days after MCAo. The numbers of $CD11b^+$ myeloid cells in SNS block group had decreased between day 3 and 14 after MCAo (day 3, N=4; day 14, N=8; U=3.0; p=0.028).

Administration of preventive antibiotic resulted in a different pattern of cellular distribution in spleen 14 days after MCAo. The numbers of $B220^+$ B cells, $CD4^+$ T cells and $CD8^+$ cytotoxic T cells were reduced among the splenocytes of mice belonging to SNS block group compared with vehicle group (Figure 8F and G). In addition, using enrofloxacin in a preventive manner reduced the numbers of $CD3^+$ T cells and $CD4^+$ $V\alpha3.2^+$ MOG-specific T helper cells among splenocytes in propranolol-treated mice (Figure 8F).

5.1.7 SNS block with propranolol did not affect the phenotype of myelin oligodendrocyte glycoprotein T cell receptor transgenic T cells in the spleen

ELISpot was performed 14 days after MCAo to investigate the cytokine-profile of individual MOG-specific splenocytes, based on IFN-γ, IL-4 and IL-17 secretion, after blocking SNS axis of CIDS with propranolol. Additionally, the effect of enrofloxacin on CNS-specific autoreactive responses was assessed.

Compared with vehicle-treatment, blocking SNS axis of CIDS did not influence the number of splenic T cells secreting any of the three cytokines (IFN-γ, IL-4, IL-17) upon stimulation with $pMOG_{35-55}$, independent of enrofloxacin use. Preventively administered enrofloxacin did not affect the number of MOG-reactive IFN-γ producing cells but reduced strongly the numbers of MOG-reactive IL-17-secreting splenocytes (Figure 9A). This decrease was more pronounced in SNS block group. Preventively administered enrofloxacin also reduced the number of IL-4 secreting MOG-specific T cells in the spleens of mice where the SNS axis of CIDS had been blocked (Figure 9A).

The ratio between autoreactive Th1 and Th2 cells (identified by the levels of the cytokines they produce: IFN-γ and IL-4, respectively) was calculated since it is a marker for immunological outcome (van der Graaff et al., 1998) and dependent on stress systems (Elenkov et al., 1996). This ratio was higher in 2D2 mice after blocking SNS mediated CIDS in experiments where mice were administered preventive enrofloxacin (vehicle, 3.6±1.5; SNS block, 6.0±3.2) but did not differ between vehicle (3.6±1.6) and SNS block groups (2.7±1.3) when enrofloxacin was not given (Figure 9B). The ratio between autoreactive Th17 and Th1 cells, on the other hand, can determine the phenotype of CNS-directed autoreactivity (Stromnes et al., 2008). Similar ratio between Th17 and Th1 cells in vehicle (vehicle, 0.12±0.05; vehicle+AB, 0.08±0.06) and SNS block groups (SNS block, 0.10±0.05; SNS block+AB, 0.05±0.07; Figure 9C) indicates that autoreactive phenotype is not affected by blocking SNS mediated CIDS.

In summary, blocking SNS axis of CIDS did not alter the absolute numbers of splenocytes but reduced the frequencies of splenic myeloid cells or, combined with preventive antibiotic, splenic B cells, helper T cells and effector T cells. Autoreactive potential in the spleen was not increased by blocking SNS axis of CIDS but combination with preventive antibiotics

resulted in imbalance between autoreactive Th1 and Th2 cells and reduced the numbers of IL-17 secreting MOG-specific splenocytes.

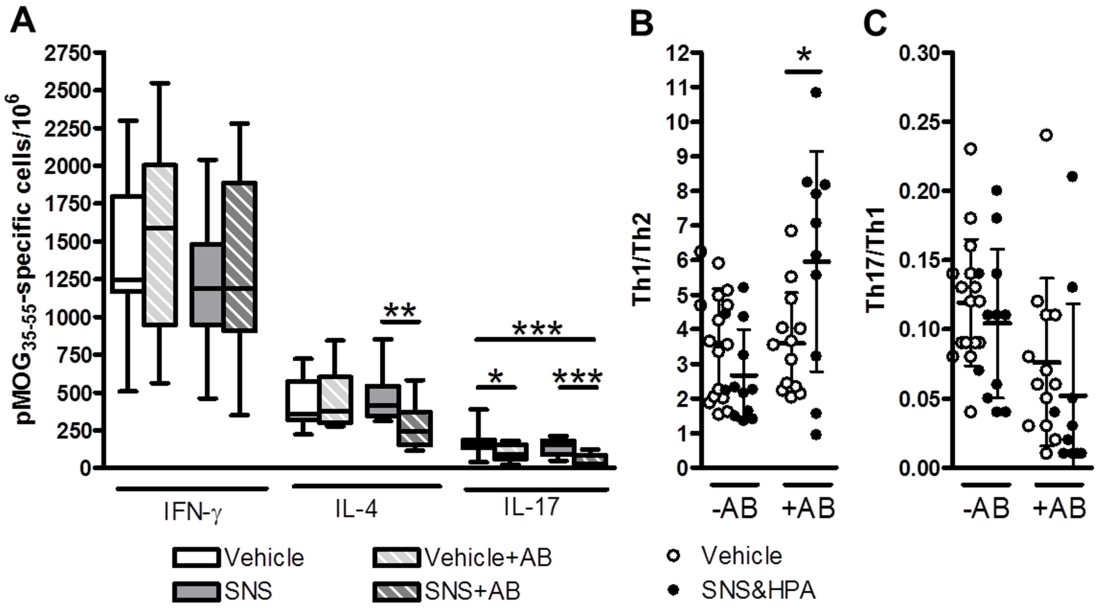

Figure 9. Frequencies of MOG-reactive cells per 1x10^6 splenocytes in 2D2 mice after blocking SNS axis of CIDS and vehicle treatment. Effect of enrofloxacin on autoreactive responses. ***A***, The numbers of MOG-reactive IFN-γ (Th1 signature cytokine), IL-4 (Th2 signature cytokine) and IL-17 (Th17 signature cytokine) secreting splenocytes were similar in vehicle (vehicle, N=16; vehicle+AB, N=13) and SNS block groups (SNS block, N=12; SNS block+AB, N=10). The number of IFN-γ secreting MOG-reactive cells (Th1 cells) was not affected by preventive enrofloxacin treatment. Enrofloxacin had no effect on MOG-specific cells responding with IL-4 secretion in vehicle group but reduced that in SNS block group (One-way ANOVA with Bonferroni post-hoc, F=4.0, p=0.007). The number of IL-17 secreting cells upon peptide stimulation was reduced by preventive antibiotic in vehicle and SNS block groups (F=10.6, vehicle *versus* vehicle+AB: p=0.020; SNS block *versus* SNS block+AB: p=0.001). Reduction in SNS block group was significant also in comparison with vehicle group of mice that were not given enrofloxacin (F=10.6, p<0.0005). ***B***, Ratio of autoreactive Th1/Th2 cells based on their cytokine secretion profile differed between vehicle and SNS block groups when preventive enrofloxacin was administered (Student's t-test, t(21)=-2.4, p=0.027). This effect was not observed when enrofloxacin was not applied. ***C***, Ratio between autoreactive Th17 and Th1 cells was not affected by blocking SNS axis of CIDS and enrofloxacin use. Abbreviations: AB, antibiotic (enrofloxacin); IFN-γ, interferon gamma; IL-4, interleukin 4; IL-17, interleukin 17; pMOG$_{35-55}$, peptide fragment (amino acids 35-55) from myelin oligodendrocyte glycoprotein; SNS, sympathetic nervous system block group. *, p<0.05; **, p<0.01; ***, p<0.001.

5.1.8 SNS block with propranolol increased the number of myelin oligodendrocyte glycoprotein specific CD4$^+$ and CD8$^+$ T cells in the thymus of 2D2 mice

T cell development takes place in thymus (Murphy, 2008). To investigate whether cellular composition of thymus was affected by blocking SNS mediated CIDS with propranolol, I obtained absolute thymocyte numbers and analyzed thymi of C57Bl/6J and 2D2 mice with

FACS three days after MCAo. Absolute numbers of thymocytes did not differ between the groups and strains (Figure 10A).

Cellular composition of the thymus was not affected by propranolol in C57Bl/6J mice (Figure 10B and C) but increased the frequencies of $CD4^+$ and $CD8^+$ single-positive MOG-specific ($V\alpha3.2^+$) T cells in the thymus of 2D2 mice (Figure 10D and E). Compared with 2D2 mice, the thymi of C57Bl/6J mice contained more $CD8^+$ cytotoxic T cells (Mann-Whitney *U*-test, between SNS block groups: U=6.0; p=0.009; between vehicle groups: U=0.0; p<0.0005).

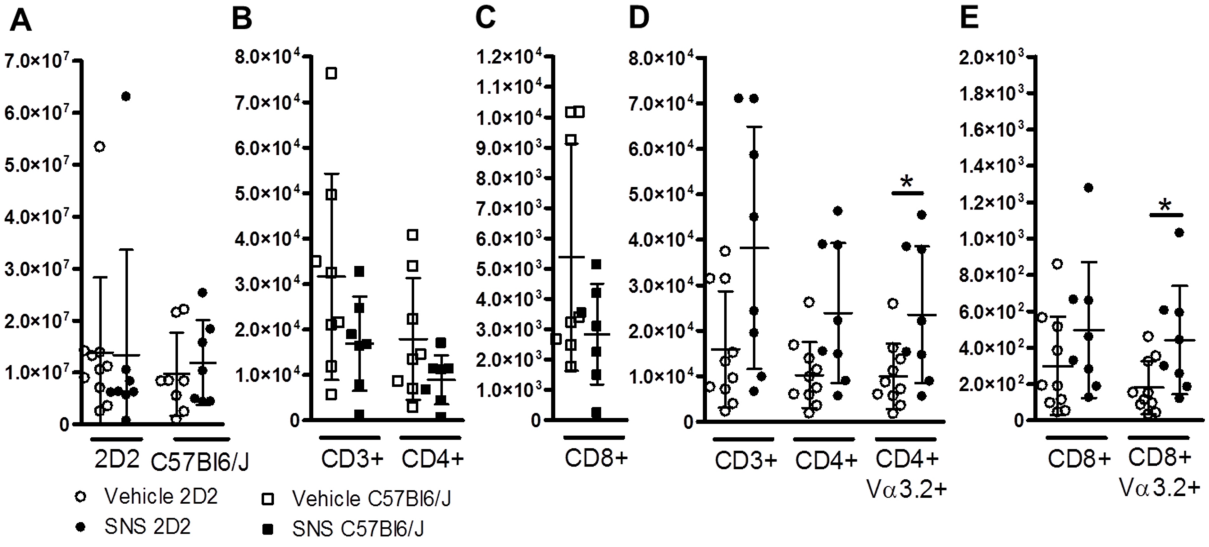

Figure 10. Absolute numbers of thymocytes and their composition (presented per 1x10^5 thymocytes) in C57Bl/6J and 2D2 mice three days after MCAo and vehicle or propranolol treatment (enrofloxacin was not provided) analysed with FACS. ***A***, Absolute numbers of live thymocytes were similar in C57Bl/6J (vehicle, N=8; SNS block, N=7) and 2D2 mice (vehicle, N=10; SNS block, N=8) three days after MCAo independent of blocking the SNS axis of CIDS with propranolol. ***B*** and ***C***, The fractions of thymocytes ($CD3^+$, $CD4^+$, $CD8^+$) were not affected by propranolol treatment in C57Bl/6J mice. ***D*** and ***E***, The fraction of $CD4^+$ $V\alpha3.2^+$ MOG-specific helper T cells (Mann-Whitney *U*-test, U=17.0; p=0.043) and $CD8^+$ $V\alpha3.2^+$ MOG-specific cytotoxic effector T cells (U=15.0; p=0.027) was higher among the thymocytes of 2D2 mice after blocking the SNS axis of CIDS. Abbreviations: SNS, sympathetic nervous system block group. *, p<0.05.

5.1.9 SNS block with propranolol or lack of β2-adrenoreceptor did not affect the cellular composition of leukocytes infiltrating the ischemic brain

$CD45^+$ leukocytes from the brains of 2D2 mice 14 days after MCAo and blocking SNS axis of CIDS were quantified, analyzed with FACS and compared with vehicle-treated 2D2 mice. The numbers of $CD45^+$ leukocytes in ipsi- and contralateral hemispheres were not affected by blocking the SNS axis of CIDS with propranolol (Figure 11A and B; Figure 12A and B).

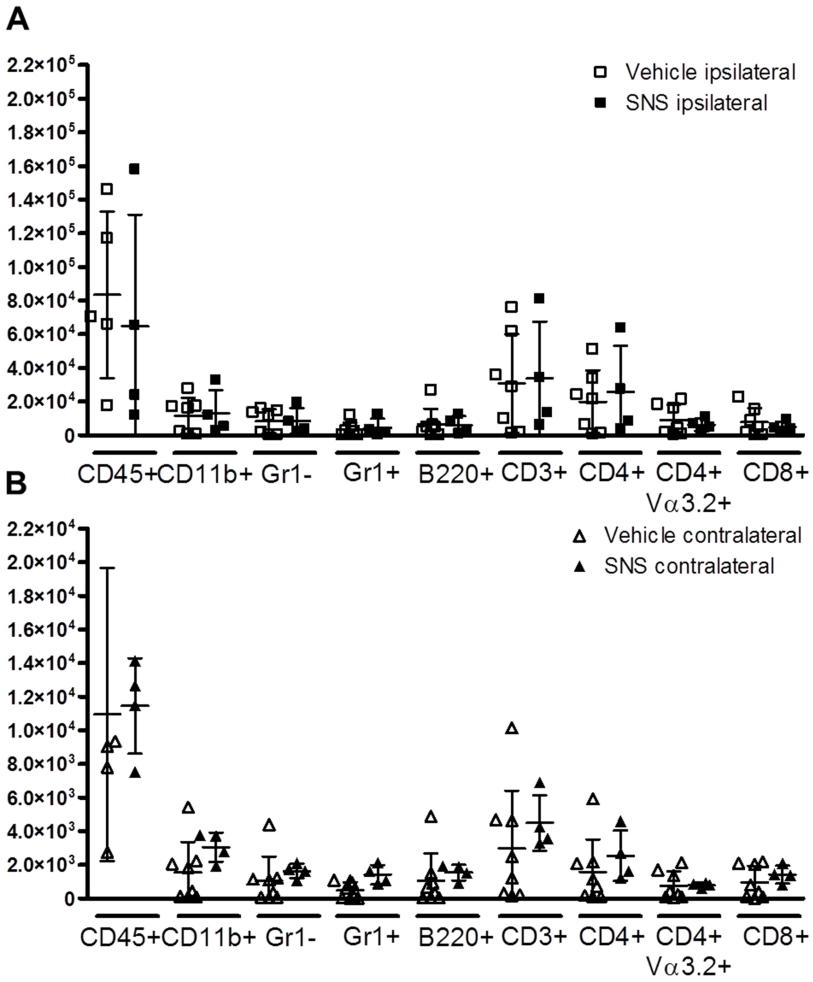

Figure 11. FACS analysis of leukocyte subpopulations from the brains of 2D2 mice which were treated with propranolol (N=4) to block the SNS axis of CIDS or vehicle (N=7) 14 days after MCAo. Enrofloxacin was not provided. Absolute numbers of leukocytes from ipsi- (***A***) and contralateral (***B***) hemispheres are presented. Blocking SNS axis of CIDS with propranolol neither affected the numbers of myeloid ($CD11b^+$, $CD11b^+$ $Gr1^-$ monocytes/macrophages, $CD11b^+$ $Gr1^+$ granulocytes) nor lymphoid cells ($B220^+$ B cells, $CD3^+$ T cells, $CD4^+$ helper T cells, $CD4^+$ $V\alpha3.2^+$ MOG-specific helper T cells and $CD8^+$ effector T cells) infiltrating brain ipsi- and contralateral hemisphere. Abbreviations: SNS, sympathetic nervous system block group.

Detailed analysis of the composition of brain infiltrating leukocytes revealed that 2D2 mice from vehicle and SNS block groups did not differ in terms of ipsi- and contralateral infiltration of $CD11b^+$ myeloid cells ($CD11b^+$ $Gr1^-$ monocytes/macrophages, $CD11b^+$ $Gr1^+$ granulocytes) and $CD11b^-$ lymphoid cells ($B220^+$ B cells, $CD3^+$ T cells and its subtypes $CD4^+$ helper T cells, $CD4^+$ $V\alpha3.2^+$ 2D2 transgenic helper T cells, cytotoxic $CD8^+$ T cells) in experiments where enrofloxacin was not provided (Figure 11A and B).

This held true also for experiments where enrofloxacin was preventively administered to minimize the likelihood of infections (Figure 12A and B). Analysis included $B220^+$ B cells, $CD3^+$ T cells, further divided into $CD4^+$ helper T cells and $CD8^+$ cytotoxic T cells, $V\alpha3.2^+$ transgenic MOG-specific $CD4^+$ and $CD8^+$ T cells, antigen-experienced $CD44^+$ transgenic,

MOG-specific $CD4^+$ and $CD8^+$ T cells, and $CD25^+$ regulatory MOG-specific T cells. In addition to lymphocytes, the $CD11b^+$ myeloid cells were analyzed ($CD11b^+$ $Gr1^-$ monocytes/macrophages and $CD11b^+$ $Gr1^+$ granulocytes). Comparisons of 2D2 mice that received half a dose of propranolol (3x15 mg/kg) with those that received full dose (3x30 mg/kg) revealed increased migration of T cells ($CD3^+$) and subsequently $CD4^+$ helper T cells and $CD8^+$ cytotoxic T cells to the ipsilateral hemisphere of mice receiving full dose of propranolol.

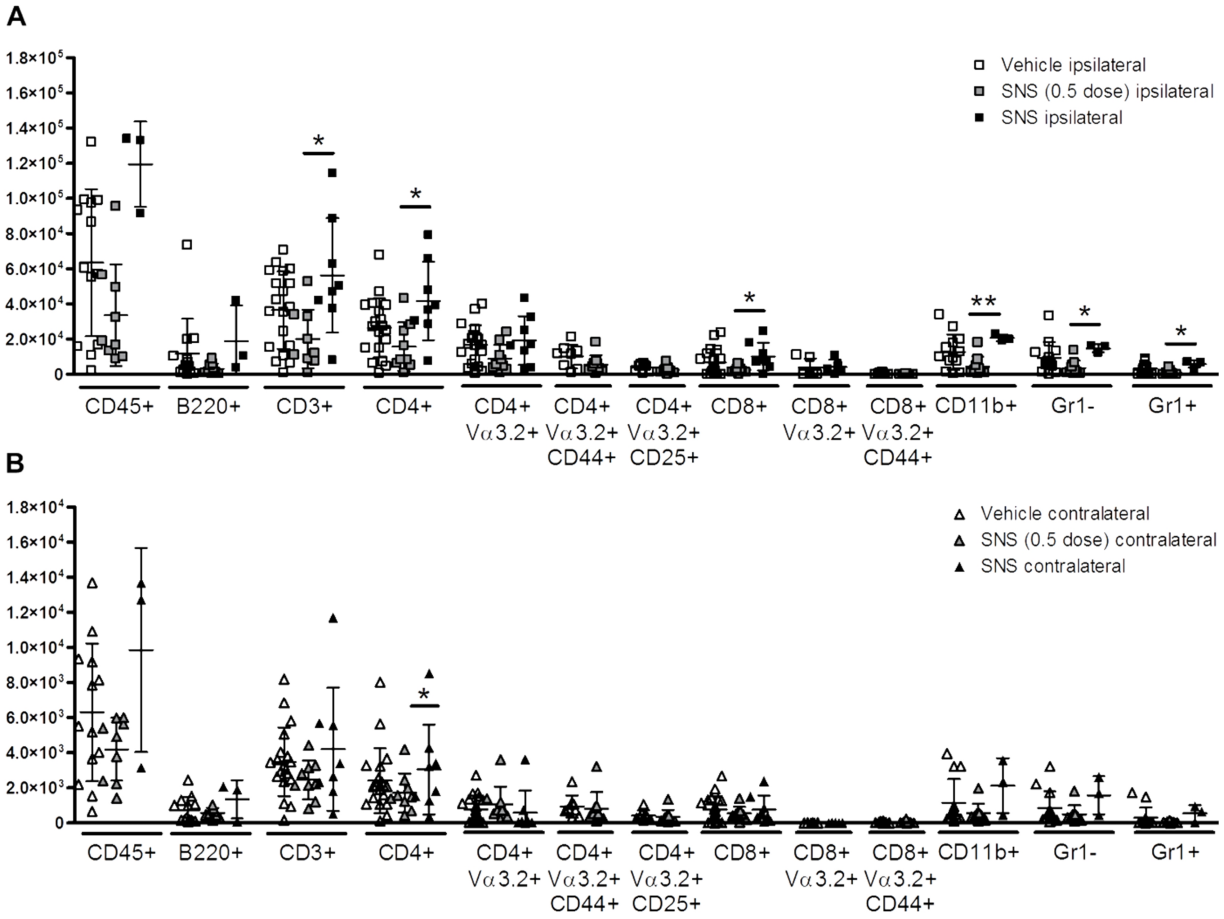

Figure 12. FACS analysis of leukocyte subpopulations in the brains of 2D2 mice which were treated with propranolol to block the SNS axis of CIDS (0.5 dose; N=9; full dose, N=3-8) or vehicle (N=13-19) 14 days after MCAo. All mice received enrofloxacin. Absolute numbers of leukocytes from ipsilateral (***A***) and contralateral (***B***) hemispheres are presented. Vehicle and SNS block groups differed from each other neither ipsi- nor contralaterally regarding analyzed cellular subsets. ***A***, Some differences were found in ipsilateral hemisphere infiltrating leukocytes between the mice receiving 0.5 dose and full dose of propranolol (all analyzed with Mann-Whitney *U*-test). These included $CD3^+$ T cells (U=11.0; p=0.015), $CD4^+$ helper T cell (U=10.0; p=0.011) and $CD8^+$ cytotoxic T cell populations (U=10.0; p=0.011). Also $CD11b^+$ myeloid cells (U=0.0; p=0.009), $CD11b^+$ $Gr1^-$ monocytes/macrophages (U=1.0; p=0.018) and $CD11b^+$ $Gr1^+$ granulocytes (U=1.0; p=0.018) were found in greater numbers in the ipsilateral hemsiphere of mice receiving full dose of propranolol. ***B***, Contralaterally, 2D2 mice receiving full dose of propranolol had less $CD4^+$ $V\alpha3.2^+$ MOG-specific helper T cells compared with those receiving only 0.5 dose of the substance (Mann-Whitney *U*-test, U=14.0; p=0.036). Abbreviations: SNS, sympathetic nervous system block group. *, $p<0.05$; **, $p<0.01$.

These mice had also a higher infiltration of myeloid cells, monocytes/macrophages ($CD11b^+$ $Gr1^-$) and granulocytes ($CD11b^+$ $Gr1^+$) to the ipsilateral hemisphere (Figure 12A). Leukocyte infiltration to brain in vehicle and propranolol-treated mice was not affected by enrofloxacin.

To investigate whether lack of β2-AR could influence leukocyte infiltration to brain, composition of brain infiltrating MNCs in β2-AR ko mice and their wild-type littermate controls was analyzed with FACS 14 days after MCAo. Enrofloxacin was not provided. No differences in infiltrating $CD11b^+$ myeloid cells, $B220^+$ B cells, $CD3^+$ T cells, $CD4^+$ helper T cells, $CD8^+$ cytotoxic T cells, and antigen-experienced ($CD44^+$) $CD4^+$ and $CD8^+$ T cells were observed (Figure 13A and B). The numbers of different leukocytes in brain corresponded well with those from vehicle- and propranolol-treated 2D2 mice.

Therefore, the quantities of leukocytes infiltrating brain, including those of MOG TCR transgenic $CD4^+$ T cells, were not affected by lack of β2-AR or blocking SNS mediated CIDS with propranolol.

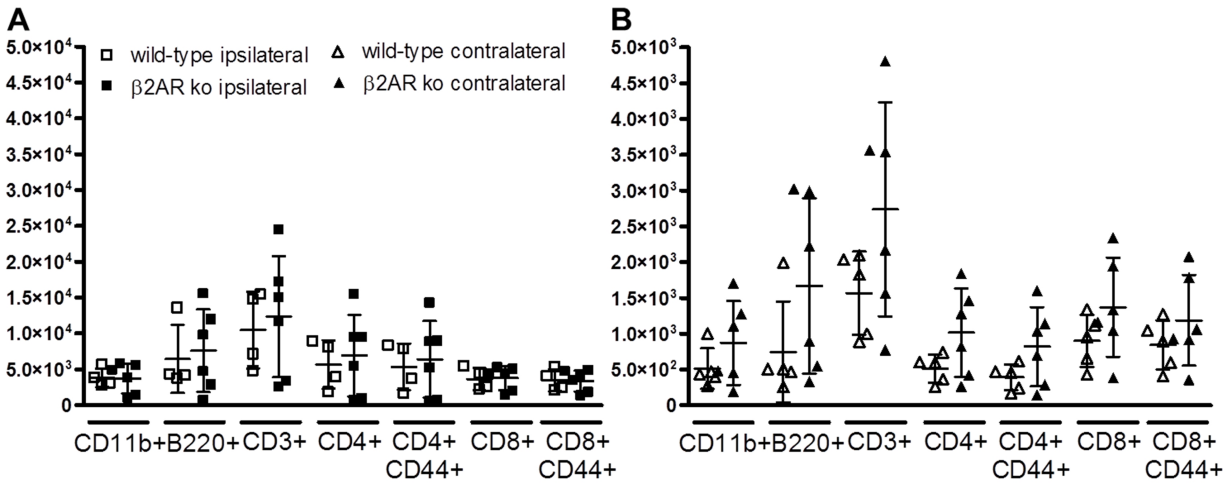

Figure 13. FACS analysis of leukocyte subpopulations in the brains of β2-AR ko mice (N=6) and their wild-type littermates (N=4-5) 14 days after MCAo. Enrofloxacin was not provided. Absolute numbers of leukocyte subpopulations from ipsilateral (***A***) and contralateral (***B***) hemispheres were similar between β2-AR ko mice and their wild-type littermates. Abbreviations: β2-AR ko, β2-adrenoreceptor knockout. *, $p<0.05$.

5.1.10 SNS block with propranolol increased Th1-type autoreactive myelin oligodendrocyte glycoprotein specific immune responses in the ischemic brain

To assess the autoreactive potential of brain infiltrating leukocytes after propranolol and vehicle treatment, equal number of brain MNCs, harvested 14 days after MCAo from 2D2

mice, were subjected to ELISpot assay. Responses to MOG-peptide ($pMOG_{35-55}$) stimulation with interferon-gamma (IFN-γ), interleukin-4 (IL-4) and IL-17 secretion were monitored.

Results from ELISpot demonstrated that the number of brain MNCs responding to MOG-stimulation with IFN-γ secretion was higher in the ipsilateral hemisphere of the mice where SNS mediated CIDS was blocked with propranolol (Figure 14A and D). Hence, indicating higher CNS-antigen specific Th1-type autoreactive potential. The number of brain MNCs reacting to peptide stimulation with IL-4 (signature cytokine for Th2 cells) or IL-17 production (Th17 cells) was not affected by treatment (Figure 14B, C, E, and F).

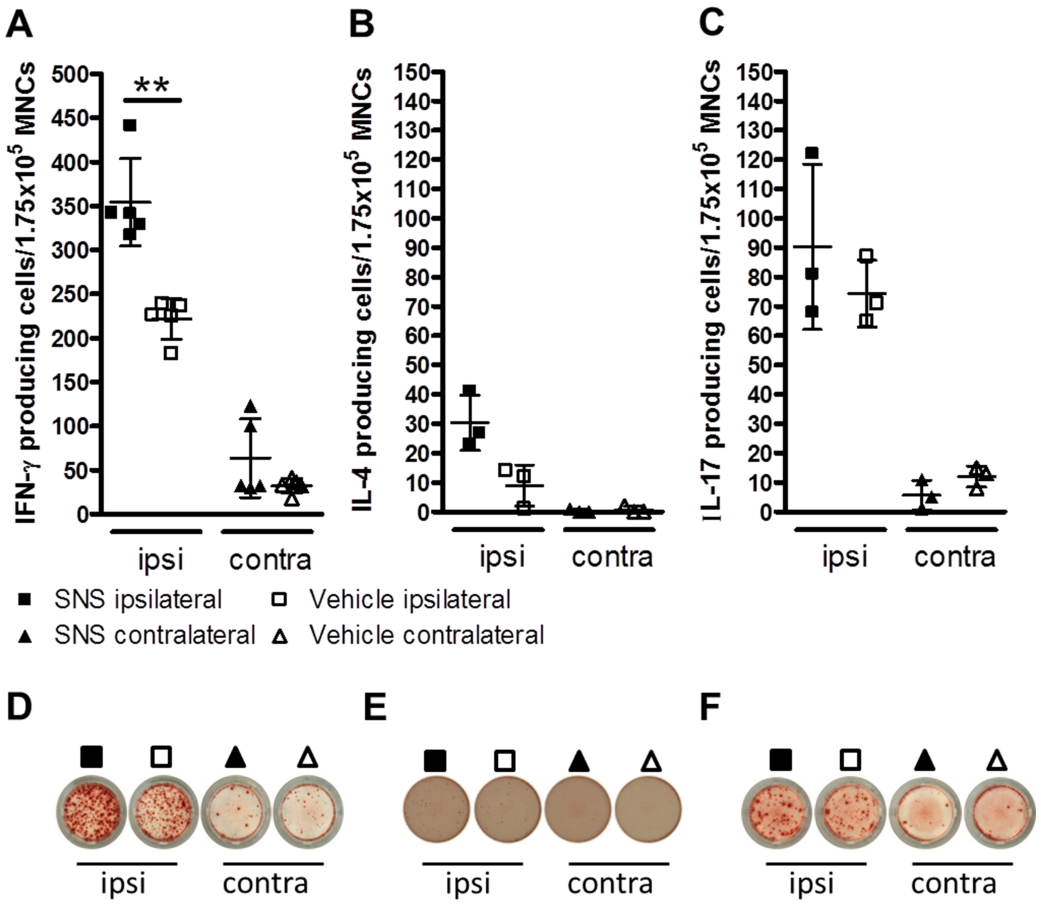

Figure 14. ELISpot analysis of numbers of MOG-reactive cells per 1.75x10^5 brain MNCs secreting IFN-γ (*A*), IL-4 (*B*) and IL-17 (*C*) in 2D2 mice treated with propranolol, to block the SNS axis of CIDS, or vehicle, 14 days after MCAo. Enrofloxacin was not provided. ***A***, Blocking SNS axis of CIDS increased ipsilaterally the number of brain MNCs responding to $pMOG_{35-55}$ stimulation with IFN-γ secretion [individual repetitions: 2 (first with vehicle, N=8; SNS block, N=7; second with vehicle, N=5; SNS block, N=6; number of wells analyzed: vehicle, N=5; SNS block; N=5; Mann-Whitney *U*-test, *U*=0.0; *p*=0.008]. The numbers of MOG-specific IL-4 (***B***) and IL-17 (***C***) producing cells were neither ipsi- nor contralaterally affected by blocking SNS axis of CIDS [individual repetitions: 1 (vehicle, N=8; SNS block, N=7); number of wells analyzed: vehicle, N=3; SNS block; N=3]. Representative images of ELISpot wells showing brain MNCs reacting to $pMOG_{35-55}$ stimulation with IFN-γ (***D***), IL-4 (***E***) or IL-17 (***F***) secretion. Abbreviations: Contra, contralateral; IFN-γ, interferon-gamma; IL-4, interleukin 4; IL-17, interleukin 17; ipsi, ipsilateral; $pMOG_{35-55}$, peptide fragment (amino acids 35-55) from myelin oligodendrocyte glycoprotein; SNS, sympathetic nervous system block group. **, p<0.01.

5.2 The combined role of sympathetic nervous system (SNS) and hypothalamic-pituitary-adrenal (HPA) axis in CNS antigen specific immune responses

5.2.1 Combined block of SNS and HPA axis with propranolol and mifepristone improved survival and health status in female 2D2 and C57Bl/6J mice

Basic original injection schemes for blocking either SNS or HPA axis of CIDS with propranolol or mifepristone (both 3x30 mg/kg), respectively, have been published (Prass et al., 2003). However, I established an optimized injection solution preparation protocol for mifepristone which lead to a very high dissolution in diluent. Consequently, I conducted a dose finding study with the minimum of 3x20 mg/kg and a maximum of 3x30 mg/kg. Particularly male mice were sensitive to the high doses of mifepristone. This served as an argument to conduct further experiments in female mice.

In a first set of experiments female 2D2 mice were administered 3x30 mg/kg propranolol and 3x30 mg/kg mifepristone together with preventive antibiotic according to the scheme (Figure 1A) and their health status was monitored. The acute mortality among treated mice within the first 24 h after MCAo was high (Figure 15A), probably due to direct toxicity from the treatment applied. This might arise from missing stress response and body's need to activate the cardiovascular system which is blocked.

In further experiments a dose of 3x20 mg/kg mifepristone was used. 2D2 mice where SNS and HPA mediated CIDS was simultaneously blocked with 3x30 mg/kg propranolol and 3x20 mg/kg mifepristone (referred to as SNS&HPA block group in the following passages) showed a trend towards improved acute survival 24 h after MCAo (SNS&HPA block, 3x30 mg/kg mifepristone, 66.7%; SNS&HPA block, 3x20 mg/kg mifepristone, 90.0%; Chi square=3.3, df=1, p=0.070; Figure 15A, B and C). Moreover, 2D2 mice from SNS&HPA block group survived over the 30-day observation period better compared with vehicle group (Figure 15B), had subsequently better health status and faster recovery (Figure 15E). 2D2 and C57Bl/6J mice from SNS&HPA block group maintained their physiological temperatures after MCAo whereas vehicle-treated mice were prone to hypothermia (Figure 15K and L).

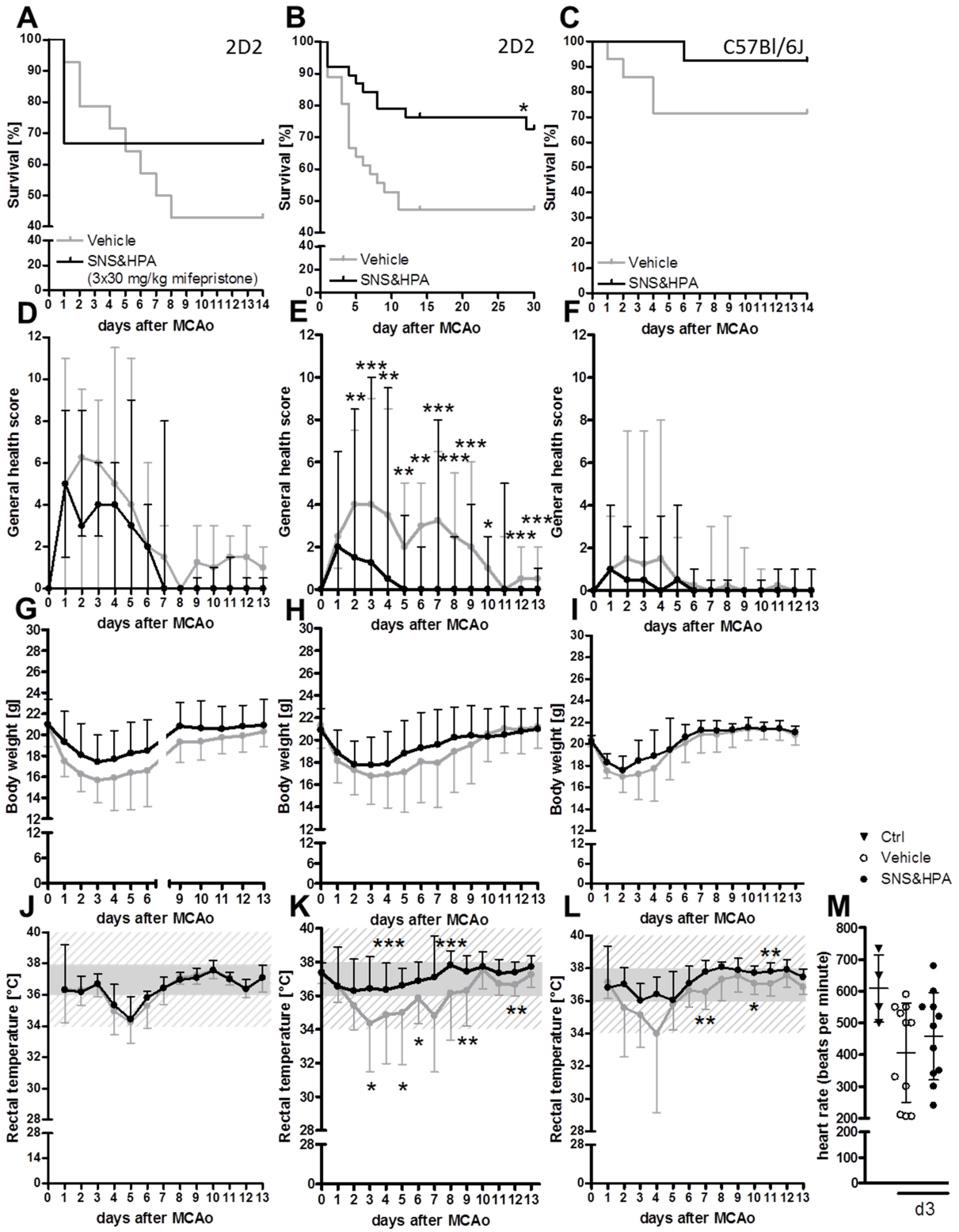

Figure 15. Simultaneous blocking of SNS and HPA axes of CIDS (SNS&HPA block group) improved long-term survival and promoted faster recovery from stroke compared with vehicle treatment (vehicle group). Preventive enrofloxacin was provided. ***A***, ***D***, ***G***, ***J***, Female 2D2 mice: ***A***, survival (vehicle, N=14; SNS&HPA block, N=12), ***D***, general health score (vehicle, N=11; SNS&HPA block, N=9), ***G***, body weight loss and ***J***, rectal temperature (for both: vehicle, N=13; SNS&HPA block, N=9) between vehicle and SNS&HPA block group where a treatment regime of 3x30mg/kg propranolol and 3x30mg/kg mifepristone was applied. ***B***, ***E***, ***H***, ***K***, Female 2D2 mice: ***B***, survival (vehicle, N=35; SNS&HPA block, N=39), ***E***, general health score (vehicle, N=20; SNS&HPA block, N=29), ***H***, body weight loss and ***K***, rectal temperature (for both: vehicle, N=31; SNS&HPA block, N=36) between vehicle and SNS&HPA block group, corresponding to treatment

regime of 3x30mg/kg propranolol and 3x20mg/kg mifepristone. Mice from SNS&HPA block group were characterized by improved survival for up to 30 days after MCAo (vehicle, 49%; SNS&HPA block, 72%; Chi square=4.4, df=1, p=0.037; ***B***). Mice from SNS&HPA block group had better health status, demonstrated by lower general health scores, and faster recovery compared with mice from vehicle group (***D***; Mann-Whitney *U*-test: day 2: U=116.5; p=0.003; day 3: U=108.5; p=0.001; day 4: U=76.5; p=0.006; day 5: U=61.0; p=0.002; day 6: U=61.0; p=0.003; day 7: U=52.5; p<0.0005; day 8: U=47.0; p=0.001; day 9: U=35.5; p<0.0005; day 10: U=52.0; p=0.018; day 12: U=42.0; p=0.001; day 13: U=46.5; p=0.004). Vehicle-treated mice developed hypothermia after MCAo whereas mice from SNS&HPA block group maintained physiological temperatures (***H***; Mann-Whitney *U*-test: day 3: U=428.5; p=0.031; day 4: U=278.5; p=0.001; day 5: U=257.5; p=0.024; day 6: U=227.5; p=0.023; day 8: U=165.0; p=0.001; day 9: U=155.5; p=0.008; day 12: U=122.5; p=0.004). ***C***, ***F***, ***I***, ***L***, Female C57Bl/6J mice: ***C***, survival (vehicle, N=14; SNS&HPA block, N=13), ***F***, general health score (vehicle, N=11; SNS&HPA block, N=13), ***I***, body weight loss and ***L***, rectal temperature (for both: vehicle, N=13; SNS&HPA block, N=13) between vehicle and SNS&HPA block group. Rectal temperatures between the groups differed also in C57Bl/6J mice (Mann-Whitney *U*-test: day 7: U=17.0; p=0.003; day 10: U=24.5; p=0.017; day 11: U=21.0; p=0.008). ***M***, Heart rate (beats per minute), measured three days after MCAo, was similar in SNS&HPA block and vehicle groups of mice and did not differ from control values from 2D2 mice. For clarity in figure, in panels ***G***, ***H***, ***I*** and ***J***, ***K***, ***L*** data from vehicle group are expressed as mean-standard deviation and in SNS&HPA block group mean+standard deviation. Optimal body temperature of a mouse is presented as a grey bar, and yet acceptable body temperature grey streaked area on a background. Abbreviations: Ctrl, control; SNS&HPA, sympathetic nervous system/hypothalamic-pituitary-adrenal axis block group. *, p<0.05; **, p<0.01; ***, p<0.001.

Health status of mice which received 3x30 mg/kg propranolol and either 3x30 mg/kg (2D2 mice) or 3x20 mg/kg mifepristone (2D2 and C57Bl/6J mice) is compared with corresponding vehicle groups in Figure 15. Heart rate (beats per minute) three days after MCAo was similar in SNS&HPA block (458±138) and vehicle (406±156) group and did not differ from those of 2D2 mice that were neither subjected to MCAo nor treated with propranolol but received preventive enrofloxacin (609±105; Figure 15M).

5.2.2 Infarct volume was smaller in female 2D2 and C57Bl/6J mice after combined SNS and HPA block with propranolol and mifepristone

Propranolol and mifepristone treatment for blocking the SNS and HPA mediated CIDS lead to 2/3 smaller infarct volume in female 2D2 mice. Reduction was robust and stable for at least seven days after MCAo suggesting that no delayed infarct maturation occurred (Figure 16A). This effect was strain independent as infarct volumes were comparably smaller after combined treatment also in female C57Bl/6J mice (Figure 16B). Infarct volume reduction in SNS&HPA block group of male C57Bl/6J mice did not reach significance one day after MCAo but became evident seven days after MCAo (Figure 16B). Dual treatment with propranolol and mifepristone was needed for clearly and robustly smaller infarct volumes. Single treatment with either propranolol or mifepristone did not show an effect with such magnitude (Figure 4 and Figure 16C).

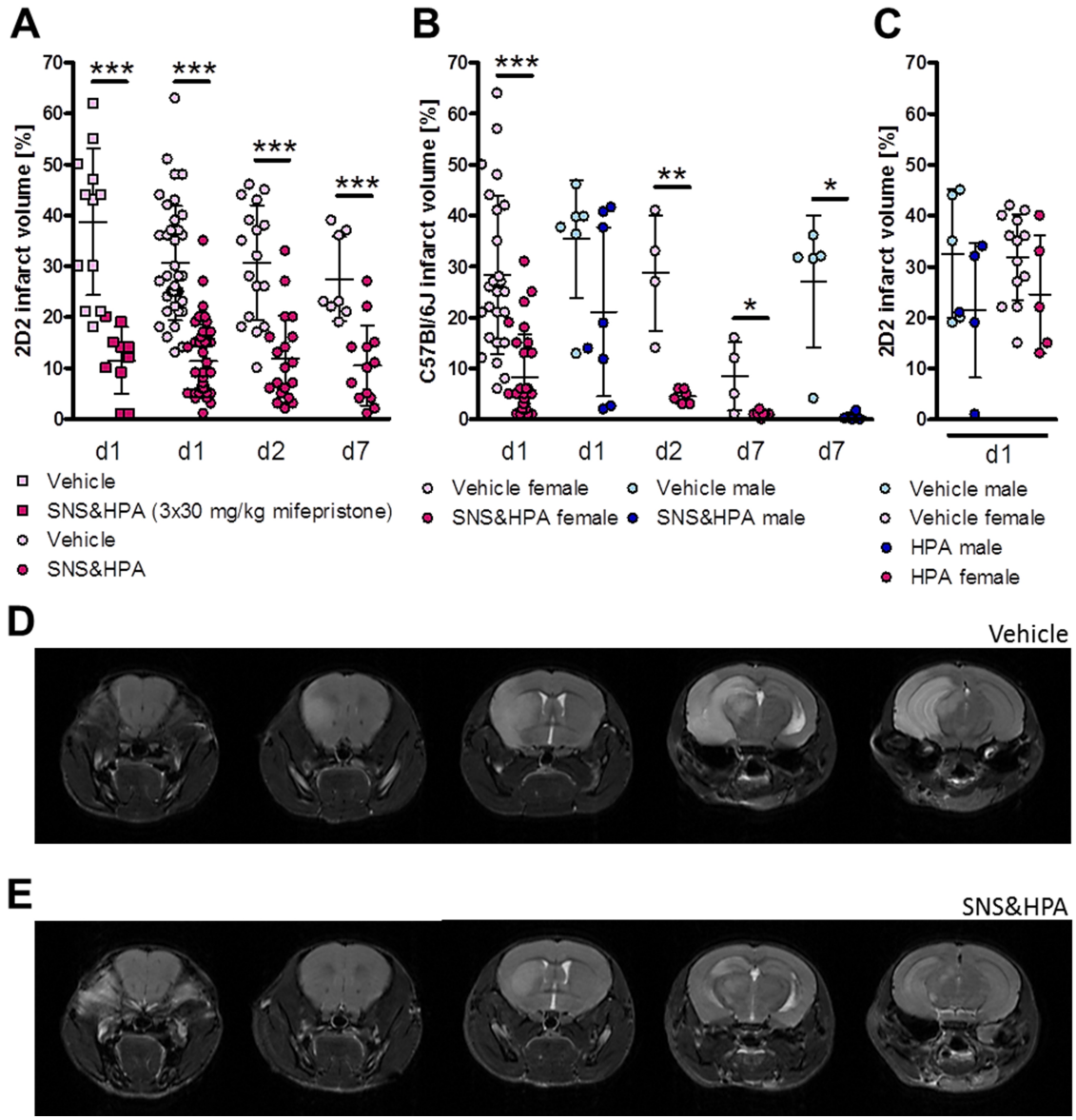

Figure 16. Blocking simultaneously SNS and HPA axes of CIDS with propranolol and mifepristone, resulted in robustly smaller infarct volume (enrofloxacin was provided). ***A***, Treatment resulted in clearly smaller infarct volumes in female 2D2 mice (day 1 after MCAo: between SNS&HPA block group receiving 3x30 mg/kg mifepristone, N=10; and vehicle group, N=12; Students' *t*-test; $t(20)=5.5$; $p<0.0005$; and between SNS&HPA block group receiving 3x20 mg/kg mifepristone, N=41; and vehicle group, N=38; $t(64)=8.1$; $p<0.0005$). The effect persisted at least seven days after MCAo (between SNS&HPA block group receiving 3x20 mg/kg mifepristone and vehicle group: day 2: vehicle, N=17; SNS&HPA block, N=19; $t(34)=5.7$; $p<0.0005$; day 7: vehicle, N=8; SNS&HPA block, N=13; $t(19)=4.7$; $p<0.0005$). ***B***, Infarct volume was smaller also in female C57Bl/6J mice that were received 3x20 mg/kg mifepristone (Mann-Whitney *U*-test; day 1: vehicle, N=25; SNS&HPA block, N=28; $U=49.0$, $p<0.0005$; day 2: vehicle, N=4; SNS&HPA block, N=6; $U=0.0$, $p=0.010$; day 7: vehicle, N=4; SNS&HPA block, N=7; $U=3.5$, $p=0.021$). In male C57Bl/6J mice, infarct volume was not significantly smaller on day 1 after MCAo (vehicle, N=6; SNS&HPA block, N=8) but 7 days after MCAo (vehicle, N=5; SNS&HPA block, N=4; Mann-Whitney *U*-test; $U=0.0$, $p=0.016$). ***C***, Blocking solely HPA axis of CIDS (enrofloxacin was not applied) did not lead to smaller infarct volumes neither in male (vehicle, N=5; HPA block, N=5) nor female 2D2 mice (vehicle, N=13; HPA block, N=5) one day after MCAo. ***D***, Vehicle-treated mice developed large thalamo-cortical ischemic lesions characteristic to a 60-minute MCAo. ***E***, Mice from SNS&HPA block group developed small ischemic foci rarely involving the cortex. Abbreviations: d, day; HPA, hypothalamic-pituitary-adrenal axis block group; SNS&HPA, sympathetic nervous system/hypothalamic-pituitary-adrenal axis block group. *, $p<0.05$; **, $p<0.01$; ***, $p<0.001$.

In addition to infarct volume, ischemic lesions in SNS&HPA block and vehicle group of mice differed anatomically. Ischemic lesions in vehicle group of mice were typical for a 60-minute MCAo (large and thalamo-cortical, as depicted in Figure 16D), whereas those in SNS&HPA block group comprised smaller ischemic foci and rarely involved the cortex (Figure 16E). Moreover, they resembled ischemic lesions from murine models of MCAo with 30-minute occlusion time [for comparison of focal ischemia filament models with 30- and 60-minute occlusion times see (Dirnagl, 2010)].

5.2.3 Altered cerebral blood flow was not the primary reason behind smaller infarcts following combined SNS and HPA block with propranolol and mifepristone

Smaller infarct volumes are often related to increased CBF (Dalkara et al., 1994). To investigate whether altered CBF was the primary reason behind the effect on infarct volumes (visible at 24 h after stroke) after simultaneous blocking of SNS and HPA axes of CIDS with propranolol and mifepristone, FAIR-MRI and DWI were performed immediately after filament insertion and 3 h after MCAo in the same mice (Figure 1B). ADC maps calculated from DWI images showed large ipsilateral lesions immediately after filament insertion. The lesions diminished within 3 h and did not differ between the groups (immediately after filament insertion: vehicle, 102±37.5 mm^3; SNS&HPA block, 86.7±51.0 mm^3; 3 h after MCAo: vehicle, 51.8±44.3 mm^3; SNS&HPA block, 33.5±31.4 mm^3; Figure 17A and B). To differentiate between the effects of pharmaceutical CIDS block and MCAo, a group of mice was treated according to the scheme (Figure 1A) and subjected to a sham-surgery. ADC lesions were small and did not differ between the vehicle and SNS&HPA block groups of sham-operated C57Bl/6J mice (Figure 17C). CBF in ipsilateral hemisphere of female C57Bl/6J mice from both groups was strongly reduced following MCAo but was not affected by pharmaceutical blocking of CIDS [immediately after filament insertion: vehicle, ipsilaterally 0.04±0.49 and contralaterally 2.21±1.07 ml/(g*min); SNS&HPA block, ipsilaterally 0.22±0.25 and contralaterally 1.65±1.17 ml/(g*min); 3 h after MCAo: vehicle, ipsilaterally 0.49±0.32 and contralaterally 2.02±0.32 ml/(g*min); SNS&HPA block, ipsilaterally 0.48±0.60 and contralaterally 1.49±0.79 ml/(g*min); Figure 17D]. Data from sham-operated mice demonstrated that treatment alone had no effect on hemispheric CBF. CBF values neither differed between the ipsi- and contralateral hemisphere nor between the treatment groups (Figure 17E). Examples of CBF and ADC lesion size from the same C57Bl/6J mouse immediately after filament insertion are shown in Figure 17F and G.

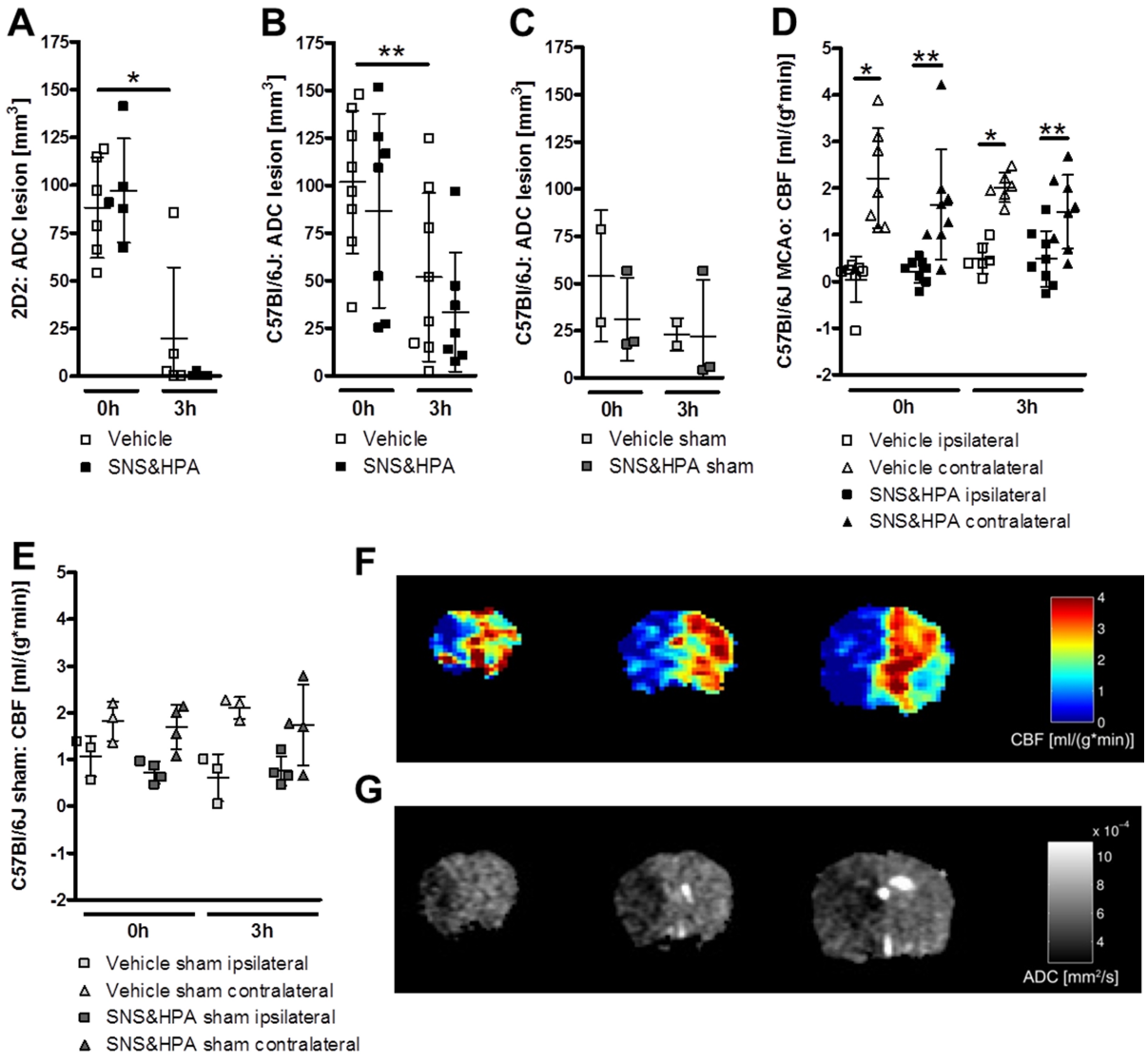

Figure 17. Altered CBF was not the primary reason behind clearly smaller infarct volumes after blocking simultaneously SNS and HPA mediated CIDS. ***A***, ADC lesions in female 2D2 mice (vehicle, N=7; SNS&HPA block, N=5) immediately after filament insertion and 3 h after MCAo. Reduction in ADC lesion size in vehicle group was significant (Wilcoxon test; *Z*=-2.2, *p*=0.031). ***B***, ADC lesions in female C57Bl/6J mice (vehicle, N=8; SNS&HPA block, N=7) at same time points. ADC lesion reduction within three hours in vehicle group was significant (Wilcoxon test; *Z*=-2.3, *p*=0.008). ***C***, ADC lesion sizes in sham-operated C57Bl/6J mice within and between the groups did not differ. ***D***, Ipsilateral CBF was equally reduced in vehicle and SNS&HPA block group of C57Bl/6J mice immediately after filament insertion (Wilcoxon test; vehicle, N=7; *Z*=-2.4, *p*=0.016, SNS&HPA block, N=8; *Z*=-2.5, *p*=0.008) and 3 h after MCAo (vehicle, N=6; *Z*=-2.2, *p*=0.031, SNS&HPA block, N=8; *Z*=-2.5, *p*=0.008). ***E***, Ipsi- and contralateral CBF in sham-operated mice (vehicle, N=3; SNS&HPA block, N=4) within and between the groups did not differ. ***F***, CBF map immediately after MCAo, illustrating diminished blood flow ipsilateral to MCAo. ***G***, ADC map from the same animal, demonstrating lesion in left hemisphere. Abbreviations: ADC, apparent diffusion coefficient; CBF, cerebral blood flow; SNS&HPA, sympathetic nervous system/hypothalamic-pituitary-adrenal axis block group. *, $p<0.05$; **, $p<0.01$.

5.2.4 Combined SNS and HPA block with propranolol and mifepristone improved survival and promoted recovery of mice with bronchopulmonary infections

In order to analyze if, in spite of preventive enrofloxacin treatment, infections contributed to the hypothermia and high mortality in vehicle group of mice between days three and ten after MCAo, the BAL fluid was collected three days after MCAo for microbiological analysis. Infection was diagnosed when CFU/ml (LOG10) in BAL fluid exceeded five. Trachea and emerging bronchi in these mice were covered with a thicker layer of mucus compared with healthy animals. Average bacterial load in the bronchi was similar in vehicle [4.0±1.9 CFU/ml (LOG10)] and SNS&HPA block group of female 2D2 mice [3.7±1.7 CFU/ml (LOG10)], did not differ from those of sham-operated mice (Figure 18A). However, single mice developed a bacterial burden in the BAL fluid where the CFU/ml (LOG10) was above 5.

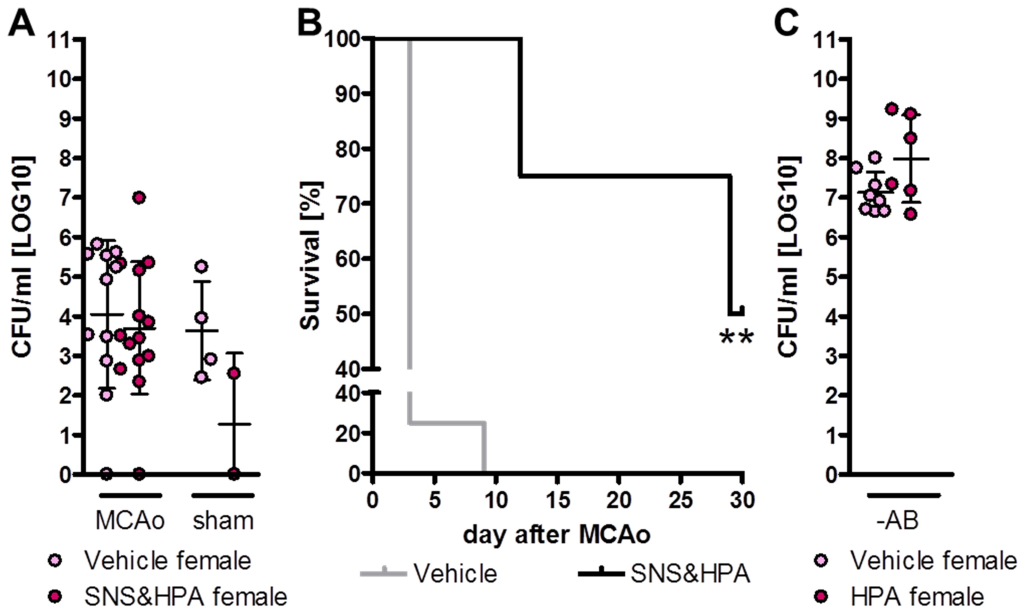

Figure 18. Bacterial load in BAL fluid was similar in vehicle and SNS&HPA block group of female 2D2 mice. Blocking CIDS with propranolol and mifepristone promoted recovery and elongated the life expectancy of infected mice (CFU/ml BAL fluid (LOG10) above five). ***A***, 2D2 mice from vehicle (N=11) and SNS&HPA block (N=14) group (preventive enrofloxacin was provided) did not differ from each other and sham-operated 2D2 mice (vehicle, N=4; SNS&HPA block, N=2) in terms of the bacterial burden in BAL fluid. ***B,*** Mice from SNS&HPA block group with infection, identified by CFU/ml BAL fluid being above 5 (LOG10) on panel ***A*** (N=5) recovered or had elongated life expectancy compared with vehicle treated mice (N=4) over 30 days after MCAo (Chi square=7.6, df=1, p=0.006). ***C***, HPA block alone with 3x30 mg/kg mifepristone (vehicle, N=8; SNS&HPA block, N=6; without preventive enrofloxacin) had no effect on bacterial load in the BAL fluid of female 2D2 mice. Abbreviations: CFU, colony forming units; HPA, hypothalamic-pituitary-adrenal axis block group; SNS&HPA, sympathetic nervous system/hypothalamic-pituitary-adrenal axis block group.**, p<0.01.

Blocking SNS and HPA mediated CIDS with propranolol and mifepristone promoted recovery and elongated life expectancy of mice with bronchopulmonary infections (Figure 18B). Blocking HPA axis of CIDS with 3x30 mg/kg mifepristone had no effect on bacterial load in BAL fluid [vehicle, 7.1±0.5 CFU/ml (LOG10); HPA block, 8.0±1.1 CFU/ml (LOG10); Figure 18C].

In summary, blocking simultaneously SNS and HPA mediated CIDS with propranolol and mifepristone resulted in robustly smaller infarct volumes and improved recovery and survival of mice with bronchopulmonary infections.

5.2.5 Combined SNS and HPA block with propranolol and mifepristone did not worsen symptoms of experimental autoimmune encephalomyelitis reminiscent disease in 2D2 and C57Bl/6J mice

Beyond the initial hemiparesis after MCAo, 2D2 mice developed neurological symptoms that lasted over the observation period of 30 days after MCAo. This manifested as weakness or paralysis affecting hind limbs and tail. Eighty seven percent of vehicle and 91% of mifepristone and propranolol treated female 2D2 mice developed EAE-like symptoms within 30 days after MCAo. By day 13 after MCAo, EAE-like disease was developed by 76% of mice in vehicle and 45% of mice in SNS&HPA block group. The median onset of symptoms was day 14 in SNS&HPA block group and day 9 in vehicle group. Disease progression was similar in both groups and surviving mice reached a median final score of 2 (corresponding to a hind limb weakness with or without tail paralysis). This occurred a median of 6 days earlier in vehicle group (vehicle, day 23; SNS&HPA block, day 29; Figure 19A). Female C57Bl/6J mice from vehicle and SNS&HPA block groups developed milder EAE-like symptoms after MCAo than 2D2 mice (Figure 19B).

5.2.6 Combined SNS and HPA block with propranolol and mifepristone normalized elongated F-wave latencies upon sciatic nerve stimulation

Because MOG is found also in the peripheral nervous system including the sciatic nerve (Pagany et al., 2003) and resulting from the attempt to characterize the autoreactive phenotype better, sciatic nerve conduction was evaluated electrophysiologically 14 days after MCAo in 2D2 mice. Latencies to F-wave upon stimulation were elongated in vehicle group of mice (18.2±5.9 ms) compared with pre-MCAo baseline values (13.5±2.7 ms). Blocking SNS and

HPA mediated CIDS had a normalizing effect on this (latency to F-wave 14.5±4.9 ms; Figure 19C and D). Sciatic nerve conduction velocities, measured by latencies to F-wave, did not correlate with differences in EAE score between the groups 14 days after MCAo and also not with the size of ischemic lesion (data not shown). F-wave chronodispersion was not affected by MCAo and did not differ between the groups (Figure 19E).

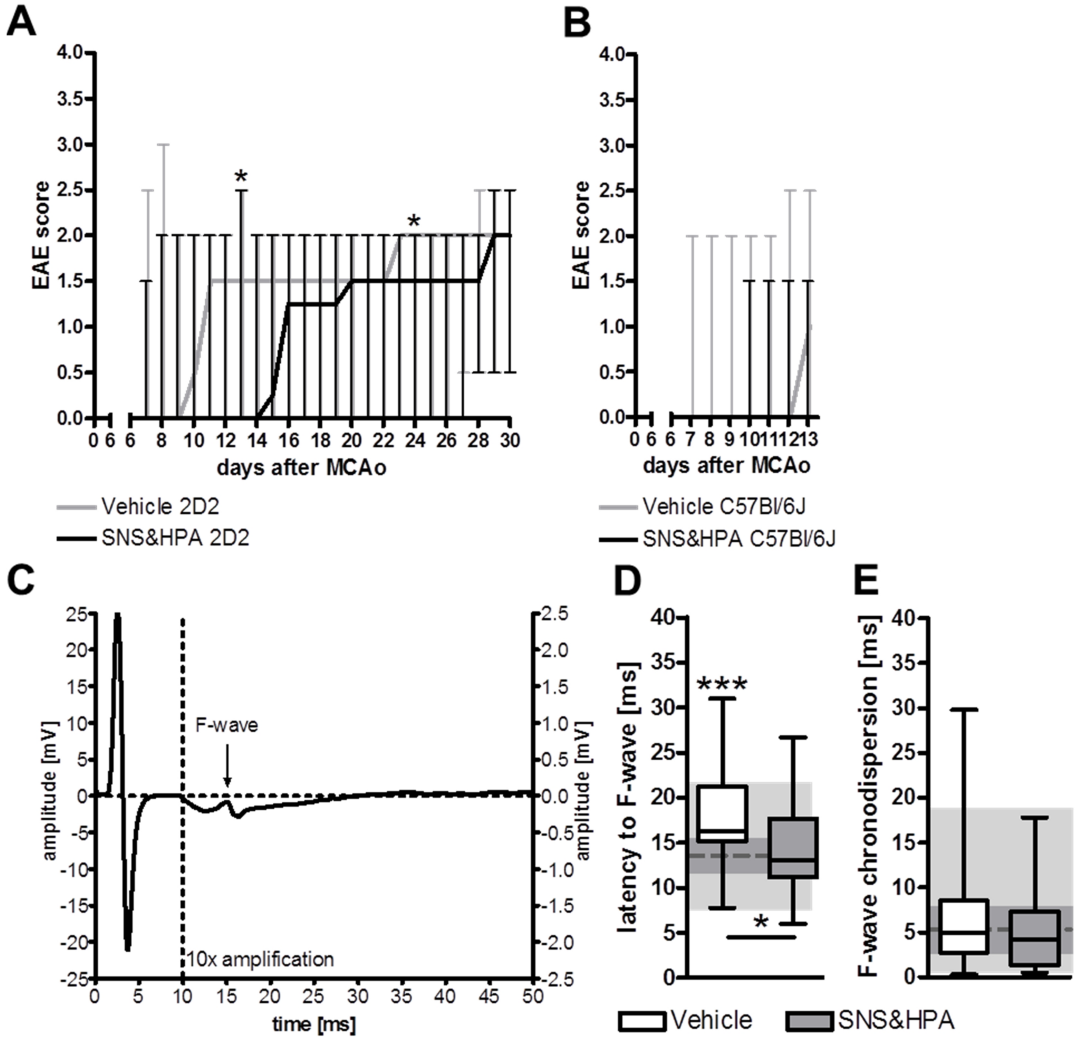

Figure 19. Blocking SNS and HPA mediated CIDS did not intensify EAE development within 30 days after MCAo and normalized the elongated latencies to F-wave upon sciatic nerve stimulation. ***A***, In spite of the median onset of EAE 5 days later in SNS&HPA block group of 2D2 mice (N=31) compared with vehicle group (N=21), the final disease severity 30 days after MCAo was similar in both groups. Differences between the groups were detected on days 13 (Mann-Whitney *U*-test, *U*=157.5; *p*=0.031) and 24 (*U*=63.5; *p*=0.047) after MCAo. ***B***, Compared with 2D2 mice, EAE symptoms were milder in C57Bl/6J mice. ***C***, Typical baseline F-wave in a 2D2 mouse from the study. ***D***, Latency to F-wave upon sciatic nerve stimulation 14 days after MCAo was elongated in vehicle group (N=24) compared with pre-MCAo (baseline) values (N=127; One-way ANOVA with Bonferroni post-hoc, *F*=13.8; *p*<0.0005) and SNS&HPA block group (N=37; *p*=0.002). Pre-MCAo baseline data are presented on a background: dotted line symbolizes the median, dark grey rectangle indicates 25th and 75th percentile and a light grey rectangle minimum and maximum values. ***E***, F-wave chronodispersion was neither affected by MCAo nor CIDS block. EAE score data are presented as median±range. Abbreviations: EAE, experimental autoimmune encephalomyelitis; MCAo, middle cerebral artery occlusion; SNS&HPA, sympathetic nervous system/hypothalamic-pituitary-adrenal axis block group. *, *p*<0.05.

5.2.7 Combined SNS and HPA block with propranolol and mifepristone reduced T cell and macrophage infiltration to peripheral nerve roots

To investigate whether myelitis contributed to observed autoreactive phenotype via CNS-antigen specific immune cell infiltration to the spinal cord, vertebral columns of 2D2 mice were collected 30 days after MCAo for immunohistochemistry. Since MOG-induced lesion pathology typically involves T cells and macrophages (Linington et al., 1993; Genain et al., 1996; Hjelmstrom et al., 1998), the cell types analyzed were T cells ($CD3^+$), macrophages ($Mac3^+$), MOG TCR trangenic $CD4^+$ T cells ($V\alpha3.2^+$) and inflamed axons (APP^+).

Immune cell infiltrates were not found in the spinal cord. Instead, they accumulated in spinal nerve roots (Figure 20A-L). Immunopositive structures were limited to specific nerve roots where they concentrated heavily. $CD3^+$ T cells and $Mac3^+$ macrophages were often found together. Quantification of the immunopositive structures revealed that infiltration of $CD3^+$ T cells (vehicle, 26.9±18.4 cells/mm^2; SNS&HPA block, 8.2±7.8 cells/mm^2) and $Mac3^+$ macrophages (vehicle, 85.1±49.4 cells/mm^2; SNS&HPA block, 52.0±47.1 cells/mm^2) was reduced in the nerve roots of animals treated with propranolol and mifepristone to block the SNS and HPA mediated CIDS compared with vehicle-treated mice (Figure 20M). Frequencies of cells with MOG TCR and APP^+ inflamed axons were similar in SNS&HPA block and vehicle groups of mice (Figure 20N). In SNS&HPA block group of mice the number of $V\alpha3.2^+$ cells per mm^2 spinal nerve root was associated with higher number of inflamed axons (APP^+) (Figure 20O).

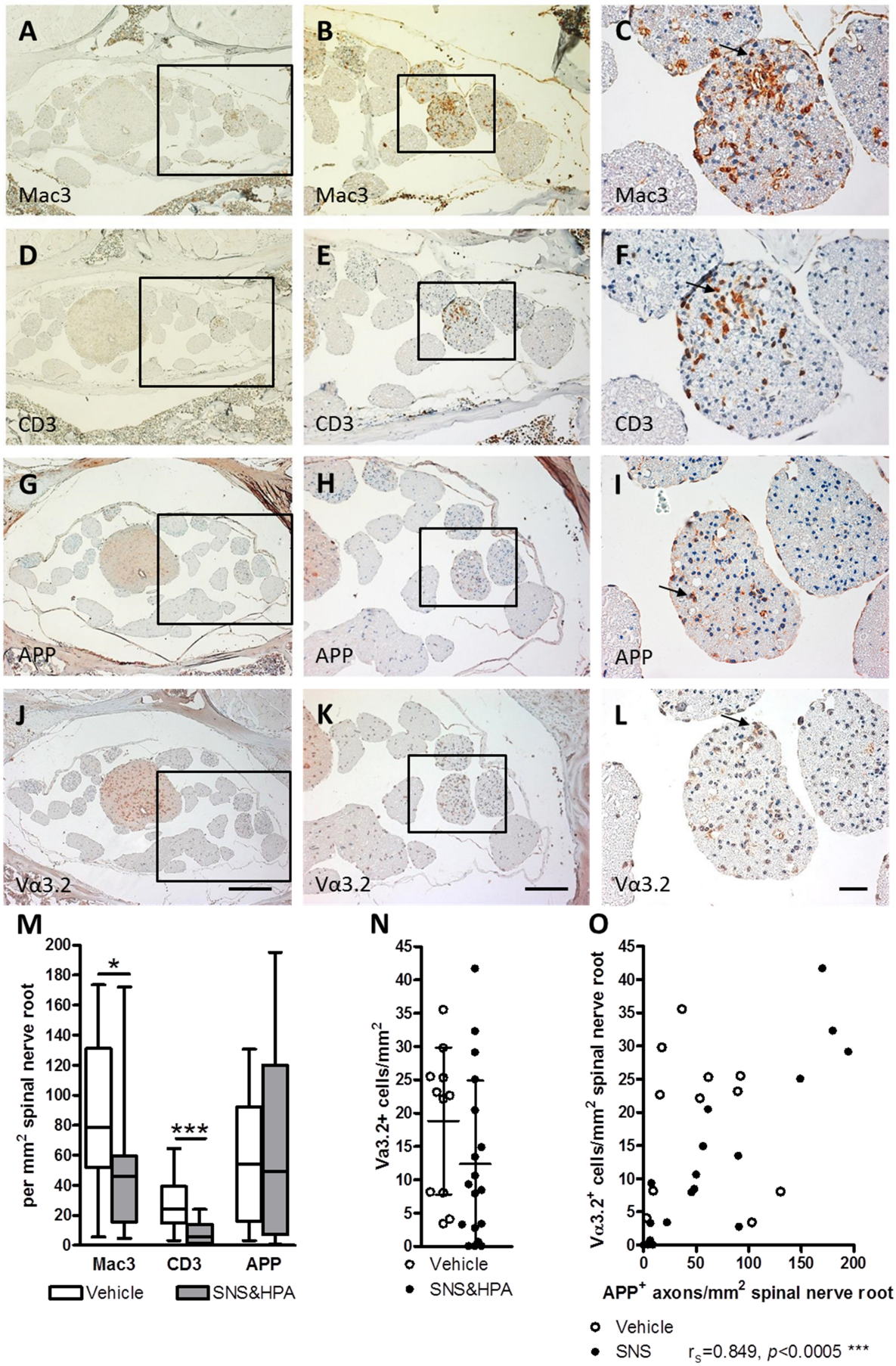
A
Mac3
B
Mac3
C
Mac3
D
CD3
E
CD3
F
CD3
G
APP
H
APP
I
APP
J
Vα3.2
K
Vα3.2
L
Vα3.2
M
per mm2 spinal nerve root
200
180
160
140
120
100
80
60
40
20
0
*
***
Mac3
CD3
APP
Vehicle
SNS&HPA
N
Va3.2+ cells/mm2
45
40
35
30
25
20
15
10
5
0
Vehicle
SNS&HPA
O
Vα3.2+ cells/mm2 spinal nerve root
45
40
35
30
25
20
15
10
5
0
0
50
100
150
200
APP+ axons/mm2 spinal nerve root
Vehicle
SNS
rs=0.849, p<0.0005 ***

Figure 20. Infiltration of T cells and macrophages to peripheral nerve roots was reduced after blocking of SNS and HPA axis mediated CIDS with propranolol and mifepristone (N=18) compared with vehicle treatment (N=11). Microphotographs demonstrating Mac3 (macrophages; ***A***), CD3 (T cells; ***D***), APP (inflamed axons; ***G***) and Vα3.2 (MOG TCR; ***J***) staining of 2D2 mouse vertebral columns at sacral level where most of the *cauda equina* locates. Areas outlined in ***A***, ***D***, ***G*** and ***J*** are magnified in ***B***, ***E***, ***H***, ***K*** and further in ***C***, ***F***, ***I***, ***L***, respectively. Arrows on ***C***, ***F***, ***I*** and ***L*** indicate immunostained cells (Mac3, CD3, Vα3.2) and axons (APP). ***M***, Blocking simultaneously the SNS and HPA axis mediated CIDS reduced the number of $CD3^+$ T cells (Mann-Whitney U=27.0, p=0.001) and $Mac3^+$ macrophages (Mann-Whitney U=51.0, p=0.031) in the nerve roots of 2D2 mice 30 days after MCAo. ***O***, There was no significant difference between the number of $V\alpha3.2^+$ cells per mm^2 spinal nerve root between the groups. ***N***, The number of APP^+ inflamed axons per mm^2 spinal nerve root correlated with that of $V\alpha3.2^+$ cells in SNS&HPA block group of mice (Spearman's rank-order correlation). Scale bars in ***A***, ***D***, ***G***, ***J***, 200 µm; in ***B***, ***E***, ***H***, ***K***, 100 µm; in ***C***, ***F***, ***I***, ***L***, 20 µm. Abbreviations: SNS&HPA, sympathetic nervous system/hypothalamic-pituitary-adrenal axis block group. *, p<0.05; ***, p<0.001.

5.2.8 Combined SNS and HPA block with propranolol and mifepristone did not aggravate long-term locomotor deficits

Symptoms of CNS-directed autoreactive immune responses might develop over a longer period following initializing event. To detect subtle locomotor differences between 2D2 mice from vehicle and SNS&HPA block group their gait was analyzed before MCAo, 10 and 30 days after MCAo. Typical stroke-induced alterations in male C57Bl/6J mice (Hetze et al., 2012) like decreased maximum contact areas and stride lengths, increased stand times and increased base of support (distance between front or hind paws) were observed 10 days after MCAo in both groups of female 2D2 mice (Table 2). Blocking simultaneously SNS and HPA mediated CIDS did not intensify or introduce new gait impairments. Nevertheless, 30 days after MCAo the gait of 2D2 mice from SNS&HPA block group deviated more from pre-MCAo baseline values (Table 2). This affected duration of a paw contact with a glass plate and distances between successive steps with one paw (Figure 21). Mid-term (10 days after MCAo) post-MCAo alterations in gait were additionally analyzed in female C57Bl/6J mice following simultaneous blocking of SNS and HPA axes of CIDS. Ten days after MCAo vehicle and SNS&HPA block groups of mice did not differ in gait, confirming the observations in 2D2 mice (Table 2).

Therefore, long-term (30 days after MCAo) analysis of functional and neurological outcome demonstrated that simultaneous blocking of SNS and HPA axes of CIDS with propranolol and mifepristone neither aggravated locomotor deficits nor enhanced CNS inflammation.

Table 2. CatWalk gait analysis of female 2D2 and C57Bl/6J mice before, 10 and 30 days after MCAo. Mice received enrofloxacin preventively.

Parameter	Definition	Paw	2D2					C57Bl/6J		
			Baseline	Vehicle 10 days after MCAo	SNS&HPA 10 days after MCAo	Vehicle 30 days after MCAo	SNS&HPA 30 days after MCAo	Baseline	Vehicle 10 days after MCAo	SNS&HPA 10 days after MCAo
Spatial characteristics										
Max contact area (mm^2)	Area of a paw print at maximal plate contact	RF	26,25±13,82	16,70±7,306 ***	16,42±5,730 ***	15,53±6,801 ***	18,00±6,306 **	17.06±2.653	15.60±3.935	16.01±5.287
		RH	19,82±14,68	12,92±6,435 *	11,79±5,158 **	13,99±8,764	15,51±6,447 #	16.02±3.310	13.12±4.818	12.69±5.544
		LF	26,89±14,05	19,00±5,348 **	18,79±6,448 ***	18,77±5,564 **	21,59±6,505 *	17.52±2.779	16.79±3.995	18.87±4.539
		LH	19,73±14,06	14,51±5,684 *	15,51±8,000	17,42±9,744	22,00±10,09 #	17.67±3.956	17.30±4.965	18.81±4.623
Kinetic characteristics										
Run duration (s)	Time for passing the walkway		2,120±0,562	2,798±0,664 ***	2,559±0,683 **	2,666±0,539 **	2,759±0,564 ***	2.074±0.404	2.802±0.628 ***	2.891±0.473 ***
Normalized swing speed (s)	Swing speed*Run duration	RF	1167±235,4	998,9±212,5 **	973,0±258,5 **	939,4±186,9 ***	931,1±179,5 ***	1171±153.4	1220±212.2	1171±105.8
		RH	983,8±242,4	820,2±185,0 **	791,7±194,1 ***	804,3±197,9 **	778,2±223,7 **	1110±150.2	1063±239.6	1025±129.8
		LF	1168±233,6	1073±177,2	1008±228,4 **	1001±238,0 *	967,4±216,3 **	1181±142.8	1177±138.0	1174±89.57
		LH	992,3±235,8	912,7±230,9	881,8±255,9	906,5±272,1	882,0±234,7	1149±139.3	1224±209.0	1217±171.7
Stand (s)	Duration of a paw contact with plate	RF	0,137±0,033	0,161±0,048 *	0,156±0,049	0,164±0,054	0,172±0,039 **	0.127±0.028	0.181±0.034 ***	0.173±0.031 ***
		RH	0,115±0,033	0,132±0,039	0,131±0,041	0,138±0,046	0,142±0,041 *	0.123±0.024	0.153±0.040 **	0.155±0.027 *
		LF	0,140±0,031	0,166±0,039 **	0,162±0,043 *	0,170±0,044 *	0,176±0,041 **	0.128±0.025	0.173±0.034 ***	0.175±0.022 ***
		LH	0,114±0,032	0,146±0,041 **	0,140±0,047 *	0,154±0,052 *	0,163±0,041 ***	0.127±0.025	0.172±0.035 ***	0.179±0.035 ***
Comparative statistics										
Regularity index (%)	Regularity of gait		92,01±7,358	87,91±18,94	88,34±14,22	93,13±4,871	93,41±5,221	95.53±3.596	92.33±4.556	91.62±5.918
Base of support (mm)	Distance between paws	RF-LF	7,928±5,334	10,06±5,463	12,77±8,814 *	14,19±8,221 *	13,26±7,772 *	11.05±7.104	6.840±4.997	11.92±8.874
		RH-LH	14,26±9,701	20,16±12,49	26,26±17,40 **	28,33±15,53 **	27,04±16,87 **	17.75±11.55	14.95±8.842	21.02±13.57
Stride length (mm)	Distance between successive steps with one paw	RF	63,88±9,181	50,63±17,19 **	50,19±17,06 ***	48,94±15,76 **	47,82±14,02 ***	60.10±6.581	55.48±7.374	53.72±5.749 *
		RH	60,60±8,631	46,11±18,55 **	53,62±21,15	47,50±17,36 *	43,92±13,39 ***	58.20±5.646	52.86±8.181	51.33±6.077 *
		LF	64,25±8,651	48,94±16,65 ***	51,13±16,95 ***	50,13±16,35 **	47,22±13,09 ***	60.39±5.906	56.22±9.730	53.14±5.550 *
		LH	58,37±10,93	45,78±16,57 **	46,78±15,37 ***	48,35±17,09	45,48±12,75 ***	57.34±6.421	53.58±7.076	49.09±4.905 **
Phase dispersions (%)	Contact of a target paw in relation to a step cycle of the anchor paw	RF-LH	6,663±7,276	9,099±7,519	6,526±6,815	1,815±9,420	2,952±4,866 *	1.916±5.339	2.511±5.106	4.956±8.010
		LF-RH	5,535±5,437	7,898±6,963	4,049±6,621	5,380±6,284	7,249±7,746	0.758±4.977	7.470±4.614 ***	4.936±5.681
		LH-RH	42,65±8,210	44,10±10,07	42,69±8,282	44,96±7,445	44,08±7,502	45.11±8.595	43.63±8.856	47.72±7.052
		LF-RF	49,45±3,765	50,25±3,931	47,88±7,821	51,76±3,799	50,94±4,265	50.34±2.496	49.63±2.076	51.41±3.541
		RF-RH	50,66±5,702	49,11±11,09	49,90±8,948	49,40±6,656	48,90±5,527	48.12±4.609	48.70±4.491	48.96±5.246
		LF-LH	48,34±6,634	50,45±4,274	48,06±5,767	49,27±6,122	49,21±6,429	46.01±5.118	46.04±4.443	44.29±5.120

* compared with baseline: One-way ANOVA for multiple comparisons with Bonferroni correction (*, $p<0.05$; **, $p<0.01$; ***, $p<0.001$)
# compared with SNS&HPA group day 10 after MCAo: One-way ANOVA for multiple comparisons with Bonferroni correction (#, $p<0.05$)
Abbreviations: RF, right front paw; RH, right hind paw; LF, left front paw; LH, left hind paw; SNS&HPA, sympathetic nervous system/ hypothalamic-pituitary-adrenal axis block group; MCAo, middle cerebral artery occlusion

2D2 mice: Female. Baseline N=44; Vehicle after MCAo N=35 (day 10 N=21, day 30 N=14), SNS&HPA after MCAo N=48 (day 10 N=29, day 30 N=19)
C57Bl/6J mice: Female. Baseline N=31; Vehicle N=12; SNS&HPA N=9

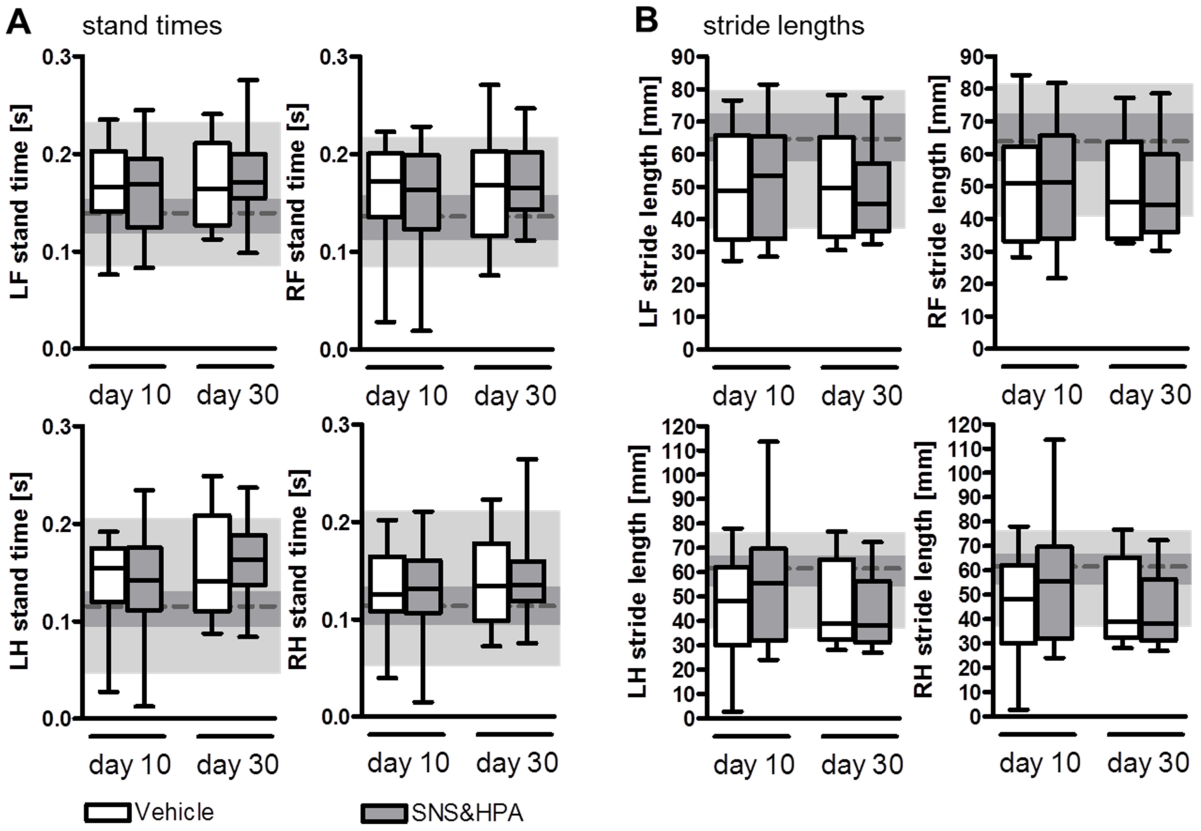

Figure 21. Stand times and stride lengths measured 30 days after MCAo, analyzed with CatWalk gait analysis, deviated in SNS&HPA block group from baseline slightly more than in vehicle group of 2D2 mice. All mice received preventively enrofloxacin. No differences were detected between vehicle and SNS&HPA block groups at analyzed time points. Please see Table 2 for details and statistics. Abbreviations: SNS&HPA, sympathetic nervous system/hypothalamic-pituitary-adrenal axis block group.

5.2.9 Combined SNS and HPA block with propranolol and mifepristone increased the absolute number of splenocytes but reduced the relative frequency of lymphocytes among splenocytes in 2D2 mice

Spleen is the peripheral lymphoid organ where circulating antigens are presented to T cells (Murphy, 2008). To investigate whether blocking simultaneously SNS and HPA axes of CIDS affects the cellular composition of spleen, splenocytes were analyzed with FACS 14 days after MCAo. Compared with vehicle group of 2D2 mice, those from SNS&HPA block group had less lymphocytes ($B220^+$ B cells, $CD3^+$ T cells, $CD4^+$ helper T cells, $CD4^+$ $V\alpha3.2^+$ MOG TCR transgenic helper T cells) among splenocytes with the exception of cytotoxic effector T cells (Figure 22A). Lymphocyte numbers in the spleens of female C57Bl/6J mice, on the other hand, were not affected by SNS and HPA block with propranolol and mifepristone (Figure 22B). Absolute number of splenocytes was nevertheless higher in 2D2 mice from SNS&HPA block group ($1.5x10^8 \pm 6.1x10^7$) compared with vehicle group ($6.2x10^7 \pm 5.0x10^7$).

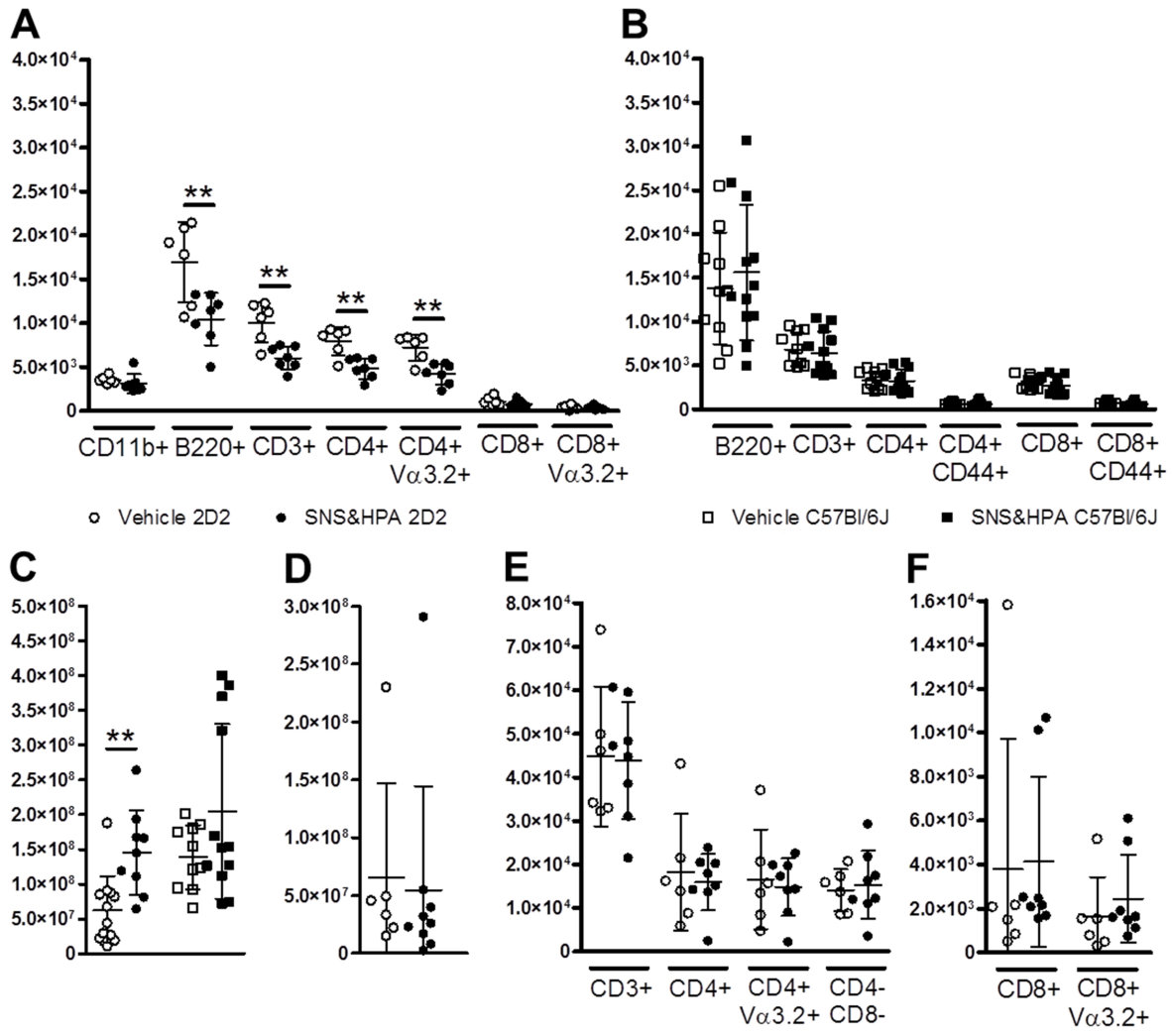

Figure 22. Blocking simultaneously SNS and HPA axes of CIDS reduced the numbers of lymphocytes per 1x10^5 splenocytes in female 2D2 mice but did not affect cellular composition of thymus 14 days after stroke. ***A***, FACS analysis for cellular composition of spleen in 2D2 mice revealed lower frequencies of B220$^+$ B cells [Student's *t*-test, $t(11)=3.1$, $p=0.010$], CD3$^+$ T cells [$t(11)=4.0$, $p=0.002$], CD4$^+$ helper T cells [$t(11)=4.0$, $p=0.002$] and CD4$^+$ Vα3.2$^+$ transgenic MOG TCR carrying helper T cells [$t(11)=4.0$, $p=0.002$] per 1x10^5 splenocytes in mice from SNS&HPA block group (N=7) compared with vehicle group (N=6). ***B***, Cellular composition of spleen in vehicle (N=10) and SNS&HPA block group of C57Bl/6J mice (N=12) did not differ. ***C***, Absolute numbers of splenocytes in vehicle and SNS&HPA block groups of 2D2 (vehicle; N=12; SNS&HPA block, N=7) and C57Bl/6J mice (vehicle; N=10; SNS&HPA block, N=12). Absolute number of splenocytes was increased in 2D2 mice from SNS&HPA block group (Kruskal-Wallis, Chi-Quadrat=14.9, df=3, $p=0.002$; Mann-Whitney *U*-test, $U=16.0$; $p=0.006$). ***D***, Absolute number of thymocytes in 2D2 mice were not affected by CIDS block (vehicle, N=6; SNS&HPA block, N=7). ***E*** and ***F***, Cellular composition of thymus was similar in vehicle and SNS&HPA block groups of 2D2 mice. FACS data are presented as counts per 1x10^5 measured cells. Abbreviations: SNS&HPA, sympathetic nervous system/hypothalamic-pituitary-adrenal axis block group.

This difference was not observed in C57Bl/6J mice (vehicle, 1.4x10^8±4.6x10^7; SNS&HPA block, 2.1x10^8±1.3x10^8; Figure 23C). Absolute number of thymocytes in 2D2 mice (vehicle, 6.6x10^7±8.2x10^7; SNS&HPA block, 5.5x10^7±9.0x10^7) and cellular composition of thymus including CD3$^+$ CD4$^-$ CD8$^-$ undifferentiated T cells, single positive CD4$^+$ and CD8$^+$ T cells,

transgenic MOG TCR carrying $CD4^+$ and $CD8^+$ T cells, 14 days after MCAo was not affected by blocking SNS and HPA axis with propranolol and mifepristone (Figure 22D, E and F).

5.2.10 Combined SNS and HPA block with propranolol and mifepristone did not affect Th1-type autoreactive myelin oligodendrocyte glycoprotein specific immune responses in the spleen

Results from the ischemic brains of female 2D2 mice 14 days after MCAo demonstrated higher Th1- as well as Th2-type autoreactive potential towards MOG after blocking simultaneously SNS and HPA axes of CIDS compared with vehicle treatment. To investigate, whether autoreactive potential differed also in the spleen, splenocytes from 2D2 mice were stimulated with MOG 14 days after MCAo and their cytokine-profile was analyzed. Simultaneous blocking of SNS and HPA mediated CIDS did not alter the frequency of MOG-reactive IFN-γ, IL-4 or IL-17 secreting cells in the spleens of female 2D2 mice (Figure 23A). The ratio between autoreactive Th1 (IFN-γ producing) and Th2 cells (IL-4 producing) was 4.5±1.7 in vehicle and 5.4±1.7 in SNS&HPA block group and thus not different (Figure 23B). Also the ratio between autoreactive Th17 (IL-17 producing) and Th1 cells was not affected by CIDS block (0.11±0.03 in vehicle and 0.12±0.08 in SNS&HPA block group; Figure 23C).

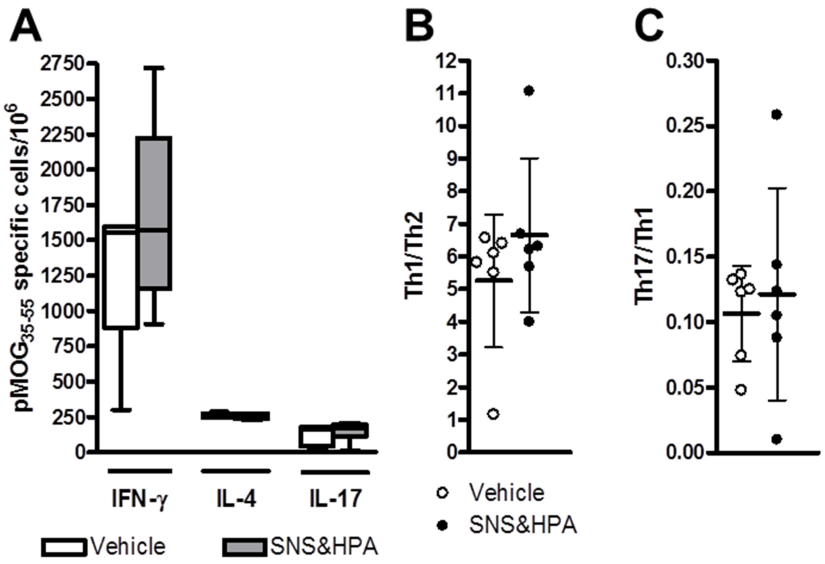

Figure 23. Cytokine-profile of MOG-reactive cells per 1x10^6 splenocytes in female 2D2 mice after simultaneous blocking of SNS and HPA mediated CIDS and vehicle treatment 14 days after stroke. ***A***, The number of IFN-γ (Th1), IL-4 (Th2) or IL-17 (Th17) secreting MOG-specific cells per 1x10^6 splenocytes did not differ between vehicle (N=6 for all) and SNS&HPA block group (IFN-γ, N=6; IL-4 and IL-17, N=9). ***B***, The ratio between MOG-specific Th1 and Th2 cells in the spleen was not increased in SNS&HPA block group. ***C***, The ratio between MOG-specific Th17 and Th1 cells in the spleen was similar and below one in both groups. Abbreviations: IFN-γ, interferon gamma; IL-4, interleukin 4; IL-17, interleukin 17; $pMOG_{35-55}$, peptide fragment (amino acids 35-55) from myelin oligodendrocyte glycoprotein; SNS&HPA, sympathetic nervous system/hypothalamic-pituitary-adrenal axis block group; Th, T helper cells (number indicates type).

5.2.11 Combined SNS and HPA block with propranolol and mifepristone increased Th1-type autoreactive myelin oligodendrocyte glycoprotein specific immune responses in the ischemic brain

In line with ischemic lesion reduction by two thirds following SNS and HPA block with propranolol and mifepristone (Figure 16A) the average number of brain MNCs was both, ipsi- and contralaterally lower in the brains of 2D2 mice belonging to SNS&HPA block group compared with vehicle treatment (Figure 24A). CNS-antigen (MOG) specific autoreactive potential of these cells was evaluated with ELISpot 14 days after MCAo. Simultaneous blocking of SNS and HPA mediated CIDS doubled the fraction of MOG-specific IFN-γ producing brain MNCs (598 per $3.25x10^5$ total brain MNCs in vehicle and 1122 per $3.25x10^5$ of total brain MNCs in SNS&HPA block group), indicating increased MOG-specific Th1 response (Figure 24B).

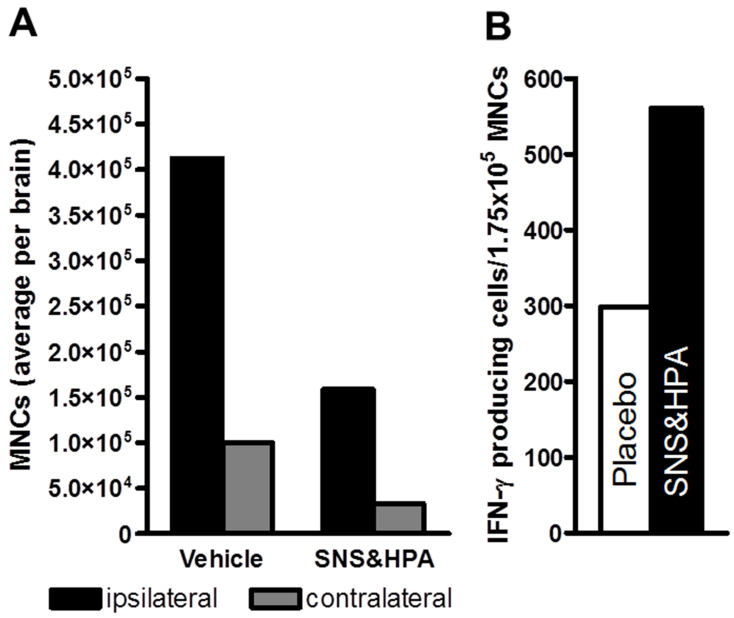

Figure 24. Simultaneous blocking of SNS and HPA axes of CIDS increased the fraction of IFN-γ producing MOG-specific brain MNCs in 2D2 mice 14 days after stroke. Average number of brain infiltrating MNCs was lower (***A***) but the fraction of MOG-specific IFN-γ secreting brain MNCs twice as high in SNS&HPA block group (***B***). Presented are mean values per brain per group (***A***) or per $1.75x10^5$ brain MNCs per group (***B***). Abbreviations: IFN-γ, interferon-γ; MNCs, mononuclear cells; SNS&HPA, sympathetic nervous system/hypothalamic-pituitary-adrenal axis block group.

Therefore, in line with the results from blocking SNS axis alone, higher Th1-type autoreactive potential of brain MNCs in 2D2 mice after simultaneous block of SNS and HPA mediated CIDS was limited to the CNS. In spleen, the treatment increased absolute number of splenocytes but decreased the fraction of lymphocytes, including MOG TCR transgenic $CD4^+$ T cells.

5.3 The role of stroke-activated 2D2 $CD4^+$ T cells adoptively transferred to Rag-1KO mice after stroke

Adoptive transfer experiments were designed to investigate, how the MOG TCR expressing $CD4^+$ helper T cells, primed by MCAo, behaved when transferred to lymphocyte-deficient Rag-1KO mice 6 h after MCAo. Another goal was to examine whether the development of functional neurological symptoms of autoreactive immune responses was hampered by smaller infarct volumes in SNS&HPA block group of female 2D2 mice and attempt to provide clarity about the role for higher frequency of IFN-γ secreting MOG-specific Th1 cells in the brain. Based on the treatment received by donor 2D2 mice, Rag-1KO recipients were divided into three groups: naïve (non-manipulated 2D2 mice), vehicle and SNS&HPA block group. All donor (and recipient) mice were administered preventively enrofloxacin and $CD4^+$ T cells were harvested seven days after MCAo from spleen and lymph nodes.

5.3.1 Adoptive transfer of $CD4^+$ T cells from stroked mice treated with propranolol and mifepristone increased post-stroke mortality in Rag-1KO mice

Based on the treatment of donor 2D2 mice, Rag-1KO recipient mice were divided into naïve, vehicle and SNS&HPA block groups. Eighty-two per cent of naïve, 62% of vehicle and 40% of SNS&HPA block group of Rag-1KO mice survived until the end of the study on day 30 after MCAo. The mortality in SNS&HPA block group of Rag-1KO mice was significantly higher than in naïve group but did not differ from vehicle group of mice (Figure 25A). In spite of the high mortality, Rag-1KO mice maintained stable body weight and temperature post-MCAo independent of the treatment in $CD4^+$ T cell donor 2D2 mice (Figure 25B and C).

5.3.2 Infarct volumes in Rag-1KO mice were not affected by the treatment of donor 2D2 mice

Rag-1KO mice from all three groups developed equally severe infarcts 24 h after MCAo, independent of gender (naïve, male 28±14%; female 39±11%; vehicle, male 27±14%; female 27±14%; SNS&HPA block, male 32±16%; female 20±16%). Therefore, the origin and phenotype of $CD4^+$ T cells determined by the treatment of 2D2 donor mice had no significant effect on infarct volumes in Rag-1KO recipient mice (Figure 25D).

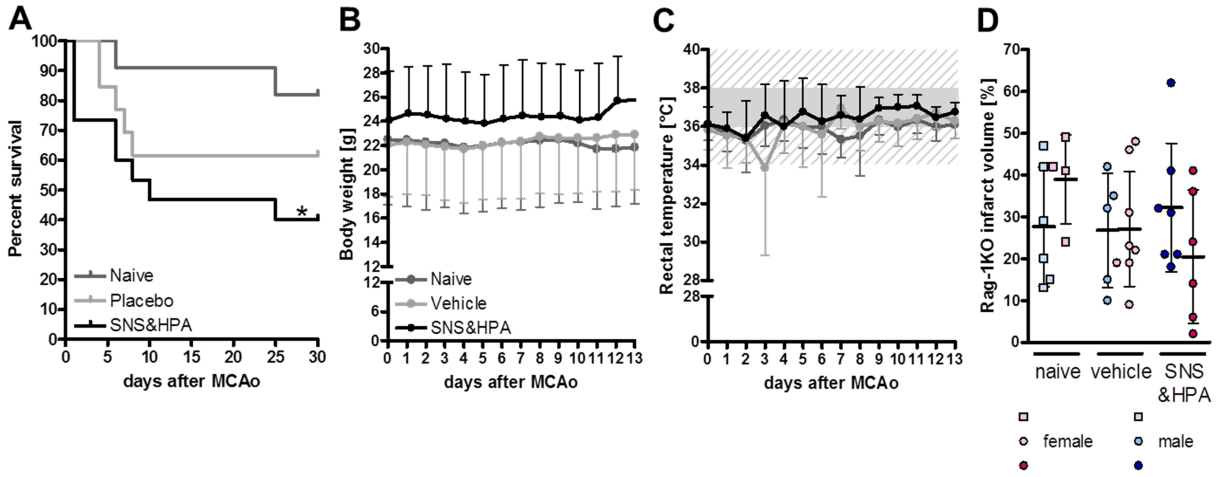

Figure 25. Rag-1KO mice, adoptively transferred with CD4$^+$ T cells 6 h after MCAo from naïve (non-manipulated) 2D2 mice or from seven days post-stroke 2D2 mice (vehicle and SNS&HPA block groups) developed ischemic lesions of similar size. Mortality was higher in SNS&HPA block group of Rag-1KO mice compared with naïve group. All mice received preventively enrofloxacin. A, Survival curves of Rag-1KO mice (naïve, N=10; vehicle, N=13; SNS&HPA block, N=14) until 30 days post-MCAo. Mortality was higher in SNS&HPA block group compared with naïve group (Chi square=4.6, df=1, p=0.032). Rag-1KO mice from all groups maintained stable body weight (B) and temperature (C) after MCAo. Optimal body temperature of a mouse is presented as a grey bar, and yet acceptable body temperature with grey streaked area on a background. For clarity, in panels B and C data from naïve and vehicle groups are experssed as mean-standard deviation and from SNS&HPA block group as mean+standard deviation. D, Ischemic lesion sizes 24 h after MCAo did not differ between Rag-1KO mice from naïve (male, N=6; female, N=4), vehicle (male, N=5; female, N=8) and SNS&HPA block group (male, N=7; female, N=6) and between genders. Abbreviations: MCAo, middle cerebral artery occlusion; SNS&HPA, sympathetic nervous system/hypothalamic-pituitary-adrenal axis block group.

5.3.3 Functional neurological deficits and immune cell infiltrates into spinal nerve roots of Rag-1KO mice were not affected by the treatment of donor 2D2 mice

Majority of Rag-1KO recipients (90% from naïve, 89% from vehicle and 78% from SNS&HPA block group) developed EAE-like symptoms within the 30-day observation period after MCAo. EAE-like disease was not aggravated in Rag-1KO mice from SNS&HPA block group. Compared with 2D2 mice, median disease onset was delayed and symptoms milder in Rag-1KO mice (Figure 26A and B).

Electrophysiological recordings 14 days after MCAo demonstrated that upon sciatic nerve stimulation Rag-1KO mice from all three groups had similar latencies to F-wave (naïve, 16.0±3.9 ms; vehicle, 15.0±2.7 ms; SNS&HPA block, 17.8±4.4 ms) and F-wave chronodispersion (naïve, 6.2±4.6 ms; vehicle, 5.2±2.9 ms; SNS&HPA block, 6.4±4.5 ms). These values did not differ from pre-MCAo baseline values (latency to F-wave: 16.6±4.4 ms; F-wave chronodispersion: 5.2±5.4 ms; Figure 26C and D).

Immunohistochemical analysis of spinal nerve roots for immune cell infiltrates and inflamed axons 30 days after MCAo and adoptive transfer of $CD4^+$ T cells from 2D2 donor mice supported the findings of milder neurological deficits in the Rag-1KO mice. Some adoptively transferred $CD4^+$ T cells had migrated to spinal nerve roots of Rag-1KO mice and located preferentially near $Mac3^+$ macrophages. $Mac3^+$ macrophages (naïve, 22.8±10.7 cells/mm^2; vehicle, 20.3±7.0 cells/mm^2; SNS&HPA block, 20.8±7.3 cells/mm^2), $CD4^+$ T cells (naïve, 3.6±8.0 cells/mm^2; vehicle, 1.2±1.1 cells/mm^2; SNS&HPA block, 0.2±0.2 cells/mm^2) and APP^+ inflamed axons (naïve, 7.0±6.3 cells/mm^2; vehicle, 7.7±4.5 cells/mm^2; SNS&HPA block, 10.3±8.6 cells/mm^2) were approximatley four times less frequent in the nerve roots of Rag-1KO mice compared with 2D2 mice. Their density in spinal nerve root of Rag-1KO mouse was not affected by the treatment of donor 2D2 mice (Figure 26E). Increased infiltration of $Mac3^+$ macrophages was in vehicle and SNS&HPA block groups associated with higher densities of APP^+ inflamed axons (Spearman's rank-order correlation: vehicle, r_s=0.810, p=0.015; SNS&HPA block, r_s=1.000, p<0.0005; data not shown).

Locomotor deficits were evaluated in Rag-1KO mice using CatWalk gait analysis system 10 and 30 days after MCAo, corresponding to mid- and long-term outcome, respectively. In line with better post-stroke health status in Rag-1KO mice compared with 2D2 mice, lower EAE scores and normal electrophysiological findings, gait deficits in Rag-1KO recipient mice after MCAo were minor and are summarized in Table 3.

In conclusion, with adoptive transfer experiments where $2x10^6$ $CD4^+$ T cells from differently treated 2D2 mice (naïve, vehicle and SNS&HPA block group) seven days after MCAo were injected i.v. to Rag-1KO recipients 6 h after MCAo demonstrated that $CD4^+$ T cells from propranolol and mifepristone treated 2D2 mice, primed by first stroke, reduced survival 30 days post-MCAo compared with animals receiving naïve but not vehicle-treated 2D2 $CD4^+$ T cells, do not enhance long-term functional neurological deficits in Rag-1KO mice supported by EAE score, electrophysiological recordings, quantification of immune cells and inflamed axons in spinal nerve roots and analysis of locomotor deficits.

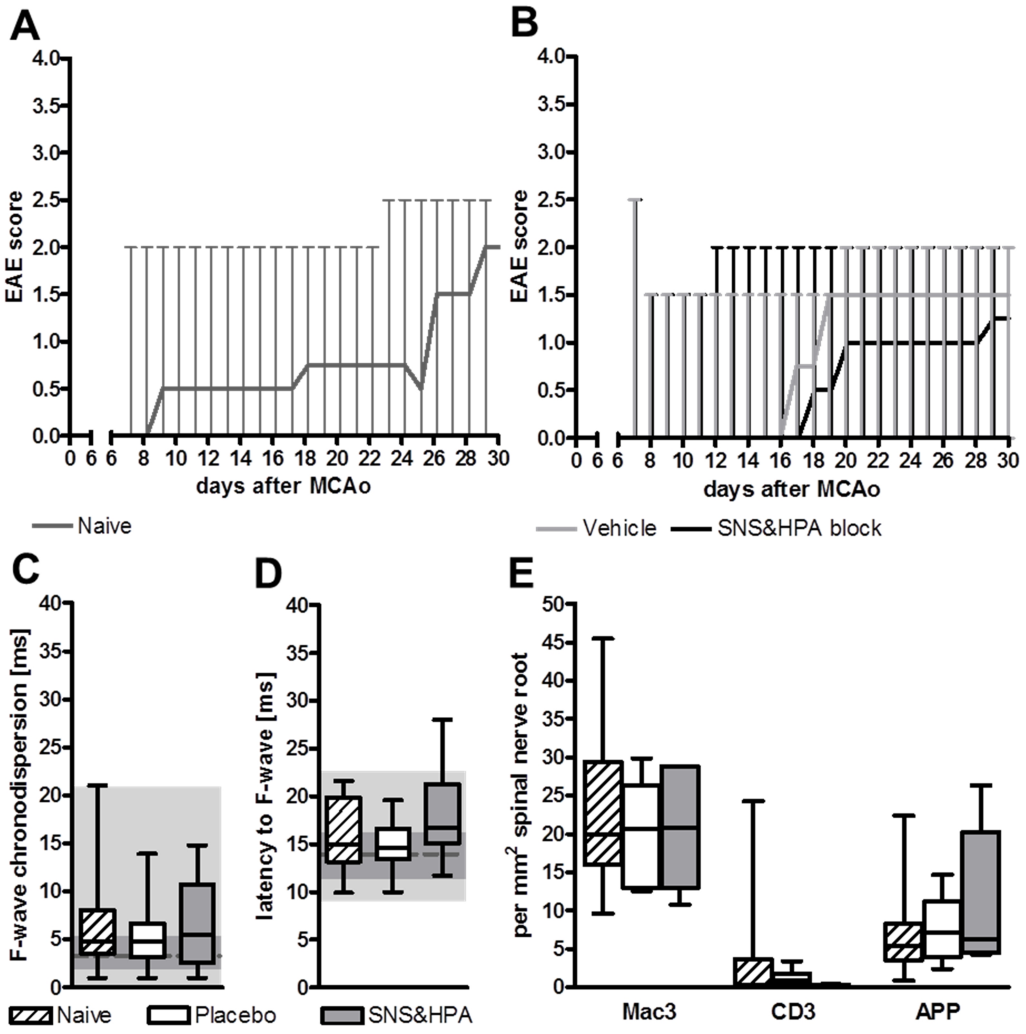

Figure 26. Rag-1KO mice adoptively transferred with CD4$^+$ T cells from 2D2 donor mice where SNS and HPA mediated CIDS had been simultaneously blocked did not show aggravation of EAE-like symptoms over the 30 day observation period after MCAo. Sciatic nerve conduction and immune cell infiltration to spinal nerve roots was not affected by the treatment of donor mice. ***A***, Rag-1KO mice adoptively transferred with naïve 2D2 CD4$^+$ T cells (N=10) developed mild EAE-like symptoms already 8 days after MCAo, compared with day 16 in vehicle (N=9) and day 17 in SNS&HPA block group of mice (N=9; ***B***). ***C***, Latencies to F-wave upon sciatic nerve stimulation 14 days after MCAo did not differ between the groups of Rag-1KO mice (naïve, N=20; vehicle, N=16; SNS&HPA block, N=14) and also not from pre-MCAo baseline values (N=19; dotted line symbolizes the median value, dark grey rectangle indicates 25th and 75th percentile of the values and a light grey rectangle minimum and maximum values). ***D***, F-wave chronodispersion did not differ between the groups and from baseline. ***E***, Densities of immune cells (Mac3$^+$ macrophages, CD3$^+$ T cells) and inflamed axons (APP$^+$) in spinal nerve roots did not differ between the groups 30 days after MCAo. Abbreviations: EAE, experimental autoimmune encephalomyelitis; MCAo, middle cerebral artery occlusion; SNS&HPA, sympathetic nervous system/hypothalamic-pituitary-adrenal axis block group.

Table 3. CatWalk gait analysis of Rag-1KO mice, adoptively transferred with $CD4^+$ T cells from 2D2 mice, before, 10 and 30 days after MCAo.

Parameter	Definition	Paw	Baseline	Naive	Vehicle	SNS&HPA	Naive	Vehicle	SNS&HPA
				10 days after MCAo			30 days after MCAo		
Spatial characteristics									
Max contact area (mm^2)	Area of a paw print at maximal plate contact	RF	21,25±5,527	23,67±7,136	23,22±6,561	24,84±3,533	22,97±5,236	22,79±6,385	24,20±3,530
		RH	21,12±7,832	19,33±8,356	20,10±9,184	20,73±6,547	17,90±4,554	21,20±9,228	24,17±4,913
		LF	21,57±6,009	25,65±7,226	24,66±6,798	27,00±6,075 *	23,28±5,720	24,58±3,944	26,47±8,105
		LH	19,96±9,057	22,76±11,83	23,95±8,893	24,11±11,31	23,63±6,860	23,83±2,684	25,86±10,17
Kinetic characteristics									
Run duration (s)	Time for passing the walkway		3,229±0,538	2,681±0,692 *	2,777±0,694	2,523±0,467 **	3,068±0,649	3,047±0,361	2,464±0,409 ** $
Normalized swing speed (s)	Swing speed*Run duration	RF	818,9±80,61	761,6±58,86	801,1±84,01	783,7±82,51	775,4±81,49	775,8±98,62	725,1±55,87 **
		RH	781,5±136,0	632,6±58,64 *	691,8±157,1	692,4±81,93	622,7±69,35 ***	685,9±93,24	665,6±113,2
		LF	804,9±88,92	767,4±79,03	846,6±125,3	819,8±34,49	787,3±109,9	809,0±77,35	739,9±68,64
		LH	750,3±115,7	707,3±119,9	693,6±80,48	692,3±69,65	790,8±146,2	807,7±88,51	666,6±65,39 $$
Stand (s)	Duration of a paw contact with plate	RF	0,188±0,031	0,163±0,041	0,178±0,038	0,167±0,017	0,183±0,028	0,189±0,035	0,168±0,026
		RH	0,186±0,040	0,141±0,041 *	0,163±0,059	0,158±0,032	0,156±0,032 *	0,172±0,034	0,161±0,026
		LF	0,186±0,033	0,162±0,041	0,176±0,026	0,174±0,021	0,188±0,035	0,201±0,038	0,164±0,021 $
		LH	0,184±0,039	0,150±0,045	0,163±0,040	0,159±0,025	0,192±0,047 &	0,197±0,022	0,152±0,028 * $$ #
Comparative statistics									
Regularity index (%)	Regularity of gait		93,63±4,010	96,95±1,810 *	94,66±4,873	95,34±2,171	94,44±4,369	95,87±4,348	89,79±4,163 * $ #
Base of support (mm)	Distance between paws	RF-LF	9,846±6,232	12,80±10,50	15,13±8,574	9,566±8,308	10,41±6,275	14,95±10,97	10,77±8,926
		RH-LH	17,20±13,17	23,57±17,09	31,12±15,74	19,67±10,85	17,97±9,297	26,92±20,24	22,77±26,11
Stride length (mm)	Distance between successive steps with one paw	RF	32,66±4,376	35,66±4,684	36,20±2,512	37,59±4,518 *	33,36±4,479	33,32±2,752	37,87±6,750
		RH	32,21±4,093	34,19±5,051	32,89±3,962	37,63±4,489 *	32,40±3,913	31,77±4,858	35,36±5,686
		LF	32,75±3,849	34,86±5,406	35,65±3,465	38,86±4,548 **	33,27±3,948	33,50±3,006	37,75±6,058
		LH	31,73±3,830	33,55±5,376	33,64±3,789	36,86±5,411 *	31,93±2,403	32,00±3,858	33,47±4,786
Phase dispersions (%)	Contact of a target paw in relation to a step cycle of the anchor paw	RF-LH	4,839±5,433	6,297±4,508	5,214±5,297	6,736±1,370	2,814±4,077	4,142±6,855	7,605±5,798
		LF-RH	3,891±4,772	5,406±6,143	7,804±11,41	6,091±2,098	10,01±6,367 *	6,223±2,959	4,431±9,084
		LH-RH	45,70±6,639	45,64±8,512	44,16±4,996	48,63±3,273	47,89±11,92	49,44±8,360	41,33±12,53
		LF-RF	49,17±3,273	50,33±2,945	51,05±3,185	50,03±3,588	48,91±5,418	49,45±4,308	49,85±3,958
		RF-RH	49,85±4,148	52,83±3,542	47,06±4,787	51,28±2,268	53,24±3,699 *	51,91±3,595	48,98±3,077 #
		LF-LH	49,31±4,062	52,41±4,022 *	51,20±4,462	52,49±5,355 *	50,97±5,518	50,39±3,416	47,08±8,204

* compared with baseline: Kruskal-Wallis with Mann-Whitney *U*-test (*, $p<0.05$; **, $p<0.01$; ***, $p<0.001$)
& compared with Naive d10: Wilcoxon for paired comparisons (&, $p<0.05$)
# compared with Naive d30: Kruskal-Wallis with Mann-Whitney *U*-test (#, $p<0.05$)
$ compared with Vehicle d30: Kruskal-Wallis with Mann-Whitney *U*-test ($, $p<0.05$; $$, $p<0.01$)
Abbreviations: RF, right front paw; RH, right hind paw; LF, left front paw; LH, left hind paw; SNS&HPA, sympathetic nervous system/hypothalamic-pituitary-adrenal axis block group; MCAo, middle cerebral artery occlusion

Rag-1KO mice: Gender-mixed. Baseline N=37; Naive after MCAo N=17 (day 10 N=8, day 30 N=9); Vehicle after MCAo N=12 (day 10 N=4, day 30 N=8); SNS&HPA after MCAo N=12 (day 10 N=6, day 30 N=6)

5.3.4 $CD4^+$ T cells and macrophages were found in the brains of Rag-1KO mice 30 days after adoptive transfer and stroke but their frequency per volume was not affected by treatment of donor 2D2 mice

To follow whether the treatment of 2D2 donor mice affected brain's local inflammatory milieu in lymphocyte-deficient Rag-1KO mice 30 days after MCAo, immunohistochemistry with markers for CD4 (for $CD4^+$ T cells) and Iba-1 (for microglia/macrophages) was performed. $CD4^+$ T cells were still observed in the brains of Rag-1KO mice 30 days after MCAo and adoptive transfer of $CD4^+$ T cells from naïve, vehicle and propranolol/mifepristone treated 2D2 mice. $CD4^+$ T cells had accumulated preferentially at peri-infarct area (Figure 27A, C, F and I). Activated Iba-1^+ microglia/macrophages were found abundantly at peri-infarct areas and within infarct core (Figure 27B, D, G and J). Ramified resting Iba-1^+ microglia obtained an ameoboid-like morphology with thickened processes (Figure 27E, arrows) upon migrating towards ischemic core. There, their somata became oval or irregular (Figure 27H) and they were found extravagating through local blood vessels (Figure 27K). No significant differences were detected in the quantities of brain infiltrating $CD4^+$ T cells (naïve, 20.8±16.3 cells/mm^2; vehicle, 27.0±20.7 cells/mm^2; SNS&HPA block, 12.5±7.6 cells/mm^2 ipsilateral hemisphere) and Iba-1^+ microglia/ macrophages (naïve, 6.9±5.6 cells/mm^2; vehicle, 7.5±5.5 cells/mm^2; SNS&HPA block, 4.5±3.7 cells/mm^2 ipsilateral hemisphere) between the groups (Figure 27L). Infiltration of $CD4^+$ T cells and Iba-1^+ microglia/macrophages did not depend on the size of ischemic lesion (data not shown). These data demonstrate that blocking simultaneously the SNS and HPA mediated CIDS does not enhance $CD4^+$ T cell and macrophage infiltration to ischemic brains compared with vehicle treatment.

Figure 27 (see following page). $CD4^+$ T cells and Iba-1^+ macrophages were found in Rag-1KO mice brains 30 days after MCAo and adoptive transfer of $CD4^+$ T cells from naïve and treated 2D2 donors, the latter underwent MCAo 7 days before transfer. Images from CD4 (green) and Iba-1 (red) stained brain sections were taken from three regions indicated in ***A*** and ***B***. Ischemic core is outlined with a black solid line. Region ***1*** represents contralateral hemisphere, ***2*** non-ischemic area around ischemic core and ***3***, peri-infarct region in ipsilateral hemisphere. ***(1) C, D, E*** (thick arrow indicates resting microglia with thin processes) ***(2) F, G, H*** (thick arrow indicates activated microglia with an amoeboid-like shape, large cell body and thick processes) ***(3) I, J, K*** (immune cell infiltration was highest around and within ischemic core). ***L,*** Densitites of $CD4^+$ and Iba-1^+ cells per mm^2 ipsilateral hemisphere in Rag-1 KO mice from naïve (N=8), vehicle (N=6) SNS&HPA block group (N=4) did not differ. Abbreviations: VL, vessel lumen. Scale bar: 20 µm.

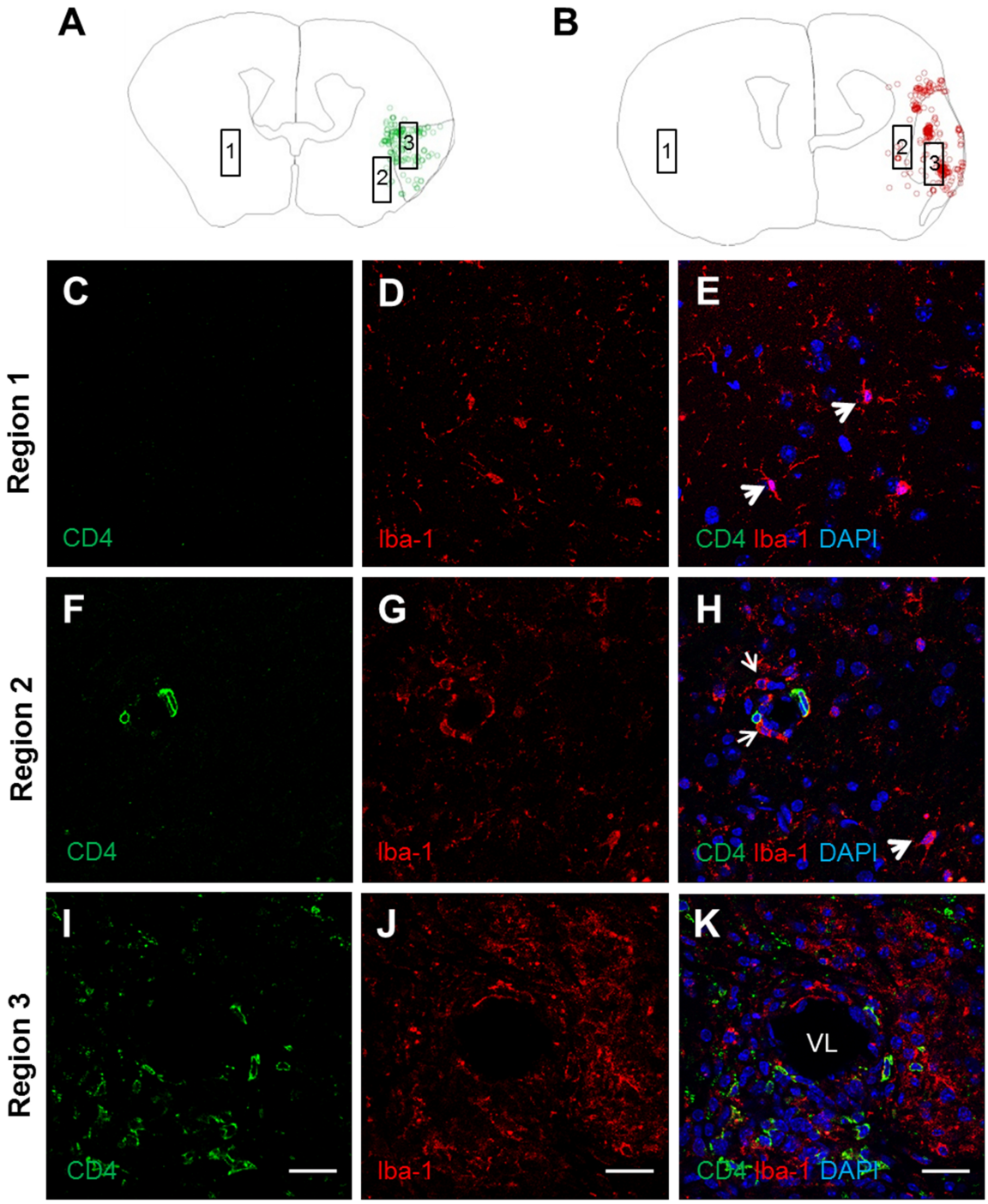
A
B
1
2
3
1
2
3
C
D
E
Region 1
CD4
Iba-1
CD4 Iba-1 DAPI
F
G
H
Region 2
CD4
Iba-1
CD4 Iba-1 DAPI
I
J
K
Region 3
CD4
Iba-1
CD4 Iba-1 DAPI
VL

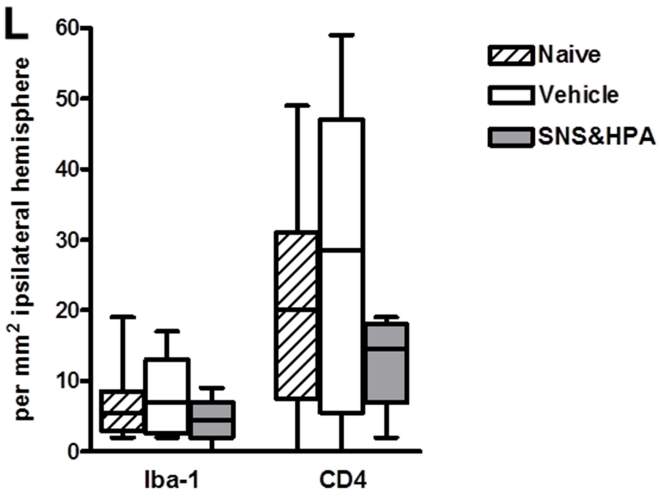
L
per mm2 ipsilateral hemisphere
60
50
40
30
20
10
0
Iba-1
CD4
Naive
Vehicle
SNS&HPA

6. Discussion

The goal of this thesis was to elucidate whether CIDS comprises a built-in mechanism to reduce the likelihood of CNS-antigen specific autoreactive responses in case of a CNS injury such as stroke. Autoreactive immune responses are classically associated with Th1 cells. Therefore, in a murine model of MCAo, I blocked the two main communication pathways between the CNS and the immune system that mediate CIDS mainly by suppressing cell-mediated immune responses (particularly the function of Th1 cells and antigen presenting cells): the SNS and the HPA axis. If CIDS were to reduce the likelihood of CNS-directed autoreactivity, blocking CIDS should, on the contrary, promote CNS-directed autoreactivity. Understanding that CIDS is an independent risk factor for stroke patients' high susceptibility to infections and poor neurological outcome has initiated the search for immunomodulatory therapies for this socioeconomically relevant disease. The drawback of most of these studies is their focusing on early effects and benefit while conditions like CNS-antigen directed autoreactive immune responses develop slow. The aims of this thesis were thus the characterization of immune cells and phenotype of T cells infiltrating ischemic brain at the time of peak T cell infiltration 14 days after MCAo (and CIDS block); follow-up of long-term (30 days) functional and neurological outcome after blocking the SNS or simultaneously the SNS and HPA axes of CIDS at the time of stroke; and investigation of the role of stroke-primed MOG TCR transgenic T cells in a setting of a "second stroke" in lymphocyte-deficient Rag-1KO mice.

The key findings of this thesis are the following: first, CIDS block (either SNS block alone or simultaneous block of SNS and HPA axes with propranolol and mifepristone) increases delayed MOG-specific Th1-type autoreactive immune responses by IFN-γ secreting MNCs in the brains of MOG TCR transgenic 2D2 mice 14 days after MCAo. Second, intravenously transferred 2D2 $CD4^+$ T cells are still found in the brain and spinal nerve roots of lymphocyte-deficient Rag-1KO mice 30 days after MCAo and cell transfer. Third, functional symptoms of CNS antigen specific autoreactive immune responses based on EAE-like disease and polyradiculitis phenotype measured by EAE score, gait analysis, EMG/ENoG and spinal nerve root immunohistochemistry, is not augmented by CIDS block in 2D2, C57Bl/6J and Rag-1KO mice. Fifth, lack of β2-AR at birth (β2-AR ko mice) is associated with aggravation of EAE-like symptoms after MCAo. Sixth, simultaneous block of SNS and HPA with propranolol and mifepristone improves post-stroke health status, promotes recovery and elongates life expectancy in mice with bronchopulmonary infections. Seventh, infarct volume

is lastingly two thirds smaller after simultaneous block of SNS and HPA mediated CIDS with propranolol and mifepristone; altered CBF can be excluded as the primary reason of this effect.

6.1 Methodological considerations

Four different mouse strains were used in this thesis: MOG TCR transgenic 2D2, C57Bl/6J, β2-AR ko and lymphocyte-deficient Rag-1KO mice. Majority of experiments were carried out on 2D2 mice. This is an artificially created mouse strain where a vast majority (above 80%) of peripheral $CD4^+$ T cells carry a functional receptor for MOG fragment ($pMOG_{35-55}$) (Bettelli et al., 2003). $pMOG_{35-55}$ is a highly encephalitogenic peptide fragment within the extracellular Ig Variable region like domain of MOG (Pham-Dinh et al., 1993; Mendel et al., 1995; Kroepfl et al., 1996), a minor myelin component (Amiguet et al., 1992). Being located on outermost myelin sheath (Brunner et al., 1989), MOG would be easily accessible to immune cells upon blood-brain-barrier damage like that occurring in stroke. Its extracellular domain (Pham-Dinh et al., 1993; Kroepfl et al., 1996) is encephalitogenic (Mendel et al., 1995) and plays a role in CNS inflammation by activating the C1q component of the complement and consequently causing damage to mature oligodendrocytes (Scolding et al., 1989; Johns and Bernard, 1999). These mice are thus well-suited to study if a link existed between CIDS and CNS-directed autoreactive immune responses and to characterize it. Many of the effects observed in 2D2 mice in the present thesis were additionally confirmed in wild-type C57Bl/6J mice and in an adoptive transfer experiment to Rag-1KO mice. The role for SNS mediated CIDS was, in addition to SNS block with propranolol in 2D2 mice, assessed in β2-AR ko mice which lack the crucial receptor mediating immunomodulatory effects of the SNS. Cholinergic anti-inflammatory pathway mediating the fast and local effects of CIDS was not of interest in the present thesis. Unlike the SNS and HPA axis (Levine et al., 1962), stimulation of cholinergic anti-inflammatory pathway does not counteract autoreactive CNS inflammation in a model of EAE (Nicolussi et al., 2009).

The pharmaceutical agents used here to block the SNS and HPA axes of CIDS were propranolol and mifepristone, respectively. Propranolol is a non-selective β-blocker and mifepristone a glucocorticoid receptor antagonist. S(-)-propranolol was used as this is the most potent enantiomer and has higher affinity towards the β1-AR and β2-AR. Single treatment schemes for propranolol and mifepristone for the purpose of blocking immunodepression via SNS and HPA activation have been published (Prass et al., 2003).

Here, drug preparation, dosage and injection scheme was shifted for the combined treatment and to decrease acute mortality and adverse effects.

Murine transient (60-minute) MCAo was used as a model for stroke. MCAo is the most commonly used animal model for stroke. It mimics focal ischemia and reperfusion injury and resembles human stroke with a therapy-induced or spontaneous reperfusion which accounts for the majority of stroke cases. Size of the ischemic lesion in this model is regulated by the occlusion time. A 60-minute MCAo classifies as severe and causes infarcts involving lateral striatum, the cortex and the hypothalamus. These lesions are highly reproducible and the method is minimally invasive (Durukan and Tatlisumak, 2007; Dirnagl, 2010).

To investigate the autoreactive phenotype of brain infiltrating MNCs after MCAo and CIDS block, ELISpot assay was performed. Th1, Th2 and Th17 ELISpots were chosen based on the critical involvement of these T cell populations in autoreactive diseases. In particular Th1 but also Th17 responses are typically associated with detrimental autoreactivity (Ando et al., 1989; Cua et al., 2003), whereas Th2 cells alleviate autoreactive symptoms (Webster et al., 2002). The advantage of ELISpot over ELISA and other similar techniques is that it enables to enumerate specific cells in the sample producing certain cytokine, such as IFN-γ for Th1 cells, IL-4 for Th2 cells and IL-17 for Th17 cells, upon stimulation (for example with MOG peptide fragment). IFN-γ specific Th1 cell ELISpot is, for example, acknowledged in transplantation research (Augustine and Hricik, 2012). However, beside the invaluable information that ELISpot provides, the obvious limitation becomes evident in analyzing the autoreactive phenotype of mouse brain MNCs after stroke. The assay is based on equal number of brain MNCs ($1.75x10^5$) being stimulated together with naïve feeder cells to achieve optimal density for cellular interactions within the ELISpot analysis plate well. A prerequisite for such a high number of brain MNCs for ELISpot assay (per one cytokine ELISpot a minimum of positive control, peptide stimulation and negative control are needed) and consequently increased number of mice needed, led to inevitable pooling of the brains of mice belonging to one treatment group which had undergone successful MCAo confirmed by MRI. Furthermore, the number of brain infiltrating MNCs was about two thirds lower in mice treated with propranolol and mifepristone for blocking simultaneously the SNS and HPA axes of CIDS corresponding to two thirds smaller infarct volume. Because of these reasons, in the present thesis only one ELISpot experiment was possible after simultaneous blocking of the SNS and HPA axes of CIDS. However, brain ELISpot was also performed after single SNS block with propranolol where a higher number of brain MNCs was available since infarct

volumes in these mice were not so much smaller. Data from these ELISpots support the findings of brain ELISpot after simultaneous blocking of the SNS and HPA axes of CIDS.

6.2 CNS antigen specific Th1-type autoreactive myelin oligodendrocyte glycoprotein specific immune responses in the ischemic brain are increased after blocking CNS injury induced immunodepression

The blood-brain-barrier damage in stroke facilitates the entry of leukocytes like neutrophils, macrophages and lymphocytes into damaged brain and allows brain antigens to enter peripheral circulation. CNS-antigens that normally are not accessible to immune cells become available in increased numbers. This might enhance priming and activation of autoreactive T cells after stroke (Becker et al., 2005).

Cerebrospinal fluid and peripheral blood of the stroke patients contains increased concentrations of antibodies and T cells specific for various CNS-antigens. These include, neurofilament-specific antibodies (Bornstein et al., 2001), autoreactive T cells recognizing myelin components such as myelin basic protein and proteolipid protein (Wang et al., 1992) and microtubule-associated protein 2 and N-methyl D-aspartate receptor subunit NR-2A (Planas et al., 2012). CNS-antigen specific T cells are often regulatory (Becker et al., 1997; Becker et al., 2005). While the key mechanism of CIDS is inhibition of T cell differentiation, proliferation and function (Prass et al., 2003), regulatory T cells are also relatively resistant to apoptosis induced by elevated glucocorticoid levels (Tischner and Reichardt, 2007) characteristic to CIDS. In order to transfer autoimmune disease like EAE, MOG TCR Th1 cells have to differentiate into effector/memory T cells that express adhesion molecule CD44 (Jager et al., 2009; Williams et al., 2011). CD44 promotes T cell rolling prior to crossing endothelial barriers, homing and cellular infiltration in early stages of a delayed-type hypersensitivity response (Borland et al., 1998). Depletion of circulating T cells, which also occurs in CIDS after stroke, reduces ischemic brain damage (Kleinschnitz et al., 2010). This might be a mechanism, how CIDS reduces the probability of developing CNS-antigen specific autoimmune responses after stroke. Accordingly, blocking CIDS would promote this.

In the present thesis, T cell subpopulations, including the MOG-specific ones, were quantified in the ischemic brains of 2D2 mice 14 days after MCAo and CIDS block. At the same time point, enumeration of phenotypically different MOG-reactive T cells among brain MNCs was performed using ELISpot assay. Peak infiltration of $CD4^+$ T cells has been shown to occur 14 days after MCAo and plateau until day 30 after stroke (Stubbe et al., 2013). Independent of

the use of preventive enrofloxacin, blocking SNS mediated CIDS with propranolol had no effect on the number of brain infiltrating leukocytes, including $CD4^+$ $V\alpha3.2^+$, $CD8^+$ $V\alpha3.2^+$ T cells and those expressing CD44 (effector/memory MOG-specific T cells) or CD25 (regulatory MOG-specific T cells). The numbers of brain infiltrating leukocytes were also not altered in C57Bl/6J mice and between β2-AR ko mice and their wild-type littermates. The latter demonstrates that leukocyte recruitment to the lesion at this time point was not significantly influenced by β2-AR. However, CIDS block affected the phenotype and autoreactive potential of T cells among brain infiltrating MNCs. ELISpot assay demonstrated that blocking SNS axis of CIDS increased the relative number of MOG-specific Th1 cells among the MNCs that react to stimulation with MOG with IFN-γ production. Thus suggesting altered autoreactive potential of MOG-specific Th1 cells after blocking SNS axis of CIDS with propranolol. MOG-specific T cell responses of Th2 and Th17 type were not affected by propranolol treatment. Increased MOG-specific Th1-type autoreactive immune responses in ischemic brain was confirmed and magnified in experiments where the SNS and HPA axes of CIDS were simultaneously blocked. Furthermore, enhanced Th1-type MOG-specific autoreactive immune responses after stroke appeared to be CNS-specific and were not found in a peripheral lymphoid organ spleen. This suggests that CIDS affects predominantly and rather specifically the development of Th1-type autoreactive immune responses to MOG-specific T cells in stroke. Th1-type autoreactive immune response from MOG-specific IFN-γ secreting T cells has been shown to be of key relevance also in MOG-induced multiple sclerosis pathology, whereas the quantity of these cells is not affected (Van der Aa et al., 2003).

Adoptive transfer experiment using 2D2 mice (naïve, vehicle or propranolol and mifepristone treated to block the SNS and HPA axes of CIDS) as $CD4^+$ T cell donors and B and T cell deficient Rag-1KO mice as recipients showed that 2D2 $CD4^+$ T cells still located around and within the ischemic lesion of Rag-1KO mice 30 days after MCAo and cell transfer. The quantity of transferred $CD4^+$ T cells in the brains of Rag-1KO mice 30 days after stroke was not affected by the treatment of donor 2D2 mice. The $CD4^+$ T cells likely proliferate in the brain or re-enter the ischemic lesion. When infiltrating brain, CNS-antigen specific T cells have been described to remain in brain parenchyma or re-enter in cycles when recognizing their antigen in a correct MHC context (Hickey et al., 1991).

6.3 Blocking CNS injury induced immunodepression does not worsen functional long-term outcome after stroke

MCAo and blocking CIDS induced specific neurological deficits in mice. In the present thesis these deficits were characterized with emphasis on signs of CNS-directed autoreactive immune responses. Functional tests were performed over a time period of 30 days after MCAo.

Blocking CIDS did not introduce new gait deficits or result in enhanced locomotor deficits compared with vehicle-treated mice. Measurements from 10 days after MCAo, reflecting mid-term outcome after MCAo revealed that mice from both groups, with and without CIDS block, developed similarly typical stroke-induced alterations in gait reported in laboratory rodents (Vandeputte et al., 2010; Hetze et al., 2012; Li et al., 2013). Vehicle treated mice and those where the SNS and HPA axes of CIDS were simultaneously blocked did also not differ 30 days after MCAo. Therefore, locomotor deficits in 2D2 mice after simultaneous blocking of SNS and HPA axes of CIDS but do not differ from those in vehicle-treated mice.

Ninety-six percent of 2D2 mice where majority of the peripheral $CD4^+$ T cells carry a functional receptor for MOG peptide fragment ($pMOG_{35-55}$) do not develop spontaneous EAE (Bettelli et al., 2003). This is because of the limited access of these MOG TCR transgenic $CD4^+$ T cells to the CNS where MOG mainly locates and the need for prior differentiation into effector/memory MOG TCR T cells (Jager et al., 2009; Williams et al., 2011). Damage to the blood-brain-barrier during stroke might thus stimulate MOG-directed autoreactive immune responses in these mice. Generally, MOG-induced EAE is a model of choice for investigating axonal damage and demyelination in multiple sclerosis (Tischner and Reichardt, 2007). MOG-induced demyelination is mediated by MOG-specific Th1 and Th17 cells (Linington et al., 1993; Genain et al., 1996; Stromnes et al., 2008; Bettini et al., 2009; Jager et al., 2009), the key players in autoreactivity. Furthermore, findings from this thesis demonstrate higher MOG-specific Th1 cell responses among brain infiltrating MNCs following CIDS block. Therefore, it was of interest to investigate whether this would also result in functional neurological symptoms indicative of CNS-antigen (such as MOG) specific autoreactive immune responses.

Despite the higher Th1 type autoreactive potential in ischemic brain after CIDS block, the development of EAE-like disease phenotype was not augmented by CIDS block. However, lack of the β2-AR at birth was associated with worse EAE-like symptoms after MCAo.

Symptoms of EAE-like disease in were generally mild, including mainly hind limb weakness with or without tail paralysis. MOG-induced EAE has been described to typically manifest with mild clinical symptoms but enhanced histopathological damage compared with, for example, myelin basic protein induced EAE. MOG-specific T cells, the primary source of MOG-induced demyelination and EAE pathology, accumulate primarily at perivascular cuffs (Linington et al., 1993; Genain et al., 1996; Bettini et al., 2009). They infiltrate the CNS poorly but yet sufficiently to induce demyelinating lesions in the brain (Jager et al., 2009) and spinal cord (Stromnes et al., 2008). In addition to the lack of difference in EAE score between vehicle-treated mice and those where CIDS was blocked, blocking simultaneously the SNS and HPA axes of CIDS delayed the onset of EAE-like disease by a median of five days. Final disease severity remained, however, similar in vehicle as well as propranolol and mifepristone treated mice. This delay in symptom onset and disease development was not observed when only the SNS axis of CIDS was blocked with propranolol, indicating that combined effects of propranolol and mifepristone, like that on infarct volume, might modulate EAE-like disease development.

The neurological phenotype of mice after vehicle or propranolol and mifepristone treatment did not only manifest with an EAE-like disease. Beyond the initial hemiparesis after stroke, 2D2 mice developed flaccid rather than spastic paralysis similar to polyradicultis. MOG is indeed also expressed in the peripheral nervous system, however, in about ten times lower amounts than in the CNS (Pagany et al., 2003). To better characterize the observed neurological phenotype, sciatic nerve conduction was assessed electrophysiologically and immune cell infiltration to spinal cord and nerve roots was analyzed immunohistochemically. Findings from both, electrophysiology and immunohistochemistry supported the polyradiculitis like phenotype which, however, was also not augmented by blocking the SNS and HPA axes of CIDS. Latencies to F-wave upon sciatic nerve stimulation were elongated in vehicle group of 2D2 mice, suggestive of higher degree of demyelination in vehicle-treated mice. This electrophysiological observation is supported by findings of pathological ulnar F-wave variables in severely affected stroke patients (Chroni et al., 2006; Chroni et al., 2007). Blocking CIDS with propranolol and mifepristone had a normalizing effect on sciatic nerve F-wave latencies after stroke. Because the inflammatory infiltrates characteristic to MOG-induced demyelinating lesions contain predominantly (memory) T cells and macrophages (Linington et al., 1993; Genain et al., 1996; Hjelmstrom et al., 1998), these cells were of interest in immunohistochemial staining of vertebral columns. Unlike in classical MOG-induced EAE (Stromnes et al., 2008), immune cell infiltrates were not found in the spinal

cord. Immune cell infiltration was, however, observed in spinal nerve roots 30 days after MCAo. T cells were often found together with macrophages suggestive of antigen presentation. Both, T cells and macrophages were significantly more frequent in the spinal nerve roots of vehicle-treated 2D2 mice. Therefore, blocking the SNS and HPA axes of CIDS simultaneously with propranolol and mifepristone diminished the polyradiculitis like phenotype.

That blocking the SNS and HPA axes of CIDS simultaneously did not enhance the EAE-like disease and polyradiculitis phenotype, was verified in an adoptive transfer experiment where B and T cell deficient Rag-1KO mice received 6 h after MCAo $CD4^+$ T cells from either vehicle or propranolol and mifepristone treated 2D2 mice, that seven days earlier had undergone MCAo, or from naïve 2D2 mice. EAE-like disease was milder in Rag-1KO mice and immune cell infiltration to spinal nerve roots approximately four times lower than in 2D2 mice. Moreover, neither the EAE-like disease development nor the infiltrates to nerve roots differed between the three groups of Rag-1KO mice. Immune system in Rag-1KO mice is altered as they lack functional T and B cells. Even though B cells have been shown not to be relevant in MOG-induced demyelination and axonal damage (Linington et al., 1993; Genain et al., 1996; Hjelmstrom et al., 1998) the lower neurological deficits in Rag-1KO mice might be explained by the altered immunological milieu due to substantial lack of lymphocytes. Compared with Rag-1KO mice that received $CD4^+$ T cells from naïve 2D2 mice, the ones receiving $CD4^+$ T cells from 2D2 mice treated with propranolol and mifepristone to block CIDS showed higher post-stroke mortality. However, the survival rates of Rag-1KO mice adoptively transferred with $CD4^+$ T cells from vehicle-treated or propranolol and mifepristone treated 2D2 mice did not differ. Nevertheless, it cannot be excluded that higher mortality among Rag-1KO mice adoptively transferred with $CD4^+$ T cells from 2D2 mice in which the SNS and the HPA axes of CIDS were blocked compared with those adoptively transferred with naïve $CD4^+$ T cells from 2D2 mice might reflect early (detrimental) effects of MOG-specific autoreactive immune responses.

Reduced neurological symptoms in mice after CIDS block yet the increased Th1-type MOG-specific autoreactive potential locally in ischemic brain could be explained by neuroprotective functions of these T cells as well as overall reduced post-stroke infection rate and better coping with infections after CIDS block. Infarct volume is clearly smaller in mice that received treatment to block CIDS via SNS and HPA axis. Blocking SNS axis of CIDS alone already resulted in reduced incidence of pulmonary infections. Until today, it is not clear

which exact factors and mechanisms determine the development of detrimental and protective autoreactive T cell responses. However, they likely involve antigen specificity and phenotype of T cells, genetic factors, pattern and dynamics of T cell activation as well as infections and the size of the ischemic lesion (Czlonkowska et al., 1979; Becker et al., 1997; Frenkel et al., 2003; Hofstetter et al., 2003; Becker et al., 2005; Lewitus et al., 2006; Planas et al., 2012). In the absence of microbial agents in the brain, CNS-antigen specific Th1 and Th2 cells have been shown to accelerate healing in a model of severe aseptic cryoinjury to the brain (Hofstetter et al., 2003) and pro-inflammatory CNS-antigen specific Th1 cells to improve neuronal survival after the CNS injury (Kipnis et al., 2002). Inflammatory stimulus and infections at the time of stroke or later, on the other hand, promote detrimental Th1- (Becker et al., 2005; Becker et al., 2011) and Th2-type CNS-antigen specific responses in ischemic brain through stimulation of antigen presenting cells (Hofstetter et al., 2003), leading to enhanced neurological impairment. Changes in local brain microenvironment induced by inflammatory stimulus determine the type of T cell response (Becker et al., 2005). In fact, lipopolysaccharide challenge alone is sufficient to trigger EAE in mice overexpressing a TCR for myelin basic protein (Nogai et al., 2005). Detrimental CNS-antigen specific immune responses are thus promoted by infections and local inflammation in the brain. Additionally, larger infarct volumes contribute to increased risk of post-stroke infections (Czlonkowska et al., 1979; Asadullah et al., 1995; Woiciechowsky et al., 1998). The latter was confirmed in experimental stroke in the present thesis, demonstrating more frequent bronchopulmonary infections in mice with larger infarcts. Based on the above, it can be speculated that the effect of CIDS block on CNS-directed functional autoreactive immune responses in the present thesis was diluted, leading to possible underestimation of CNS-antigen specific immune responses upon CIDS block.

6.4 Incidence of bronchopulmonary infections is decreased and recovery of infected mice is promoted by blocking CNS injury induced immunodepression

Infections, particularly urinary tract and pulmonary infections, are common complications of stroke (Brown and Glassenberg, 1973; Czlonkowska et al., 1979) and the leading cause of death in post-acute phase (Vernino et al., 2003). In addition, pulmonary infections predict poorer neurological outcome after stroke (Emsley and Hopkins, 2008; Becker et al., 2011).

In mice, bronchopulmonary infections can be reliably identified based on the bacterial burden in the BAL fluid (Hetze et al., 2013). This method is minimally invasive and mice can be followed continuously thereafter. Another method to confirm bronchopulmonary infections in mice is a microbiological analysis from lung homogenates. This, however, does not allow for further monitoring of the subject. Analysis of bacterial load in the BAL fluid showed a strong positive correlation with the bacterial load in the lung, confirming this as a reliable method for identifying mice with bronchopulmonary infections. Blocking SNS axis of CIDS with propranolol decreased the incidence of bronchopulmonary infections in male 2D2 mice as indicated by the bacterial burden in both, BAL fluid as well as lung homogenates. This effect was gender specific. Previously, propranolol has been shown to reduce the bacterial burden in the lungs of gender-mixed SV129/J mice through a mechanism involving the β2-AR (Prass et al., 2003). Results from the present thesis demonstrate that this immunostimulatory effect of propranolol applies also for male 2D2 mice. Experiments with β2-AR ko mice and their wild-type littermates did not identify a significant difference between the bacterial burdens in the BAL fluid but the average values with standard deviations in these mice are highly similar to those in propranolol and vehicle-treated mice, respectively. Therefore, it cannot be excluded that this propranolol effect is indeed mediated by its antagonism of the β2-AR and that larger sample number would have been necessary pointing out a clear difference. However, neither propranolol nor mifepristone was capable of reducing the bacterial burden in the BAL fluid of female 2D2 mice. Mifepristone has been shown to have no effect on the bacterial load in the lung tissue of gender-mixed SV129/J mice (Prass et al., 2003).

Propranolol effect in reducing the bacterial load in the BAL fluid and in lung homogenates was not infarct volume dependent. In vehicle-treated mice, on the other hand, the bacterial load in the BAL fluid correlated strongly and positively with infarct volumes in these mice. Larger infarcts in stroke patients are known to magnify the extent of CIDS and consequently increase the likelihood of infections and poorer neurological outcome (Czlonkowska et al., 1979; Asadullah et al., 1995; Woiciechowsky et al., 1998).

Preventive enrofloxacin administration in experiments with simultaneous blocking of the SNS and HPA axes of CIDS was not able to fully block the development of infections in all stroked mice. Similarly, preventive antibiotic treatment in cerebral ischemia patients reduces but does not block the occurrence of pneumonia (Chamorro et al., 2012). However, blocking simultaneously the SNS and HPA axes of CIDS with propranolol and mifepristone promoted recovery from bronchopulmonary infections and elongated life expectancy of infected mice.

This was accompanied by overall improvement of health status, stable body weight and temperature as well as higher survival rate in these mice. The effect was not observed when only the SNS axis of CIDS was blocked with propranolol. Simultaneous blocking of the SNS and HPA axes of CIDS with propranolol and mifepristone thus results in more efficient coping with infections, improved health status and survival after stroke.

6.5 Infarct volume is robustly smaller after combined treatment with propranolol and mifepristone

Probably most intriguing is my finding that infarct volume is two thirds smaller in female 2D2 and C57Bl/6J mice after simultaneous blocking of SNS and HPA axes of CIDS with propranolol and mifepristone compared with vehicle treatment. This effect was stable for at least seven days after MCAo. Therefore, while delayed infarct volume maturation has often been described (Du et al., 1996; Becker et al., 1997; Frenkel et al., 2003), data from this thesis suggests it was not the case here and implies that the combined treatment protects neurons in the penumbra region surrounding the ischemic core. Even though it is not fully clear, which effects of propranolol and mifepristone predominantly and specifically contribute to the effect on infarct volume, it has to involve combined effects of both agents since alone they were not capable of diminishing infarct volume to a comparable level. Infarct volume is only moderately smaller when SNS axis of CIDS is blocked with propranolol alone. Even though there was no significant difference in infarct volumes after mifepristone treatment used for blocking the HPA axis of CIDS alone, the average infarct volume was moderately smaller in both, male and female 2D2 mice. The robust effect on infarct volume observed after blocking simultaneously the SNS and HPA mediated CIDS is most likely caused by synergistic functions of propranolol and mifepristone. SNS and HPA axis are anatomically and functionally connected and the activation of one commonly leads to potentiation of the other (Smythe et al., 1983; McEwen et al., 1987; Collins et al., 1988; Hadcock and Malbon, 1988).

Since SNS and HPA are both the central pathways in communication between the nervous and immune system, the effects of propranolol and mifepristone on immune responses and inflammation after stroke can be involved in the observed effect. This might comprise early effects on infiltrating immune cells, microglia or even T cells, which are strongly influenced by the activity of the SNS and HPA (Elenkov et al., 2000; Tischner and Reichardt, 2007). That different T cell subpopulations are capable of mediating either detrimental or protective effects in stroke, has been shown (Yilmaz et al., 2006; Hurn et al., 2007; Liesz et al., 2009;

Shichita et al., 2009; Liesz et al., 2011; Kleinschnitz et al., 2013). Whereas specific β2-AR antagonism and lack of β2-AR at birth has been shown to decrease infarct volume by about 20% (Han et al., 2009), results from the present thesis, where infarct volumes from non-specific β-blocker propranolol treated mice were compared with those from β2-AR ko mice demonstrate that mechanisms behind reduced infarct volumes are not mediated by the β2-AR. Because neuroprotection and reduction of ischemic lesion occur rapidly after MCAo, immunomodulatory effects possibly do not account for the main mechanism for infarct volume attenuation.

Propranolol and mifepristone exert also other functions that can likely contribute to smaller infarct volume. For example, mifepristone is a powerful antioxidant (Parthasarathy et al., 1994) and prevents DNA fragmentation (Behl et al., 1997). Neuroprotective effects of mifepristone are not related to glucocorticoid receptor antagonism and genomic effects. Mifepristone protects Purkinje neurons from apoptosis in a glucocorticoid-receptor independent manner by affecting membrane depolarization (Ghoumari et al., 2006). Mifepristone protects also hippocampal neurons from cell death after traumatic brain injury through a mechanism not affecting cell death related gene expression. This effect is observed as early as 24 h after the trauma (McCullers et al., 2002). Additionally, mifepristone reverses ischemic lesion aggravation by stress (Sugo et al., 2002). Propranolol, on the other hand, limits hypoxic damage (Ley et al., 2009). Propranolol also reverses the detrimental effects of elevated corticosterone levels such as augmentation of cognitive deficits and increased Alzheimer's pathology through amyloid-β plaque accumulation and tau phosphorylation (Dobarro et al., 2013). Adrenergic nerve fibers form a dense mesh around cerebral arteries (Edvinsson et al., 1975) allowing propranolol to increase cerebral perfusion upon traumatic brain injury (Edvinsson et al., 1979). The role of mifepristone in CBF regulation is marginal (Balkaya et al., 2011). Increased CBF is typically associated with decreased infarct volumes (Dalkara et al., 1994). However, altered CBF is not the primary reason behind the massive attenuation of infarct volume development after simultaneous blocking of SNS and HPA axes of CIDS with propranolol and mifepristone. Nevertheless, the cerebroprotective effects of propranolol and mifepristone might be mediated by small but prolonged elevations in CBF below the measuring threshold of FAIR-MRI (Leithner et al., 2008).

6.6 Gender differences in SNS and HPA function and immune responses

Several of the effects presented in this thesis were gender-specific. Below I will discuss some of the relevant differences between males and females in regard to immune response and stress systems: the SNS and the HPA axis.

Sex hormones influence immune system directly by binding appropriate receptors on thymocytes and peripheral immunocompetent cells. Sex hormones regulate T cell differentiation, cytokine production and adhesion molecule expression (Da Silva, 1999).

In addition to direct effects, estrogen modulates immune responses by interacting with nuclear factor kappa B transcription factor to control, for example, IL-6 synthesis. Estrogen in females stimulates B cell function and antibody production but inhibits suppressor T cell activity (Da Silva, 1999). By binding its response element on the 5'-prime flanking region of the IFN-γ gene, estrogen stimulates IFN-γ release (Fox et al., 1991) which potentiates immune reactions and might enhance the Th1-type responses in females. Furthermore, estrogen promotes $CD4^+$ T cell expansion, antigen-specific T cell expansion, IFN-γ secretion by these cells and accumulation of $CD4^+$ Th1 cells upon antigen-stimulation (Maret et al., 2003). Some of the estrogen effects, such as enhancing T cell response, T and B cell interactions, promotion of B cell growth and differentiation through, for instance CD40 ligand up-regulation on antigen-specific T cells are related to autoimmune diseases like systemic lupus erythematosus and do not apply in healthy subjects (Rider et al., 2001). However, in EAE estrogen has also been shown to ameliorate clinical symptoms through a mechanism involving IL-10 secretion from myelin basic protein specific T cells (Kim et al., 1999).

Immunosuppressive potential of endogenous androgen in males is exceeding that of glucocorticoids. Testosterone in males suppresses the function of both, B and T cells. They also potentiate glucocorticoid immunosuppressive effects on immune cells in the presence of lower hormone levels (Da Silva, 1999). In contrast to estrogen, testosterone promotes Th2 cell responses and shifts the Th1/Th2 balance towards Th2 cells. A study comparing the effects of T cell stimulation in male and female mice revealed that male mice produced two-fold more IL-4 and IL-10 but less IL-12 than the female mice. Testosterone was responsible for this increase in IL-10 release from $CD4^+$ T cells (Liva and Voskuhl, 2001). This could be one of the explanations why females are more prone than males to develop autoimmune diseases.

Male and female sex hormones elicit different and contrasting effects on the HPA axis activation resulting also in different modulation of immune responses. Gonadectomy (Da

Silva et al., 1993) and ovarectomy (Carey et al., 1995) experiments have demonstrated that androgens inhibit while estrogens enhance HPA axis activation in response to stress. Females produce higher levels of ACTH and corticosterone in resting state as well as under stress than males (Le Mevel et al., 1978; Chisari et al., 1995). Sex hormones affect corticosterone synthesis at the level of corticotropin releasing hormone synthesis from the paraventricular nucleus of the hypothalamus (Watts and Swanson, 1989) as well as from secondary peripheral sources including thymus and spleen as well as immune cells (Da Silva, 1999). Estrogen receptors are expressed in this area whereas androgen receptors are absent or very scarce in the corticotropin releasing hormone producing neurons (Simerly et al., 1990; Bingaman et al., 1994). However, androgen and estrogen receptors are both present on cells expressing mineralo- and glucocorticoid receptors. Corticotropin releasing hormone carries an estrogen response element which allows estrogen to directly regulate the hormone. Androgen effects on corticosterone synthesis are mainly mediated by neurons projecting from the hippocampus and the medial preoptic area to the paraventricular nucleus of the hypothalamus. HPA axis is sensitive to inherent testosterone concentrations (Simerly et al., 1990). Estrogen inhibits the negative feedback loop of corticosterone synthesis (Burgess and Handa, 1993). Additionally, it stimulates the HPA axis via regulating the expression of mineralocorticoid and glucocorticoid receptors and their binding affinity (Burgess and Handa, 1993; Carey et al., 1995). Androgen, on the contrary, potentiates the negative feedback loop of corticosterone synthesis. Female and male mice differ also in their response to inflammatory stimulus such as peripheral IL-1 injection or chronic cotton-induced granulomatous inflammation which enhances the activation of HPA axis in female mice. Female mice appear to be more sensitive to the factors activating the HPA axis and a have greater tendency to generate HPA axis activating signals (Da Silva et al., 1993).

Sex hormone effects on SNS activation are similar to the HPA stress axis activation in that SNS stimulation is more potent in females. Gonadectomy studies in rats have shown that orchiectomy in males increases and ovarectomy in females decreases the noradrenaline synthesis. Therefore, estrogen promotes and testosterone inhibits noradrenaline synthesis. Estradiol administration to gonadectomized rats increases gender-specifically noradrenaline turnover in the preoptic-anterior hypothalamic brain area in female rats (Hiemke et al., 1985; Miskowiak, 1985). Despite the reduced noradrenaline secretion in ovarectomized rats, the secretion of dopamine is increased (Miskowiak, 1985). Dopamine is another catecholamine in addition to noradrenaline and adrenaline which also functions as noradrenaline precursor. Thus, lack of estrogen possibly inhibits the turnover of dopamine to noradrenaline. Both,

testosterone (Jeong et al., 2006) and estrogen (Thanky et al., 2002) regulate the synthesis of thyrosine hydroxylase, a rate-limiting enzyme in dopamine and catecholamine synthesis. Utilization rate for noradrenaline in the midbrain is likely enhanced in females (Gordon and Shellenberger, 1974).

Sex steroids can also differentially affect drug absorption and function. This applies for propranolol, a non-specific β-AR antagonist used in this thesis to block the SNS mediated CIDS. Its metabolism and clearance are enhanced by testosterone in males (Walle et al., 1994). On the other hand, the binding affinity of the S-enantiomer of propranolol is greater in females than males (Gilmore et al., 1992).

Therefore, the differences observed in this thesis regarding the tolerance and toxicity of simultaneous propranolol and mifepristone treatment at the time of MCAo to block the SNS and HPA axis mediated CIDS, likely involve gender effects on stress axis activation and might suggest gender specific effects also on CIDS after stroke. The literature discussed above in this chapter can be summarized in that females are more sensitive and respond to stress axis stimulation with a higher activation level. Most likely, different doses of SNS and HPA axis blocking agents are necessary for male and female mice to avoid missing stress response and blocking of the cardiovascular system at the time of stroke.

6.7 Future challenges

Understanding that CIDS is triggered by the CNS injury, such as stroke, itself and that CIDS leads to increased susceptibility to infections and poorer neurological outcome, has opened a new avenue for the search of immunomodulatory agents and approaches in stroke. Here, I have investigated if and how blocking the SNS and HPA axes of CIDS affect the development of CNS-antigen specific autoimmune responses and long-term functional neurological outcome after stroke. SNS was blocked with propranolol and HPA axis with mifepristone. In conclusion, obtained results demonstrate that blocking the key mediators of CIDS, either SNS alone or SNS and the HPA axis simultaneously, leads to increased CNS-antigen specific Th1-type autoreactive potential among brain MNCs. However, this is not accompanied by worse functional neurological outcome. In addition, I have characterized the phenotype of neurological deficits in 2D2 mice following stroke and simultaneous blocking of the SNS and the HPA axes of CIDS.

In this thesis, I have focused on EAE-like disease phenotype, locomotor deficits, electrophysiology for sciatic nerve conduction velocities and spinal nerve root immunohistochemistry for immune cell infiltrates to characterize the polyradicultis-like phenotype. Mice where the SNS and the HPA axes of CIDS were blocked did not perform worse than vehicle-treated mice in any of these tests and examinations. Therefore increased Th1-type autoreactive potential in ischemic brain at the time of peak $CD4^+$ T cell infiltration does not result in worse autoreactive phenotype in these mice. Because SNS and HPA are stress axes and the hippocampal involvement in memory functions, it remains to be elucidated whether simultaneous blocking of the SNS and HPA axes of CIDS would affect cognition and memory using, for example, novel object recognition test.

Intriguingly, simultaneous blocking of SNS and HPA axes of CIDS also led to a massively and sustainably smaller infarct volume in MOG TCR transgenic 2D2 mice and wild-type C57Bl/6J mice. This effect was not primarily mediated by altered CBF. It cannot be excluded that smaller infarct volume was in part responsible for the better health status and unchanged or improved functional outcome in these mice. However, the adoptive transfer experiment with $CD4^+$ T cells from differentially treated 2D2 mice as donors and lymphocyte-deficient Rag-1KO mice as recipients provided similar results to those obtained with 2D2 mice. Since the observed smaller infarct volume resembled one after a 30-minute MCAo, it remains to be investigated whether performing a 30-minute MCAo in vehicle group of mice and a 60-minute MCAo in mice were the SNS and HPA axes of CIDS are blocked would result in similar infarct volumes in both groups and whether this would lead to differences in functional neurological outcome between the groups.

The findings of this thesis demonstrate that manipulating stress axes and CIDS are promising treatment targets in acute CNS lesion. In a murine model of MCAo I have shown that blocking the SNS and the HPA axis of CIDS reduces infection rate, infarct volume and appears to have no negative consequences on long-term functional outcome. Nevertheless, caution is needed because of the CNS-specific autoreactive T cell responses.

7. Conclusion

The principal goal of my doctoral thesis was to investigate whether CIDS represents a built-in mechanism to reduce the likelihood of CNS-directed autoreactivity after stroke when brain antigens become accessible to circulating immune cells. This was studied in a set of experiments divided into three main categories. The results can be summarized as follows:

1. Blocking SNS axis of CIDS with propranolol attenuated infarct volume development and reduced bacterial burden in the BAL fluid and lungs of male 2D2 mice. As hypothesized, blocking SNS axis of CIDS with propranolol increased the fraction of CNS-antigen (MOG) specific IFN-γ secreting cells ipsilaterally, indicating higher Th1-type autoreactive potential at the time of peak T cell infiltration 14 days after MCAo. This effect was limited to the CNS. The quantity of different leukocyte subsets, including the MOG-specific T cells, was, however, not altered. This suggests that not the quantity but the quality of brain infiltrating (MOG-specific) T cells is affected by CIDS block with propranolol. In spite of the increased Th1-type autoreactive potential in ischemic brain of propranolol-treated mice, locmotor deficits and EAE-like disease development were not enhanced by blocking SNS axis of CIDS. However, lack of the β2-AR at birth was associated with the development of more severe EAE-like symptoms. The number of MOG-specific T single positive helper and effector T cells was increased in the thymi of propranolol-treated mice. In the spleen, blocking SNS axis of CIDS combined with preventive enrofloxacin reduced the numbers of MOG-specific IL-17 (Th17) cells.

2. Blocking simultaneously the SNS and HPA axes of CIDS with propranolol and mifepristone attenuated strongly infarct volume resulting in two thirds smaller values and consequently reduced leukocyte infiltration to ischemic brain 14 days after MCAo. Smaller infarct volumes were accompanied by better health status, improved survival, improved coping with infections and elongated life expectancy. Similar to blocking the SNS axis of CIDS alone, blocking simultaneously the SNS and the HPA axes of CIDS increased the fraction of IFN-γ secreting MOG-specific Th1 cells among brain infiltrating MNCs. Also here, this effect was CNS-specific. Whereas after blocking only the SNS axis of CIDS these mice did not differ from vehicle-treated mice, blocking simultaneously the SNS and HPA axes of CIDS diminished the polyradiculitis phenotype observed after MCAo by normalizing F-wave latencies upon sciatic nerve stimulation and minimizing T cell and macrophage infiltration to spinal nerve roots. EAE-like

disease development and locomotor deficits after MCAo were not aggravated after blocking the SNS and the HPA axes of CIDS.

3. Adoptive transfer of $CD4^+$ T cells from naïve or differentially treated 2D2 donor mice (vehicle or combined treatment with propranolol and mifepristone to block the SNS and the HPA axes of CIDS; seven days after MCAo) to lymphocyte-deficient Rag-1KO mice demonstrated that these $CD4^+$ T cells had migrated ischemic brain and still located within and around ischemic lesion 30 days after MCAo. A low amount of transferred $CD4^+$ T cells had also migrated to spinal nerve roots 30 days after MCAo. The quantity of $CD4^+$ T cells and as well as the number of activated microglia and macrophages (in the brain) or macrophages alone (spinal nerve roots) was not affected by the treatment of donor mice. Furthermore, symptoms of CNS inflammation evaluated by EAE score and locomotor deficits in Rag-1KO mice were not augmented by transfer of $CD4^+$ T cells from 2D2 mice that had been treated with propranolol and mifepristone to block the SNS and the HPA axes of CIDS.

In summary, this thesis provides evidence that blocking CIDS in a murine model of MCAo increases the CNS-antigen specific Th1-type autoreactive potential in the ischemic brain. However, even in long-term this does not aggravate functional neurological outcome in these mice. Furthermore, blocking simultaneously SNS and HPA axes of CIDS normalized MCAo-induced elongated F-wave latencies upon sciatic nerve stimulation and diminished the polyradiculitis phenotype by reducing T cell and macrophage infiltration to spinal nerve roots. This favors the idea that blocking the SNS and HPA axes of CIDS with propranolol and mifepristone promotes beneficial type of autoreactive immune responses over detrimental ones. Additionally, after blocking SNS and HPA axes of CIDS with propranolol and mifepristone, infarct volume is two thirds smaller with no delayed infarct volume maturation. It remains to be investigated whether these agents carry therapeutic potential in stroke. Further studies with shifted injection schemes and additional investigations for additional functional tests and the effects of these drugs on cognition are guaranteed.

8. References

Aarons RD, Nies AS, Gerber JG, Molinoff PB (1983) Decreased beta adrenergic receptor density on human lymphocytes after chronic treatment with agonists. The Journal of pharmacology and experimental therapeutics 224:1-6.

Abrass CK, O'Connor SW, Scarpace PJ, Abrass IB (1985) Characterization of the beta-adrenergic receptor of the rat peritoneal macrophage. J Immunol 135:1338-1341.

Adelmann M, Wood J, Benzel I, Fiori P, Lassmann H, Matthieu JM, Gardinier MV, Dornmair K, Linington C (1995) The N-terminal domain of the myelin oligodendrocyte glycoprotein (MOG) induces acute demyelinating experimental autoimmune encephalomyelitis in the Lewis rat. J Neuroimmunol 63:17-27.

Ahlquist RP (1948) A study of the adrenotropic receptors. Am J Physiol 153:586-600.

Amiguet P, Gardinier MV, Zanetta JP, Matthieu JM (1992) Purification and partial structural and functional characterization of mouse myelin/oligodendrocyte glycoprotein. J Neurochem 58:1676-1682.

Ando DG, Clayton J, Kono D, Urban JL, Sercarz EE (1989) Encephalitogenic T-Cells in the B10.Pl Model of Experimental Allergic Encephalomyelitis (Eae) Are of the Th-1 Lymphokine Subtype. Cellular Immunology 124:132-143.

Asadullah K, Woiciechowsky C, Docke WD, Liebenthal C, Wauer H, Kox W, Volk HD, Vogel S, Von Baehr R (1995) Immunodepression following neurosurgical procedures. Crit Care Med 23:1976-1983.

Augustine JJ, Hricik DE (2012) T-cell immune monitoring by the ELISPOT assay for interferon gamma. Clinica chimica acta; international journal of clinical chemistry 413:1359-1363.

AyanlarBatuman O, Ferrero AP, Diaz A, Jimenez SA (1991) Regulation of transforming growth factor-beta 1 gene expression by glucocorticoids in normal human T lymphocytes. J Clin Invest 88:1574-1580.

Azzi M, Charest PG, Angers S, Rousseau G, Kohout T, Bouvier M, Pineyro G (2003) Beta-arrestin-mediated activation of MAPK by inverse agonists reveals distinct active conformations for G protein-coupled receptors. Proc Natl Acad Sci U S A 100:11406-11411.

Balkaya M, Prinz V, Custodis F, Gertz K, Kronenberg G, Kroeber J, Fink K, Plehm R, Gass P, Laufs U, Endres M (2011) Stress Worsens Endothelial Function and Ischemic Stroke via Glucocorticoids. Stroke 42:3258-U3539.

Banks WA, Kastin AJ, Broadwell RD (1995) Passage of cytokines across the blood-brain barrier. Neuroimmunomodulation 2:241-248.

Barrat FJ, Cua DJ, Boonstra A, Richards DF, Crain C, Savelkoul HF, de Waal-Malefyt R, Coffman RL, Hawrylowicz CM, O'Garra A (2002) In vitro generation of interleukin 10-producing regulatory CD4(+) T cells is induced by immunosuppressive drugs and inhibited by T helper type 1 (Th1)-and Th2-inducing cytokines. J Exp Med 195:603-616.

Beamer NB, Coull BM, Clark WM, Hazel JS, Silberger JR (1995) Interleukin-6 and interleukin-1 receptor antagonist in acute stroke. Ann Neurol 37:800-805.

Becker KJ, Kindrick DL, Lester MP, Shea C, Ye ZC (2005) Sensitization to brain antigens after stroke is augmented by lipopolysaccharide. Journal of Cerebral Blood Flow and Metabolism 25:1634-1644.

Becker KJ, McCarron RM, Ruetzler C, Laban O, Sternberg E, Flanders KC, Hallenbeck JM (1997) Immunologic tolerance to myelin basic protein decreases stroke size after transient focal cerebral ischemia. Proceedings of the National Academy of Sciences of the United States of America 94:10873-10878.

Becker KJ, Kalil AJ, Tanzi P, Zierath DK, Savos AV, Gee JM, Hadwin J, Carter KT, Shibata D, Cain KC (2011) Autoimmune Responses to the Brain After Stroke Are Associated With Worse Outcome. Stroke 42:2763-U2133.

Bederson JB, Pitts LH, Tsuji M, Nishimura MC, Davis RL, Bartkowski H (1986) Rat Middle Cerebral-Artery Occlusion - Evaluation of the Model and Development of a Neurologic Examination. Stroke 17:472-476.

Behl C, Trapp T, Skutella T, Holsboer F (1997) Protection against oxidative stress-induced neuronal cell death - A novel role for RU486. European Journal of Neuroscience 9:912-920.

Bell MJ, Kochanek PM, Doughty LA, Carcillo JA, Adelson PD, Clark RS, Wisniewski SR, Whalen MJ, DeKosky ST (1997) Interleukin-6 and interleukin-10 in cerebrospinal fluid after severe traumatic brain injury in children. J Neurotrauma 14:451-457.

Benschop RJ, Rodriguez-Feuerhahn M, Schedlowski M (1996) Catecholamine-induced leukocytosis: early observations, current research, and future directions. Brain, behavior, and immunity 10:77-91.

Bettelli E, Pagany M, Weiner HL, Linington C, Sobel RA, Kuchroo VK (2003) Myelin oligodendrocyte glycoprotein-specific T cell receptor transgenic mice develop spontaneous autoimmune optic neuritis. J Exp Med 197:1073-1081.

Bettini M, Rosenthal K, Evavold BD (2009) Pathogenic MOG-reactive CD8+ T cells require MOG-reactive CD4+ T cells for sustained CNS inflammation during chronic EAE. J Neuroimmunol 213:60-68.

Bingaman EW, Baeckman LM, Yracheta JM, Handa RJ, Gray TS (1994) Localization of androgen receptor within peptidergic neurons of the rat forebrain. Brain Res Bull 35:379-382.

Blotta MH, DeKruyff RH, Umetsu DT (1997) Corticosteroids inhibit IL-12 production in human monocytes and enhance their capacity to induce IL-4 synthesis in CD4+ lymphocytes. J Immunol 158:5589-5595.

Borger P, Hoekstra Y, Esselink MT, Postma DS, Zaagsma J, Vellenga E, Kauffman HF (1998) Beta-adrenoceptor-mediated inhibition of IFN-gamma, IL-3, and GM-CSF mRNA accumulation in activated human T lymphocytes is solely mediated by the beta2-adrenoceptor subtype. American journal of respiratory cell and molecular biology 19:400-407.

Borland G, Ross JA, Guy K (1998) Forms and functions of CD44. Immunology 93:139-148.

Bornstein NM, Aronovich B, Korczyn AD, Shavit S, Michaelson DM, Chapman J (2001) Antibodies to brain antigens following stroke. Neurology 56:529-530.

Borovikova LV, Ivanova S, Zhang M, Yang H, Botchkina GI, Watkins LR, Wang H, Abumrad N, Eaton JW, Tracey KJ (2000) Vagus nerve stimulation attenuates the systemic inflammatory response to endotoxin. Nature 405:458-462.

Brown M, Glassenberg M (1973) Mortality factors in patients with acute stroke. JAMA : the journal of the American Medical Association 224:1493-1495.

Brown R, Li Z, Vriend CY, Nirula R, Janz L, Falk J, Nance DM, Dyck DG, Greenberg AH (1991) Suppression of splenic macrophage interleukin-1 secretion following intracerebroventricular injection of interleukin-1 beta: evidence for pituitary-adrenal and sympathetic control. Cell Immunol 132:84-93.

Brunner C, Lassmann H, Waehneldt TV, Matthieu JM, Linington C (1989) Differential Ultrastructural-Localization of Myelin Basic-Protein, Myelin Oligodendroglial Glycoprotein, and 2',3'-Cyclic Nucleotide 3'-Phosphodiesterase in the Cns of Adult-Rats. J Neurochem 52:296-304.

Buller KM (2001) Role of circumventricular organs in pro-inflammatory cytokine-induced activation of the hypothalamic-pituitary-adrenal axis. Clinical and experimental pharmacology & physiology 28:581-589.

Burgess LH, Handa RJ (1993) Estrogen-induced alterations in the regulation of mineralocorticoid and glucocorticoid receptor messenger RNA expression in the female rat anterior pituitary gland and brain. Molecular and cellular neurosciences 4:191-198.

Bylund DB, Eikenberg DC, Hieble JP, Langer SZ, Lefkowitz RJ, Minneman KP, Molinoff PB, Ruffolo RR, Jr., Trendelenburg U (1994) International Union of Pharmacology nomenclature of adrenoceptors. Pharmacological reviews 46:121-136.

Carey MP, Deterd CH, de Koning J, Helmerhorst F, de Kloet ER (1995) The influence of ovarian steroids on hypothalamic-pituitary-adrenal regulation in the female rat. The Journal of endocrinology 144:311-321.

Chamorro A, Meisel A, Planas AM, Urra X, van de Beek D, Veltkamp R (2012) The immunology of acute stroke. Nature Reviews Neurology 8:401-410.

Chelmicka-Schorr E, Checinski M, Arnason BG (1988) Chemical sympathectomy augments the severity of experimental allergic encephalomyelitis. J Neuroimmunol 17:347-350.

Chisari A, Carino M, Perone M, Gaillard RC, Spinedi E (1995) Sex and strain variability in the rat hypothalamo-pituitary-adrenal (HPA) axis function. Journal of endocrinological investigation 18:25-33.

Chroni E, Argyriou AA, Katsoulas G, Polychronopoulos P (2007) Ulnar F wave generation assessed within 3 days after the onset of stroke in patients with relatively preserved level of consciousness. Clin Neurol Neurosurg 109:27-31.

Chroni E, Katsoulas G, Argyriou AA, Sakellaropoulos GC, Polychronopoulos P, Nikiforidis G (2006) Level of consciousness as a conditioning factor of F wave generation in stroke patients. Clinical neurophysiology : official journal of the International Federation of Clinical Neurophysiology 117:315-319.

Collins S, Caron MG, Lefkowitz RJ (1988) Beta-adrenergic receptors in hamster smooth muscle cells are transcriptionally regulated by glucocorticoids. J Biol Chem 263:9067-9070.

Compton MM, Caron LA, Cidlowski JA (1987) Glucocorticoid action on the immune system. Journal of steroid biochemistry 27:201-208.

Cruse JM, Lewis RE, Bishop GR, Kliesch WF, Gaitan E (1992) Neuroendocrine-immune interactions associated with loss and restoration of immune system function in spinal cord injury and stroke patients. Immunologic research 11:104-116.

Cua DJ, Sherlock J, Chen Y, Murphy CA, Joyce B, Seymour B, Lucian L, To W, Kwan S, Churakova T, Zurawski S, Wiekowski M, Lira SA, Gorman D, Kastelein RA, Sedgwick JD (2003) Interleukin-23 rather than interleukin-12 is the critical cytokine for autoimmune inflammation of the brain. Nature 421:744-748.

Czlonkowska A, Cyrta B, Korlak J (1979) Immunological observations on patients with acute cerebral vascular disease. J Neurol Sci 43:455-464.

Da Silva JA (1999) Sex hormones and glucocorticoids: interactions with the immune system. Ann N Y Acad Sci 876:102-117; discussion 117-108.

Da Silva JA, Peers SH, Perretti M, Willoughby DA (1993) Sex steroids affect glucocorticoid response to chronic inflammation and to interleukin-1. The Journal of endocrinology 136:389-397.

Dalkara T, Morikawa E, Panahian N, Moskowitz MA (1994) Blood Flow-Dependent Functional Recovery in a Rat Model of Focal Cerebral-Ischemia. American Journal of Physiology 267:H678-H683.

Davenport RJ, Dennis MS, Wellwood I, Warlow CP (1996) Complications after acute stroke. Stroke 27:415-420.

Dirnagl U (2010) Rodent Models of Stroke. Humana Press Springer Protocols Neuromethods 47.

Dirnagl U, Iadecola C, Moskowitz MA (1999) Pathobiology of ischaemic stroke: an integrated view. Trends Neurosci 22:391-397.

Dirnagl U, Members of the MCAO-SOP Group (2012) Standard operating procedures (SOP) in experimental stroke research: SOP for middle cerebral artery occlusion in the mouse. Nature Precedings <http://dx.doi.org/10.1038/npre.2012.3492.3>.

Dobarro M, Orejana L, Aguirre N, Ramirez MJ (2013) Propranolol reduces cognitive deficits, amyloid beta levels, tau phosphorylation and insulin resistance in response to chronic corticosterone administration. The international journal of neuropsychopharmacology / official scientific journal of the Collegium Internationale Neuropsychopharmacologicum 16:1351-1360.

Du C, Hu R, Csernansky CA, Hsu CY, Choi DW (1996) Very delayed infarction after mild focal cerebral ischemia: A role for apoptosis? Journal of Cerebral Blood Flow and Metabolism 16:195-201.

Durukan A, Tatlisumak T (2007) Acute ischemic stroke: overview of major experimental rodent models, pathophysiology, and therapy of focal cerebral ischemia. Pharmacology, biochemistry, and behavior 87:179-197.

Edvinsson L, Aubineau P, Owman C, Sercombe R, Seylaz J (1975) Sympathetic Innervation of Cerebral-Arteries - Prejunctional Supersensitivity to Norepinephrine after Sympathectomy or Cocaine Treatment. Stroke 6:525-530.

Edvinsson L, Lacombe P, Owman C, Reynierrebuffel AM, Seylaz J (1979) Quantitative Changes in Regional Cerebral Blood-Flow of Rats Induced by Alpha-Adrenergic and Beta-Adrenergic Stimulants. Acta Physiologica Scandinavica 107:289-296.

Elenkov IJ, Papanicolaou DA, Wilder RL, Chrousos GP (1996) Modulatory effects of glucocorticoids and catecholamines on human interleukin-12 and interleukin-10 production: clinical implications. Proceedings of the Association of American Physicians 108:374-381.

Elenkov IJ, Wilder RL, Chrousos GP, Vizi ES (2000) The sympathetic nerve--an integrative interface between two supersystems: the brain and the immune system. Pharmacological reviews 52:595-638.

Emorine LJ, Marullo S, Briend-Sutren MM, Patey G, Tate K, Delavier-Klutchko C, Strosberg AD (1989) Molecular characterization of the human beta 3-adrenergic receptor. Science 245:1118-1121.

Emsley HC, Hopkins SJ (2008) Acute ischaemic stroke and infection: recent and emerging concepts. Lancet neurology 7:341-353.

Engel O, Meisel A (2010) Models of Infection Before and After Stroke: Investigating New Targets. Infect Disord Drug Targets 9.

Fassbender K, Schmidt R, Mossner R, Daffertshofer M, Hennerici M (1994a) Pattern of activation of the hypothalamic-pituitary-adrenal axis in acute stroke. Relation to acute confusional state, extent of brain damage, and clinical outcome. Stroke 25:1105-1108.

Fassbender K, Rossol S, Kammer T, Daffertshofer M, Wirth S, Dollman M, Hennerici M (1994b) Proinflammatory cytokines in serum of patients with acute cerebral ischemia: kinetics of secretion and relation to the extent of brain damage and outcome of disease. J Neurol Sci 122:135-139.

Felten DL, Felten SY, Carlson SL, Olschowka JA, Livnat S (1985) Noradrenergic and Peptidergic Innervation of Lymphoid-Tissue. Journal of Immunology 135:S755-S765.

Felten DL, Felten SY, Bellinger DL, Carlson SL, Ackerman KD, Madden KS, Olschowki JA, Livnat S (1987) Noradrenergic sympathetic neural interactions with the immune system: structure and function. Immunological reviews 100:225-260.

Felten SY, Olschowka J (1987) Noradrenergic sympathetic innervation of the spleen: II. Tyrosine hydroxylase (TH)-positive nerve terminals form synapticlike contacts on lymphocytes in the splenic white pulp. J Neurosci Res 18:37-48.

Fisher MA (2007) F-waves--physiology and clinical uses. TheScientificWorldJournal 7:144-160.

Fox HS, Bond BL, Parslow TG (1991) Estrogen regulates the IFN-gamma promoter. J Immunol 146:4362-4367.

Franchimont D, Galon J, Gadina M, Visconti R, Zhou Y, Aringer M, Frucht DM, Chrousos GP, O'Shea JJ (2000) Inhibition of Th1 immune response by glucocorticoids: dexamethasone selectively inhibits IL-12-induced Stat4 phosphorylation in T lymphocytes. J Immunol 164:1768-1774.

Frenkel D, Huang ZH, Maron R, Koldzic DN, Hancock WW, Moskowitz MA, Weiner HL (2003) Nasal vaccination with myelin oligodendrocyte glycoprotein reduces stroke size by inducing IL-10-producing CD4(+) T cells. Journal of Immunology 171:6549-6555.

Fuchs BA, Albright JW, Albright JF (1988) Beta-adrenergic receptors on murine lymphocytes: density varies with cell maturity and lymphocyte subtype and is decreased after antigen administration. Cell Immunol 114:231-245.

Gee JM, Kalil A, Thullbery M, Becker KJ (2008) Induction of immunologic tolerance to myelin basic protein prevents central nervous system autoimmunity and improves outcome after stroke. Stroke 39:1575-1582.

Gee JM, Zierath D, Hadwin J, Savos A, Kalil A, Thullbery M, Becker KJ (2009) Long term immunologic consequences of experimental stroke and mucosal tolerance. Exp Transl Stroke Med 1:3.

Gelderblom M, Leypoldt F, Steinbach K, Behrens D, Choe CU, Siler DA, Arumugam TV, Orthey E, Gerloff C, Tolosa E, Magnus T (2009) Temporal and spatial dynamics of cerebral immune cell accumulation in stroke. Stroke 40:1849-1857.

Genain CP, Abel K, Belmar N, Villinger F, Rosenberg DP, Linington C, Raine CS, Hauser SL (1996) Late complications of immune deviation therapy in a nonhuman primate. Science 274:2054-2057.

Ghoumari AM, Piochon C, Tomkiewicz C, Eychenne B, Levenes C, Dusart I, Schumacher M, Baulieu EE (2006) Neuroprotective effect of mifepristone involves neuron depolarization. FASEB J 20:1377-1386.

Gilmore DA, Gal J, Gerber JG, Nies AS (1992) Age and gender influence the stereoselective pharmacokinetics of propranolol. The Journal of pharmacology and experimental therapeutics 261:1181-1186.

Gordon JH, Shellenberger K (1974) Regional catecholamine content in the rat brain: sex differences and correlation with motor activity. Neuropharmacology 13:129-137.

Hadcock JR, Malbon CC (1988) Regulation of beta-adrenergic receptors by "permissive" hormones: glucocorticoids increase steady-state levels of receptor mRNA. Proc Natl Acad Sci U S A 85:8415-8419.

Han RQ, Ouyang YB, Xu L, Agrawal R, Patterson AJ, Giffard RG (2009) Postischemic brain injury is attenuated in mice lacking the beta2-adrenergic receptor. Anesthesia and analgesia 108:280-287.

Herold MJ, McPherson KG, Reichardt HM (2006) Glucocorticoids in T cell apoptosis and function. Cellular and molecular life sciences : CMLS 63:60-72.

Hetze S, Romer C, Teufelhart C, Meisel A, Engel O (2012) Gait analysis as a method for assessing neurological outcome in a mouse model of stroke. J Neurosci Methods 206:7-14.

Hetze S, Engel O, Romer C, Mueller S, Dirnagl U, Meisel C, Meisel A (2013) Superiority of preventive antibiotic treatment compared with standard treatment of poststroke pneumonia in experimental stroke: a bed to bench approach. J Cereb Blood Flow Metab 33:846-854.

Hickey WF, Hsu BL, Kimura H (1991) T-lymphocyte entry into the central nervous system. J Neurosci Res 28:254-260.

Hieble JP, Bylund DB, Clarke DE, Eikenburg DC, Langer SZ, Lefkowitz RJ, Minneman KP, Ruffolo RR, Jr. (1995) International Union of Pharmacology. X. Recommendation for nomenclature of alpha 1-adrenoceptors: consensus update. Pharmacological reviews 47:267-270.

Hiemke C, Bruder D, Poetz B, Ghraf R (1985) Sex-specific effects of estradiol on hypothalamic noradrenaline turnover in gonadectomized rats. Experimental brain research 59:68-72.

Hjelmstrom P, Juedes AE, Fjell J, Ruddle NH (1998) B-cell-deficient mice develop experimental allergic encephalomyelitis with demyelination after myelin oligodendrocyte glycoprotein sensitization. J Immunol 161:4480-4483.

Hodge S, Hodge G, Flower R, Han P (1999) Methyl-prednisolone up-regulates monocyte interleukin-10 production in stimulated whole blood. Scand J Immunol 49:548-553.

Hofstetter HH, Sewell DL, Liu F, Sandor M, Forsthuber T, Lehmann PV, Fabry Z (2003) Autoreactive T cells promote post-traumatic healing in the central nervous system. J Neuroimmunol 134:25-34.

Howard M, O'Garra A (1992) Biological properties of interleukin 10. Immunol Today 13:198-200.

Hurn PD, Subramanian S, Parker SM, Afentoulis ME, Kaler LJ, Vandenbark AA, Offner H (2007) T- and B-cell-deficient mice with experimental stroke have reduced lesion size and inflammation. J Cereb Blood Flow Metab 27:1798-1805.

Jager A, Dardalhon V, Sobel RA, Bettelli E, Kuchroo VK (2009) Th1, Th17, and Th9 effector cells induce experimental autoimmune encephalomyelitis with different pathological phenotypes. J Immunol 183:7169-7177.

Jeong H, Kim MS, Kwon J, Kim KS, Seol W (2006) Regulation of the transcriptional activity of the tyrosine hydroxylase gene by androgen receptor. Neurosci Lett 396:57-61.

Joels M, de Kloet ER (1994) Mineralocorticoid and glucocorticoid receptors in the brain. Implications for ion permeability and transmitter systems. Progress in neurobiology 43:1-36.

Johns TG, Bernard CC (1999) The structure and function of myelin oligodendrocyte glycoprotein. J Neurochem 72:1-9.

Katsuura G, Gottschall PE, Dahl RR, Arimura A (1988) Adrenocorticotropin release induced by intracerebroventricular injection of recombinant human interleukin-1 in rats: possible involvement of prostaglandin. Endocrinology 122:1773-1779.

Khan MM, Sansoni P, Silverman ED, Engleman EG, Melmon KL (1986) Beta-adrenergic receptors on human suppressor, helper, and cytolytic lymphocytes. Biochem Pharmacol 35:1137-1142.

Kim S, Liva SM, Dalal MA, Verity MA, Voskuhl RR (1999) Estriol ameliorates autoimmune demyelinating disease: implications for multiple sclerosis. Neurology 52:1230-1238.

Kipnis J, Mizrahi T, Yoles E, Ben-Nun A, Schwartz M (2002) Myelin specific Th1 cells are necessary for post-traumatic protective autoimmunity. J Neuroimmunol 130:78-85.

Kleinschnitz C, Schwab N, Kraft P, Hagedorn I, Dreykluft A, Schwarz T, Austinat M, Nieswandt B, Wiendl H, Stoll G (2010) Early detrimental T-cell effects in experimental cerebral ischemia are neither related to adaptive immunity nor thrombus formation. Blood 115:3835-3842.

Kleinschnitz C et al. (2013) Regulatory T cells are strong promoters of acute ischemic stroke in mice by inducing dysfunction of the cerebral microvasculature. Blood 121:679-691.

Krishnamurthi R, Feigin, VL, Forouzanfar, MH, Mensah, GA, Connor, M, Bennett, DA, Moran, AE, Sacco, RL, Anderson, LM, Truelsen, T, O'Donnell, M, Venketasubramanian, N, Barker-Collo, S, Lawes, CMM, Wang, W, Shinohara, Y, Witt, E, Ezzati, M, Naghavi, M, Murray, C, GBD 2010, GBD Stroke Experts Group (2013) Global and regional burden of first-ever ischaemic and haemorrhagic stroke during 1990–2010: findings from the Global Burden of Disease Study 2010. Lancet Glob Health 1:e259-e281.

Kroepfl JF, Viise LR, Charron AJ, Linington C, Gardinier MV (1996) Investigation of myelin/oligodendrocyte glycoprotein membrane topology. J Neurochem 67:2219-2222.

Kwon OJ, Au BT, Collins PD, Baraniuk JN, Adcock IM, Chung KF, Barnes PJ (1994) Inhibition of interleukin-8 expression by dexamethasone in human cultured airway epithelial cells. Immunology 81:389-394.

Lands AM, Arnold A, McAuliff JP, Luduena FP, Brown TG, Jr. (1967) Differentiation of receptor systems activated by sympathomimetic amines. Nature 214:597-598.

Langhorne P, Stott DJ, Robertson L, MacDonald J, Jones L, McAlpine C, Dick F, Taylor GS, Murray G (2000) Medical complications after stroke: a multicenter study. Stroke 31:1223-1229.

Le Mevel JC, Abitbol S, Beraud G, Maniey J (1978) Dynamic changes in plasma adrenocorticotrophin after neurotropic stress in male and female rats. The Journal of endocrinology 76:359-360.

Leithner C, Muller S, Fuchtemeier M, Lindauer U, Dirnagl U, Royl G (2010) Determination of the brain-blood partition coefficient for water in mice using MRI. J Cereb Blood Flow Metab 30:1821-1824.

Leithner C, Gertz K, Schrock H, Priller J, Prass K, Steinbrink J, Villringer A, Endres M, Lindauer U, Dirnagl U, Royl G (2008) A flow sensitive alternating inversion recovery (FAIR)-MRI protocol to measure hemispheric cerebral blood flow in a mouse stroke model. Exp Neurol 210:118-127.

Levine S, Strebel R, Wenk EJ, Harman PJ (1962) Suppression of experimental allergic encephalomyelitis by stress. Proceedings of the Society for Experimental Biology and Medicine Society for Experimental Biology and Medicine 109:294-298.

Lewitus GM, Kipnis J, Avidan H, Ben-Nun A, Schwartz M (2006) Neuroprotection induced by mucosal tolerance is epitope-dependent: conflicting effects in different strains. J Neuroimmunol 175:31-38.

Ley EJ, Scehnet J, Park R, Schroff S, Dagliyan G, Conti PS, Margulies DR, Salim A (2009) The in vivo effect of propranolol on cerebral perfusion and hypoxia after traumatic brain injury. J Trauma 66:154-159; discussion 159-161.

Li S, Shi Z, Zhang H, Liu X, Chen S, Jin J, Wang Y, Jia W, Li H (2013) Assessing gait impairment after permanent middle cerebral artery occlusion in rats using an automated computer-aided control system. Behav Brain Res 250C:174-191.

Liesz A, Suri-Payer E, Veltkamp C, Doerr H, Sommer C, Rivest S, Giese T, Veltkamp R (2009) Regulatory T cells are key cerebroprotective immunomodulators in acute experimental stroke. Nat Med 15:192-199.

Liesz A, Zhou W, Mracsko E, Karcher S, Bauer H, Schwarting S, Sun L, Bruder D, Stegemann S, Cerwenka A, Sommer C, Dalpke AH, Veltkamp R (2011) Inhibition of lymphocyte trafficking shields the brain against deleterious neuroinflammation after stroke. Brain 134:704-720.

Linington C, Berger T, Perry L, Weerth S, Hinze-Selch D, Zhang Y, Lu HC, Lassmann H, Wekerle H (1993) T cells specific for the myelin oligodendrocyte glycoprotein mediate an unusual autoimmune inflammatory response in the central nervous system. Eur J Immunol 23:1364-1372.

Liva SM, Voskuhl RR (2001) Testosterone acts directly on CD4+ T lymphocytes to increase IL-10 production. J Immunol 167:2060-2067.

Loveland BE, Jarrott B, McKenzie IF (1981) The detection of beta-adrenoceptors on murine lymphocytes. International journal of immunopharmacology 3:45-55.

Mackenzie FJ, Leonard JP, Cuzner ML (1989) Changes in lymphocyte beta-adrenergic receptor density and noradrenaline content of the spleen are early indicators of immune reactivity in acute experimental allergic encephalomyelitis in the Lewis rat. J Neuroimmunol 23:93-100.

MacPhee IA, Antoni FA, Mason DW (1989) Spontaneous recovery of rats from experimental allergic encephalomyelitis is dependent on regulation of the immune system by endogenous adrenal corticosteroids. J Exp Med 169:431-445.

Madden KS, Sanders VM, Felten DL (1995) Catecholamine influences and sympathetic neural modulation of immune responsiveness. Annual review of pharmacology and toxicology 35:417-448.

Maret A, Coudert JD, Garidou L, Foucras G, Gourdy P, Krust A, Dupont S, Chambon P, Druet P, Bayard F, Guery JC (2003) Estradiol enhances primary antigen-specific CD4 T cell responses and Th1 development in vivo. Essential role of estrogen receptor alpha expression in hematopoietic cells. Eur J Immunol 33:512-521.

Mathiesen T, Andersson B, Loftenius A, von Holst H (1993) Increased interleukin-6 levels in cerebrospinal fluid following subarachnoid hemorrhage. J Neurosurg 78:562-567.

Mathiesen T, Edner G, Ulfarsson E, Andersson B (1997) Cerebrospinal fluid interleukin-1 receptor antagonist and tumor necrosis factor-alpha following subarachnoid hemorrhage. J Neurosurg 87:215-220.

McCullers DL, Sullivan PG, Scheff SW, Herman JP (2002) Mifepristone protects CA1 hippocampal neurons following traumatic brain injury in rat. Neuroscience 109:219-230.

McEwen B, Brinton R, Harrelson A, Rostene W (1987) Modulatory interactions between steroid hormones, neurotransmitters and neuropeptides in hippocampus. Adv Biochem Psychopharmacol 43:87-102.

McGillis JP, Park A, Rubin-Fletter P, Turck C, Dallman MF, Payan DG (1989) Stimulation of rat B-lymphocyte proliferation by corticotropin-releasing factor. J Neurosci Res 23:346-352.

Meert KL, Long M, Kaplan J, Sarnaik AP (1995) Alterations in immune function following head injury in children. Crit Care Med 23:822-828.

Meisel C, Schwab JM, Prass K, Meisel A, Dirnagl U (2005) Central nervous system injury-induced immune deficiency syndrome. Nat Rev Neurosci 6:775-786.

Mendel I, Kerlero de Rosbo N, Ben-Nun A (1995) A myelin oligodendrocyte glycoprotein peptide induces typical chronic experimental autoimmune encephalomyelitis in H-2b mice: fine specificity and T cell receptor V beta expression of encephalitogenic T cells. Eur J Immunol 25:1951-1959.

Migita K, Eguchi K, Kawabe Y, Nakamura T, Shirabe S, Tsukada T, Ichinose Y, Nakamura H, Nagataki S (1997) Apoptosis induction in human peripheral blood T lymphocytes by high-dose steroid therapy. Transplantation 63:583-587.

Millan M, Davalos A (2006) The Need for New Therapies for Acute Ischaemic Stroke. Cerebrovasc Dis 22:3-9.

Milligan NM, Newcombe R, Compston DA (1987) A double-blind controlled trial of high dose methylprednisolone in patients with multiple sclerosis: 1. Clinical effects. Journal of neurology, neurosurgery, and psychiatry 50:511-516.

Miskowiak B (1985) Effects of gonadectomy and sex hormones on the levels of noradrenaline and dopamine in rat hypothalamus. Acta physiologica Polonica 36:98-106.

Motulsky HJ, Cunningham EM, DeBlasi A, Insel PA (1986) Desensitization and redistribution of beta-adrenergic receptors on human mononuclear leukocytes. Am J Physiol 250:E583-590.

Munck A, Naray-Fejes-Toth A (1994) Glucocorticoids and stress: permissive and suppressive actions. Ann N Y Acad Sci 746:115-130; discussion 131-113.

Murphy K, Travers, P, Walter, P (2008) Janeway's immunobiology. --7th ed. Garland Science, Taylor & Francis Group.

Nicolussi EM, Huck S, Lassmann H, Bradl M (2009) The cholinergic anti-inflammatory system limits T cell infiltration into the neurodegenerative CNS, but cannot counteract complex CNS inflammation. Neurobiol Dis 35:24-31.

NINDS (1995) Tissue Plasminogen Activator for Acute Ischemic Stroke. The National Institute of Neurological Disorders and Stroke rt-PA Stroke Study Group. New Engl J Med 333:1581-1587.

Nogai A, Siffrin V, Bonhagen K, Pfueller CF, Hohnstein T, Volkmer-Engert R, Bruck W, Stadelmann C, Kamradt T (2005) Lipopolysaccharide injection induces relapses of experimental autoimmune encephalomyelitis in nontransgenic mice via bystander activation of autoreactive CD4+ cells. J Immunol 175:959-966.

Pagany M, Jagodic M, Schubart A, Pham-Dinh D, Bachelin C, Baron van Evercooren A, Lachapelle F, Olsson T, Linington C (2003) Myelin oligodendrocyte glycoprotein is expressed in the peripheral nervous system of rodents and primates. Neurosci Lett 350:165-168.

Pan J, Ju D, Wang Q, Zhang M, Xia D, Zhang L, Yu H, Cao X (2001) Dexamethasone inhibits the antigen presentation of dendritic cells in MHC class II pathway. Immunology letters 76:153-161.

Panina-Bordignon P, Mazzeo D, Lucia PD, D'Ambrosio D, Lang R, Fabbri L, Self C, Sinigaglia F (1997) Beta2-agonists prevent Th1 development by selective inhibition of interleukin 12. J Clin Invest 100:1513-1519.

Parthasarathy S, Morales AJ, Murphy AA (1994) Antioxidant: a new role for RU-486 and related compounds. J Clin Invest 94:1990-1995.

Pavlov VA, Wang H, Czura CJ, Friedman SG, Tracey KJ (2003) The cholinergic anti-inflammatory pathway: a missing link in neuroimmunomodulation. Molecular medicine 9:125-134.

Pham-Dinh D, Mattei MG, Nussbaum JL, Roussel G, Pontarotti P, Roeckel N, Mather IH, Artzt K, Lindahl KF, Dautigny A (1993) Myelin/oligodendrocyte glycoprotein is a member of a subset of the immunoglobulin superfamily encoded within the major histocompatibility complex. Proc Natl Acad Sci U S A 90:7990-7994.

Planas AM, Gomez-Choco M, Urra X, Gorina R, Caballero M, Chamorro A (2012) Brain-derived antigens in lymphoid tissue of patients with acute stroke. J Immunol 188:2156-2163.

Plaut M (1987) Lymphocyte hormone receptors. Annu Rev Immunol 5:621-669.

Prass K, Meisel C, Hoflich C, Braun J, Halle E, Wolf T, Ruscher K, Victorov IV, Priller J, Dirnagl U, Volk HD, Meisel A (2003) Stroke-induced immunodeficiency promotes spontaneous bacterial infections and is mediated by sympathetic activation reversal by poststroke T helper cell type 1-like immunostimulation. J Exp Med 198:725-736.

Ramirez F, Fowell DJ, Puklavec M, Simmonds S, Mason D (1996) Glucocorticoids promote a TH2 cytokine response by CD4+ T cells in vitro. J Immunol 156:2406-2412.

Rider V, Jones S, Evans M, Bassiri H, Afsar Z, Abdou NI (2001) Estrogen increases CD40 ligand expression in T cells from women with systemic lupus erythematosus. The Journal of rheumatology 28:2644-2649.

Rivier C, Vale W, Brown M (1989) In the rat, interleukin-1 alpha and -beta stimulate adrenocorticotropin and catecholamine release. Endocrinology 125:3096-3102.

Royl G, Balkaya M, Lehmann S, Lehnardt S, Stohlmann K, Lindauer U, Endres M, Dirnagl U, Meisel A (2009) Effects of the PDE5-inhibitor vardenafil in a mouse stroke model. Brain Res 1265:148-157.

Sanders VM, Baker RA, Ramer-Quinn DS, Kasprowicz DJ, Fuchs BA, Street NE (1997) Differential expression of the beta2-adrenergic receptor by Th1 and Th2 clones: implications for cytokine production and B cell help. J Immunol 158:4200-4210.

Sapolsky RM, Romero LM, Munck AU (2000) How do glucocorticoids influence stress responses? Integrating permissive, suppressive, stimulatory, and preparative actions. Endocrine reviews 21:55-89.

Schroeter M, Jander S, Witte OW, Stoll G (1994) Local immune responses in the rat cerebral cortex after middle cerebral artery occlusion. J Neuroimmunol 55:195-203.

Scolding NJ, Frith S, Linington C, Morgan BP, Campbell AK, Compston DA (1989) Myelin-oligodendrocyte glycoprotein (MOG) is a surface marker of oligodendrocyte maturation. J Neuroimmunol 22:169-176.

Shichita T, Sugiyama Y, Ooboshi H, Sugimori H, Nakagawa R, Takada I, Iwaki T, Okada Y, Iida M, Cua DJ, Iwakura Y, Yoshimura A (2009) Pivotal role of cerebral interleukin-17-producing gammadeltaT cells in the delayed phase of ischemic brain injury. Nat Med 15:946-950.

Simerly RB, Chang C, Muramatsu M, Swanson LW (1990) Distribution of androgen and estrogen receptor mRNA-containing cells in the rat brain: an in situ hybridization study. The Journal of comparative neurology 294:76-95.

Smythe GA, Bradshaw JE, Vining RF (1983) Hypothalamic monoamine control of stress-induced adrenocorticotropin release in the rat. Endocrinology 113:1062-1071.

Squire L, Bloom FE, McConnell SK, Roberts JL, Spitzer NC, Zigmond MJ, (Eds) (2003) Fundamental Neuroscience. Second Edition. Academic Press New York.

Stein M, Schiavi RC, Camerino M (1976) Influence of brain and behavior on the immune system. Science 191:435-440.

Stromnes IM, Cerretti LM, Liggitt D, Harris RA, Goverman JM (2008) Differential regulation of central nervous system autoimmunity by T(H)1 and T(H)17 cells. Nat Med 14:337-342.

Stubbe T, Ebner F, Richter D, Engel O, Klehmet J, Royl G, Meisel A, Nitsch R, Meisel C, Brandt C (2013) Regulatory T cells accumulate and proliferate in the ischemic hemisphere for up to 30 days after MCAO. J Cereb Blood Flow Metab 33:37-47.

Sugo N, Hurn PD, Morahan MB, Hattori K, Traystman RJ, DeVries AC (2002) Social stress exacerbates focal cerebral ischemia in mice. Stroke 33:1660-1664.

Sullivan GM, Canfield SM, Lederman S, Xiao E, Ferin M, Wardlaw SL (1997) Intracerebroventricular injection of interleukin-1 suppresses peripheral lymphocyte function in the primate. Neuroimmunomodulation 4:12-18.

Sun J, Link H, Olsson T, Xiao BG, Andersson G, Ekre HP, Linington C, Diener P (1991) T and B cell responses to myelin-oligodendrocyte glycoprotein in multiple sclerosis. J Immunol 146:1490-1495.

Sundar SK, Becker KJ, Cierpial MA, Carpenter MD, Rankin LA, Fleener SL, Ritchie JC, Simson PE, Weiss JM (1989) Intracerebroventricular infusion of interleukin 1 rapidly decreases peripheral cellular immune responses. Proc Natl Acad Sci U S A 86:6398-6402.

Szabo C, Thiemermann C, Wu CC, Perretti M, Vane JR (1994) Attenuation of the induction of nitric oxide synthase by endogenous glucocorticoids accounts for endotoxin tolerance in vivo. Proc Natl Acad Sci U S A 91:271-275.

Thanky NR, Son JH, Herbison AE (2002) Sex differences in the regulation of tyrosine hydroxylase gene transcription by estrogen in the locus coeruleus of TH9-LacZ transgenic mice. Brain research Molecular brain research 104:220-226.

Tischner D, Reichardt HM (2007) Glucocorticoids in the control of neuroinflammation. Molecular and cellular endocrinology 275:62-70.

Tracey KJ (2002) The inflammatory reflex. Nature 420:853-859.

Tuosto L, Cundari E, Gilardini Montani MS, Piccolella E (1994) Analysis of susceptibility of mature human T lymphocytes to dexamethasone-induced apoptosis. Eur J Immunol 24:1061-1065.

Van der Aa A, Hellings N, Bernard CC, Raus J, Stinissen P (2003) Functional properties of myelin oligodendrocyte glycoprotein-reactive T cells in multiple sclerosis patients and controls. J Neuroimmunol 137:164-176.

van der Graaff WL, Prins AP, Dijkmans BA, van Lier RA (1998) Prognostic value of Th1/Th2 ratio in rheumatoid arthritis. Lancet 351:1931.

Vandeputte C, Taymans JM, Casteels C, Coun F, Ni Y, Van Laere K, Baekelandt V (2010) Automated quantitative gait analysis in animal models of movement disorders. BMC Neurosci 11:92.

Vernino S, Brown RD, Jr., Sejvar JJ, Sicks JD, Petty GW, O'Fallon WM (2003) Cause-specific mortality after first cerebral infarction: a population-based study. Stroke 34:1828-1832.

Walle T, Walle K, Mathur RS, Palesch YY, Conradi EC (1994) Propranolol metabolism in normal subjects: association with sex steroid hormones. Clin Pharmacol Ther 56:127-132.

Wang H, Yu M, Ochani M, Amella CA, Tanovic M, Susarla S, Li JH, Wang H, Yang H, Ulloa L, Al-Abed Y, Czura CJ, Tracey KJ (2003) Nicotinic acetylcholine receptor alpha7 subunit is an essential regulator of inflammation. Nature 421:384-388.

Wang PY, Kao CH, Mui MY, Wang SJ (1993) Leukocyte infiltration in acute hemispheric ischemic stroke. Stroke 24:236-240.

Wang WZ, Olsson T, Kostulas V, Hojeberg B, Ekre HP, Link H (1992) Myelin antigen reactive T cells in cerebrovascular diseases. Clinical and experimental immunology 88:157-162.

Watts AG, Swanson LW (1989) Diurnal variations in the content of preprocorticotropin-releasing hormone messenger ribonucleic acids in the hypothalamic paraventricular nucleus of rats of both sexes as measured by in situ hybridization. Endocrinology 125:1734-1738.

Webster JI, Tonelli L, Sternberg EM (2002) Neuroendocrine regulation of immunity. Annu Rev Immunol 20:125-163.

Weimar C, Roth MP, Zillessen G, Glahn J, Wimmer ML, Busse O, Haberl RL, Diener HC, German Stroke Date Bank C (2002) Complications following acute ischemic stroke. European neurology 48:133-140.

Weissert R, Kuhle J, de Graaf KL, Wienhold W, Herrmann MM, Muller C, Forsthuber TG, Wiesmuller KH, Melms A (2002) High immunogenicity of intracellular myelin oligodendrocyte glycoprotein epitopes. J Immunol 169:548-556.

Weller RO, Djuanda E, Yow HY, Carare RO (2009) Lymphatic drainage of the brain and the pathophysiology of neurological disease. Acta Neuropathol 117:1-14.

Wiegmann K, Muthyala S, Kim DH, Arnason BG, Chelmicka-Schorr E (1995) Beta-adrenergic agonists suppress chronic/relapsing experimental allergic encephalomyelitis (CREAE) in Lewis rats. J Neuroimmunol 56:201-206.

Wilckens T, De Rijk R (1997) Glucocorticoids and immune function: unknown dimensions and new frontiers. Immunol Today 18:418-424.

Williams JL, Kithcart AP, Smith KM, Shawler T, Cox GM, Whitacre CC (2011) Memory cells specific for myelin oligodendrocyte glycoprotein (MOG) govern the transfer of experimental autoimmune encephalomyelitis. J Neuroimmunol 234:84-92.

Woiciechowsky C, Schoning B, Lanksch WR, Volk HD, Docke WD (1999a) Mechanisms of brain-mediated systemic anti-inflammatory syndrome causing immunodepression. J Mol Med (Berl) 77:769-780.

Woiciechowsky C, Schoning B, Daberkow N, Asche K, Stoltenburg G, Lanksch WR, Volk HD (1999b) Brain-IL-1beta induces local inflammation but systemic anti-inflammatory response through stimulation of both hypothalamic-pituitary-adrenal axis and sympathetic nervous system. Brain Res 816:563-571.

Woiciechowsky C, Asadullah K, Nestler D, Eberhardt B, Platzer C, Schoning B, Glockner F, Lanksch WR, Volk HD, Docke WD (1998) Sympathetic activation triggers systemic interleukin-10 release in immunodepression induced by brain injury. Nat Med 4:808-813.

Yilmaz G, Arumugam TV, Stokes KY, Granger DN (2006) Role of T lymphocytes and interferon-gamma in ischemic stroke. Circulation 113:2105-2112.

Yukawa T, Ukena D, Kroegel C, Chanez P, Dent G, Chung KF, Barnes PJ (1990) Beta 2-adrenergic receptors on eosinophils. Binding and functional studies. The American review of respiratory disease 141:1446-1452.

Zierath D, Thullbery M, Hadwin J, Gee JM, Savos A, Kalil A, Becker KJ (2010) CNS immune responses following experimental stroke. Neurocrit Care 12:274-284.

9. Abbreviations

aa	amino acid
AB	antibiotic (enrofloxacin)
ADC	apparent diffusion coefficient
ANOVA	analysis of variance
APC	allophycocyanin
β2-AR (ko)	β2-adrenoreceptor (knockout)
BAL	bronchoalveolar lavage
bp	basepair
BSA	bovine serum albumin
CBF	cerebral blood flow
CFU	colony forming unit
CIDS	central nervous system injury induced immunodepression
CNS	central nervous system
Ctrl	control
CW	CatWalk gait analysis
Cy	cyanine
dATP	desoxyadenosintriphosphat
dCTP	desoxycytidintriphosphat
dGTP	desoxyguanosintriphosphat
DNA	deoxyribonucleic acid
dTTP	desoxythymidintriphosphat
DWI	diffusion-weighted imaging
EAE	experimental autoimmune encephalomyelitis
EPI	echo planar imaging
FACS	fluorescence-activated cell sorting
FAIR-MRI	flow sensitive alternating inversion recovery magnetic resonance imaging
FCS	fetal calf serum
FITC	fluorescein isothiocyanate
FLASH	fast low angle shot
FOV	field of view
FSC	forward light scatter
HPA	hypothalamic-pituitary-adrenal
IFN-γ	interferon-γ
IgG	immunoglobulin G
IHC	immunohistochemistry
IL-#	interleukin-(number indicates type)
i.p.	intraperitoneal
i.v.	intravenous
ko	knockout
LB	Lysogeny Broth
LF	left front paw
LH	left hind paw
MACS	magnetic-activated cell sorting

MCA(o)	middle cerebral artery (occlusion)
MNC	mononuclear cell
MHC	major histocompatibility complex
MOG	myelin oligodendrocyte glycoprotein
MRI	magnetic resonance imaging
MSME	multi-slice multi-echo
PB	pacific blue
PBS	phosphate-buffered saline
PCR	polymerase chain reaction
PE	phycoerythrin
PE-Cy7	tandem conjugate (PE and a cyanine dye 7)
PerCP	peridinin chlorophyll protein
PFA	paraformaldehyde
$pMOG_{35-55}$	MOG peptide (amino acids 35-55)
PO	pacific orange
RARE	rapid acquisition with relaxation enhancement
RF	right front paw
RH	right hind paw
RPMI 1640	Roswell Park Memorial Institute 1640
RT	room temperature
s.c.	subcutaneous
SDS	sodium dodecyl sulfate
SNS	sympathetic nervous system
SNS&HPA	sympathetic nervous system/hypothalamic-pituitary-adrenal axis block group
SSC	side light scatter
T2-wt MRI	T2-weighted magnetic resonance imaging
TBE	Tris-boric acid-ethylene-diaminetetraacetic acid
TCR	T cell receptor
TE	time to echo
Th#	helper T cells (number indicates type)
TNF-α	tumor necrosis factor-α
TR	time of repetition
UV	ultraviolet
wt	wild-type

10. Eidesstattliche Versicherung

„Ich, Christine Römer, versichere an Eides statt durch meine eigenhändige Unterschrift, dass ich die vorgelegte Dissertation mit dem Thema ‚Stroke-induced immunodepression syndrome and central nervous system autoreactivity' selbstständig und ohne nicht offengelegte Hilfe Dritter verfasst und keine anderen als die angegebenen Quellen und Hilfsmittel genutzt habe.

Alle Stellen, die wörtlich oder dem Sinne nach auf Publikationen oder Vorträgen anderer Autoren beruhen, sind als solche in korrekter Zitierung (siehe „Uniform Requirements for Manuscripts (URM)" des ICMJE www.icmje.org) kenntlich gemacht. Die Abschnitte zu Methodik (insbesondere praktische Arbeiten, Laborbestimmungen, statistische Aufarbeitung) und Resultaten (insbesondere Abbildungen, Graphiken und Tabellen) entsprechen den URM (s. o.) und werden von mir verantwortet.

Meine Anteile an etwaigen Publikationen zu dieser Dissertation entsprechen denen, die in der untenstehenden gemeinsamen Erklärung mit dem/der Betreuer/in, angegeben sind. Sämtliche Publikationen, die aus dieser Dissertation hervorgegangen sind und bei denen ich Autor bin, entsprechen den URM (s. o.) und werden von mir verantwortet.

Die Bedeutung dieser eidesstattlichen Versicherung und die strafrechtlichen Folgen einer unwahren eidesstattlichen Versicherung (§156,161 des Strafgesetzbuches) sind mir bekannt und bewusst."

Datum Unterschrift

Anteilserklärung an etwaigen erfolgten Publikationen

Christine Römer hatte folgenden Anteil an den folgenden Publikationen (siehe auch 12.):

Römer C, Engel O, Winek K, Hochmeister S, Zhang T, Royl G, Klehmet J, Dirnagl U, Meisel C, Meisel, A.

Blocking stroke-induced immunodeficiency increases CNS antigen specific autoreactivity but does not worsen functional outcome after experimental stroke.

In revision phase, the Journal of Neuroscience, 2014 Apr 15

Beitrag im Einzelnen: 80 %. Optimierung von Arbeitsschritten, Planung und Durchführung der Experimente sowie Datenauswertung, Schreiben des Manuskriptes. Submission.

Hetze S, Engel O, **Römer C**, Mueller S, Meisel C, Meisel A.

Superiority of preventive antibiotic treatment compared to standard treatment of post-stroke pneumonia in experimental stroke: A bed to bench approach.

Journal of Cerebral Blood Flow Metabolism, 2013 Jun;33(6):846-54. Epub 2013 Jan 30

Beitrag im Einzelnen: 30 %. Beitrag zur Durchführung der Experimente, umfangreiche Datenauswertung, Beitrag zum Schreiben des Manuskriptes.

Hetze S[1], **Römer C[1]**, Teufelhart C, Meisel A, Engel O.

Gait analysis as a method for assessing neurological outcome in a mouse model of stroke.

Journal of Neuroscience Methods, 2012 Apr 30;206(1):7-14. Epub 2012 Feb 10

[1]Geteilte Erstautorenschaft.

Beitrag im Einzelnen: 45 %. Optimierung von Arbeitsschritten, Beitrag zur Durchführung der Experimente, umfangreiche Datenauswertung, Beitrag zum Schreiben des Manuskriptes.

Unterschrift, Datum und Stempel des betreuenden Hochschullehrers

Unterschrift der Doktorandin

11. Curriculum Vitae

Mein Lebenslauf wird aus datenschutzrechtlichen Gründen in der elektronischen Version meiner Arbeit nicht veröffentlicht.

12. Publication list

1. **Römer C,** Engel O, Winek K, Hochmeister S, Zhang T, Royl G, Dirnagl U, Meisel C, Meisel A.

   Blocking stroke-induced immunodeficiency (SIDS) increases CNS antigen specific autoreactivity but does not worsen functional outcome after experimental stroke.

   In revision phase, the Journal of Neuroscience, 2014 Apr 15

2. Huusko N, **Römer C**, Ndode-Ekane XE, Lukasiuk K, Pitkänen A.

   Loss of hippocampal interneurons and epileptogenesis: a comparison of two animal models of acquired epilepsy.

   Brain Structure and Function; Epub 2013 Oct 6

3. Hetze S, Engel O, **Römer C**, Mueller S, Meisel C, Meisel A.

   Superiority of preventive antibiotic treatment compared to standard treatment of post-stroke pneumonia in experimental stroke: A bed to bench approach.

   Journal of Cerebral Blood Flow Metabolism, 2013 Jun;33(6):846-54. Epub 2013 Jan 30

4. Hetze S[1], **Römer C[1]**, Teufelhart C, Meisel A, Engel O

   Gait analysis as a method for assessing neurological outcome in a mouse model of stroke.

   [1]Geteilte Erstautorenschaft

   Journal of Neuroscience Methods, 2012 Apr 30;206(1):7-14. Epub 2012 Feb 10

5. Immonen RJ, Kharatishvili I, Sierra A, **Einula C**, Pitkänen A, Gröhn OH

   Manganese enhanced MRI detects mossy fiber sprouting rather than neurodegeneration, gliosis or seizure-activity in the epileptic rat hippocampus.

   Neuroimage, 2008 May 1;40(4):1718-30. Epub 2008 Feb 7

13. Acknowledgements

Experimental part of this thesis was carried out at Charite, Department of Experimental Neurology.

I would like to express my gratitude towards Prof. Andreas Meisel for supervising my doctoral thesis and for his support and belief in this project.

I am grateful to Prof. Ulrich Dirnagl for his valuable advice at critical stages.

I am thankful to the Neurocure committee for the Neurocure scholarhip that funded the three years of my doctoral studies and to the MedNeuro graduate program.

I thank my co-authors, particularly Dr. Sonja Hochmeister, Tian Zhang, Dr. Georg Royl, Susann Hetze, Odilo Engel and Dr. Katarzyna Winek for their valuable contribution. I thank Dr. Petra Hünchen for showing me the technique of electromyography/electroneurography in a live mouse. I am grateful to Claudia Conert for her expert assistance in the early phases of my doctoral thesis.

I thank my daily colleagues from the office and the team of AG Andreas Meisel. It has been a truly educating experience to work together with so diverse people. I thank Christa and Ingo for their advice and pleasant atmosphere in the lab.

I owe thanks to my friends, particularly Egle, Julia, Sille, Kätlin and Kasia.

I am most grateful to my family in Germany and Estonia. Ma tänan vanat ja ema, et nad on olnud valmis mind alati ära kuulama ja nõustama, oma venda ja isa. Ich danke meinem Mann Lutz für seine Unterstützung während meiner Doktorarbeit, sein Verständnis und seine Liebe. Ich danke meinem Sohn Joonatan für unzählige besondere und glückliche Momente und seine Liebe.